

**Structural studies on the enzymes of the complement  
convertases:**

**factor B, C2a and the inhibitor SCIN**

Milder, F. J. (2007)  
Structural studies on the enzymes of the complement convertases: factor B, C2a and the inhibitor SCIN  
ISBN: 978-90-393-4620-4

# **Structural studies on the enzymes of the complement convertases:**

## **factor B, C2a and the inhibitor SCIN**

Structurele studies aan de enzymen van de complement convertases:

factor B, C2a en de remmer SCIN

*(met een samenvatting in het Nederlands)*

### **Proefschrift**

ter verkrijging van de graad van doctor aan de Universiteit Utrecht  
op gezag van de rector magnificus, prof. dr. W.H. Gispen,  
ingevolge het besluit van het college voor promoties  
in het openbaar te verdedigen op  
woensdag 26 september 2007 des middags te 2.30 uur

door

**Ferdinand Jacobus Milder**

geboren op 30 april 1977 te Arnhem, Nederland

Promotor: Prof. Dr. P. Gros

Het in dit proefschrift beschreven onderzoek werd gefinancierd door de Nederlandse organisatie voor Wetenschappelijk Onderzoek (NWO), Gebied Chemische Wetenschappen (CW)

# Contents

<b>Chapter 1</b>	General introduction	7
<b>Chapter 2</b>	Structure of complement component C2a: implications for convertase formation and substrate binding	29
<b>Chapter 3</b>	Factor B structure provides insights into activation of the central protease of the complement system	53
<b>Chapter 4</b>	Staphylococcal complement inhibitor: structure and active sites	75
<b>Chapter 5</b>	Summarizing discussion	101
	<b>Samenvattende discussie</b>	109
	<b>Dankwoord</b>	115
	<b>Curriculum vitae</b>	117
	<b>List of publications</b>	119
	<b>Appendix: color figures</b>	121



# 1

## **General introduction**

## **1 The complement system**

The complement system is a key component of the mammalian innate immune system and provides one of the major effector mechanisms of antibody-mediated immunity (Walport 2001a; 2001b). Complement was discovered in the late 19<sup>th</sup> century by Jules Bordet (Bordet, 1909). He showed that blood serum contains a component that assists, or complements, antibodies in the killing of bacteria. Similar to the blood clotting system, activated complement produces an expanding cascade of activity via a pattern of sequential activation. The primary function of the complement system is to recognize pathogens or immunogenic particles and label these cells or particles for clearance. Activated complement evokes a range of immune responses, including inflammatory responses, phagocytosis by macrophages, and B-cell stimulation. The complement system comprises over 30 soluble and cell-bound proteins that together account for more than 3 g per liter blood plasma. To avoid complement mediated self-injury almost half of the complement proteins serve as regulators or inhibitors. Deficiencies of or mutations in complement components may distort this finely balanced system. As such complement plays a role in many diseases with an immune component. Insight into the molecular mechanisms underlying activation and amplification of the complement response is important for the understanding of host self-defense and pathogen immune evasion and to the development of complement-immune therapies.

### **The complement cascade**

The complement system is activated via two specific recognition pathways, the Classical Pathway (CP) and Lectin Pathway (LP), which are amplified by the Alternative Pathway (AP). Antigen-antibody complexes and mannose-containing polysaccharides present on pathogenic surfaces respectively activate the classical and lectin pathway. The alternative pathway is activated continuously at a low rate. All three pathways of activation are triggered enzyme cascades that converge to the assembly of protease complexes, the so-called C3-convertases, on the pathogen cell surface (Figure 1.1). The C3-convertases of the classical and lectin pathway consist of C4b in complex with activated C2. The alternative pathway C3-convertase comprises C3b and activated factor B, which are homologous to C4b and C2, respectively (Xu et al., 2001). The C3 convertases catalyse the key reaction during complement activation, i.e. the conversion of C3 into C3a and C3b. C3a is a mediator of inflammation while C3b covalently binds to the nearby pathogen surface marking it for phagocytosis and initiating formation of additional C3 convertase, thus provides amplification. Due to high local concentrations of C3b



the C3 convertases may bind a C3b molecule, which changes the convertase substrate specificity from C3 to C5 (Rawal and Pangburn 2001). This C5 convertase mediates cleavage of C5 into C5a, one of the most potent mediators of inflammation, and C5b that initiates the terminal or lytic pathway. Produced C5b rapidly associates with complement proteins C6, C7 and C8 and inserts into the membrane. Subsequently, multiple C9 molecules (10-16) bind to the C5b-8 complex creating the Membrane Attack Complex (MAC). The MAC is a pore like structure with a diameter of ~100 Å through which the cellular contents leak resulting in lysis of the cell.

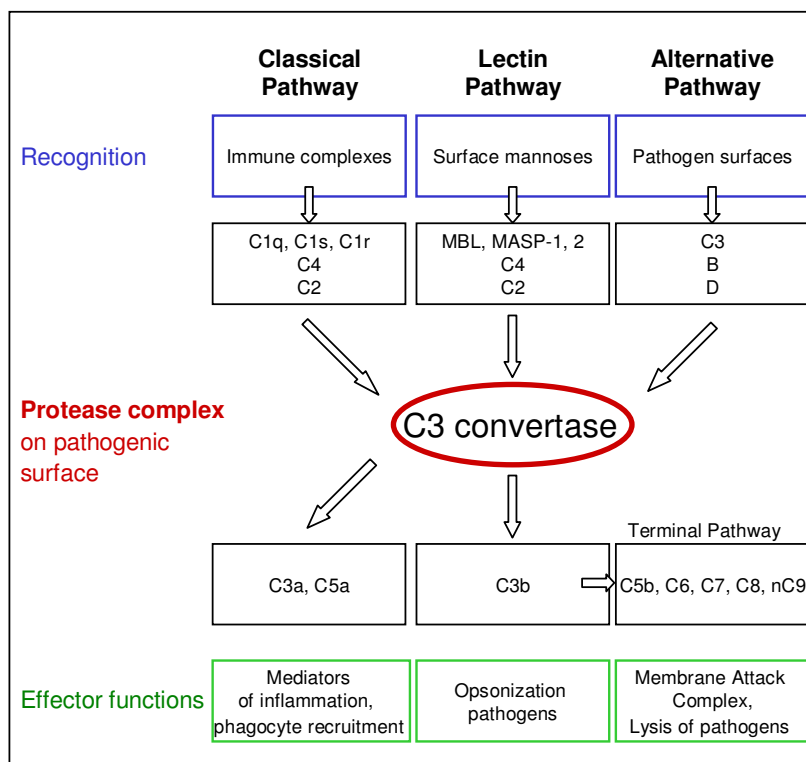


Figure 1.1 The complement cascade

## **Complement regulation**

The complement system is tightly regulated to ensure complement activation is focused on the surface of invading pathogens and to limit complement deposition on normal cells and tissues. A large part of the complement proteins serve as regulators or inhibitors and assist in this discrimination between self and non-self and keep the explosive potential of complement under control. These proteins are present in the fluid phase and on cell membranes. Most of the regulatory proteins downregulate the activity of the central C3 convertases. These Regulators of Complement Activation (RCA), are a family of related proteins that almost entirely consist of Complement Control Protein (CCP) domains arranged in a beads-on-a-string fashion (Kirkitadze and Barlow 2001). The RCA proteins inhibit the C3 convertases by causing decay of these enzymes and/or by acting as cofactors for serine protease factor I that inactivates C3b and C4b. Surface bound regulators Complement Receptor 1 (CR1/CD35) and Decay Accelerating Factor (DAF/CD55) enhance decay acceleration of all C3 convertases whereas the soluble regulators C4 Binding Protein (C4BP) and factor H act specifically on the C3 convertases of the classical/lectin and alternative pathway, respectively. In addition, factor H and CR1, together with Membrane Cofactor Protein (MCP), exhibit “cofactor activity” for the C3b and C4b inactivation by factor I.

The early (regulation of C1 activity) and final (regulation of MAC formation) stages of the complement cascade are regulated by complement proteins C1 inhibitor (C1 INH) and CD59, respectively. Complement C1 mediates activation of C4 and C2 in the initial steps of the classical pathway. C1 INH is a soluble regulator that inhibits spontaneous activation of free pro-enzyme C1 in serum and inhibits activated C1 bound to immune complexes. CD59 is a regulator expressed on most human cell surfaces. By binding to the C5b-8 complex CD59 inhibits C9 polymerisation, thus prevents formation of the pore forming membrane attack complex on self-cells.

## **2 Complement and disease**

The complement system is called a double-edged sword because, next to its defensive role, it may cause serious damage to self-cells when it runs out of control. Complement related diseases are either due to invading organisms that have developed specific strategies to overcome or to take advantage of complement mediated immune responses (Lindahl et al., 2000), or to inherited deficiencies and/or mutations in complement components and regulators.

### Pathogenic infections

By avoiding recognition and eradication pathogens may increase their survival rate (Wurzner, 1999). Most effective in evasion are pathogens that disguise themselves by pretending to be 'self'. Other pathogens may block immune responses by acquisition of host RCA proteins or by expressing either structural mimics of RCA proteins or other complement inhibiting proteins. *Streptococcus pyogenes* recruits C4BP. Binding to *S. pyogenes*' surface M protein immobilizes C4BP and protects the bacterium against phagocytosis via inhibition of opsonization (Thern et al., 1995). An example of molecular mimicry is the Vaccinia virus Complement-control Protein (VCP). This secretory protein inhibits both the classical and alternative pathway and consists of four domains homologous to the complement control protein (CCP) domains. VCP can bind to C3b and C4b and acts as a cofactor for factor I that inactivates both these proteins. Secretion of small molecules that inhibit complement is a strategy employed by the human pathogen *Staphylococcus aureus*. The recently discovered Staphylococcal Complement Inhibitor (SCIN) blocks all three complement activation pathways by specific inhibition of the C3-convertases (Rooijackers et al., 2005). Consequently, formation and deposition (opsonization) of C3b on the pathogenic surface is limited, thus, phagocytosis and eradication by human neutrophils is reduced. The characterization of the structure and active site of SCIN is described in **Chapter 4** of this thesis.

Next to evasive tactics, certain pathogens have developed methods to use the complement system for their own benefit, e.g. the Epstein-Barr virus (EBV). Infection of B cells by this herpesvirus is associated with a variety of human cancers (Serraino et al., 2005). Viral attachment is achieved through binding of EBV major membrane glycoprotein-350/220 to B cell-specific Complement Receptor-2 (CR2). At the same time this attachment prevents binding of the natural ligand, i.e. cleavage products of C3, and thereby blocks downstream immune response signalling by CR2.

### Distortion of complement regulation

Distortions in the complement cascade due to deficiencies of or mutations in complement components predispose patients to infectious diseases and are involved in immune related diseases. C2 deficiency is the most common of all complement deficiencies (Johnson et al., 1992), but, surprisingly, does not result in enhanced bacterial infections. However, persons lacking C2 frequently suffer from the immune-complex disorder System Lupus Erythematosus (SLE). This chronic rheumatic disease affects joints, muscles and other parts of the body. Mutations in C2 and factor B are linked to Age-related Macular Degeneration (AMD) (Gold et al., 2006), a disease that gradually destroys sharp, central vision. Furthermore,

mutations in factor B are associated with atypical Haemolytic Uraemic Syndrome (aHUS), a disease characterized by thrombocytopenia, microangiopathic haemolytic anaemia and renal (kidney) failure (Goicoechea de Jorge et al., 2007). Patients that are C3 deficient suffer from recurrent bacterial infections by organisms that are normally susceptible to opsonisation or lysis by complement. Persons with inherited C9 deficiency do not encounter problems with bacterial infections because the membrane inserted C5b-8 complex by itself, although less effective, is able to lyse bacteria.

Deficiencies of or mutations in complement regulators result in excessive activation and tissue injury. C1-INH deficiency is associated with the development of hereditary angioedema (Donaldson and Evans 1963). Patients are subjective to occasional explosive complement activation resulting in massive release of anaphylatoxins that cause dangerous swelling (odema) of the airways, skin and intestine. Factor H deficiency leads to uncontrolled activation of the alternative pathway C3 convertase. Deficiency of factor H has been associated with aHUS (Pichette et al., 1994). Mutations in factor H, MCP, and factor I have been linked to aHUS as well. In addition, mutations in factor H (Edwards et al., 2005; Haines et al., 2005), like mutations in factor B and C2, are associated with AMD.

### 3 The C3 convertases

The key offensive step in complement activation is the assembly of the C3 convertases on the pathogenic cell surface. These large enzymatic complexes consist of a catalytic component (Bb or C2a) non-covalently associated with a surface bound cofactor (C3b or C4b). Recent advances indicate that formation of the C3 convertases results in large conformational rearrangements in both the cofactor (Janssen et al., 2006; Wiesmann et al., 2006) and the catalytic component (**Chapters 2 and 3** of this thesis).

#### **Convertase formation**

Binding of multi-subunit complement protein C1 (C1q, C1r and C1s) to antigen-antibody complexes initiates the classical pathway. Binding of C1q to the Fc region of immunoglobulins activates the serine protease C1r which in turn activates serine protease C1s. Subsequently, activated C1s cleaves C4 into C4a (9 kDa) and C4b (193 kDa). C4a dissociates whereas C4b may become covalently attached to the nearby pathogenic cell surface via its thioester. The lectin pathway is initiated by binding of the complex consisting of Mannose-binding lectin (MBL) and the MBL Associated Serine Protases 1 and 2 (MASP-1 and 2) to mannose-containing

polysaccharides present on the pathogenic surface. This complex is homologous to C1 and cleaves C4 as well. Recently it has been shown that other lectins, i.e. some of the ficolins, and their associated serine proteases may activate C4 likewise. In a magnesium dependent manner, pro-enzyme C2 binds C4b deposited on the cell surface (Figure 1.2A). Complex formation induces conformational changes such that C2 becomes susceptible to cleavage by either C1s or MASP-2. C2 cleavage by these proteases yields C2b (30 kDa) and C2a (70 kDa). C2b dissociates from the complex leaving behind the C3-convertase (C4b2a) of the classical/lectin pathway.

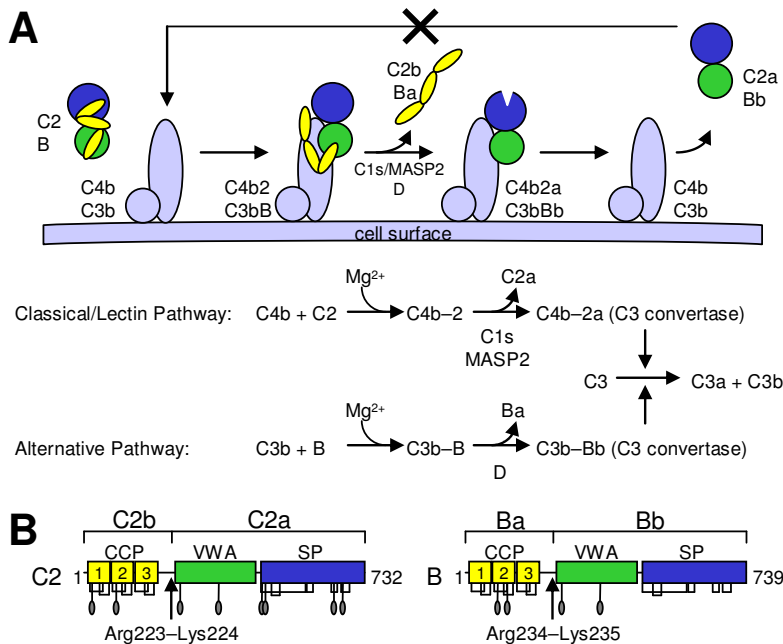


**Figure 1.2 Convertase formation and domain topology of C2 and factor B**  
**A)** Cartoon and schematic representation of C3 convertase formation. **B)** Schematic representation of C2 and factor B, indicated are the domains, N-linked glycans, and disulphide bridges.

The alternative pathway is continuously turned on at a low rate via the so-called “C3 tick-over”. This spontaneous hydrolysis of complement C3, which is homologous to C4, yields C3a (9 kDa) and C3b (177 kDa). C3a is an anaphylatoxin that mediates inflammatory responses whereas C3b may bind to nearby cell-surfaces forming a platform for factor B to bind. Factor B is homologous to C2 and is activated following association with C3b by serine protease factor D. This protease cleaves factor B into Ba, which dissociates from the complex, and Bb,

which remains bound to C3b forming the alternative pathway C3-convertase (C3bBb).

#### **Convertase dissociation**

The C3 convertases are intrinsically unstable and their dissociation is irreversible (Figure 1.2A). Once dissociated from their cofactors the proteases C2a and Bb almost completely lose their catalytic activity towards C3 (Fishelson and Muller-Eberhard 1984). The regulators of complement activation (factor H, DAF, CR1, C4BP, and MCP) enhance dissociation of the C3 convertase. As a result the complexes have a short half-life time in vivo, ~90 s and ~60 s at 37 °C for the classical/lectin and alternative pathway C3 convertases, respectively (Fishelson et al., 1984; Kerr and Parkes 1984).

## **4 The central proteases of the complement system**

#### **Enzymatic data C2 and factor B**

In the convertase setting activated C2 and factor B are highly specific serine proteases that cleave C3 and C5. Once dissociated from the convertase Bb retains 1% of its proteolytic activity in a hemolytic assay using factor B or factor D depleted normal human serum (Fishelson and Muller-Eberhard 1984). Isolated pro-enzymes C2 and factor B and fragments C2a and Bb all display significant reactivity towards small synthetic thioester substrates (Kam et al., 1987). Toward these substrates factor B is 10 times less reactive than Bb. No such difference is present in between C2 and C2a that both are as reactive as Bb. The four proteins are relative poor esterases since hydrolysis of the same substrates by trypsin is 3 orders of magnitude more efficient.

#### **Domain topology of factor B and C2**

The homologous pro-enzymes factor B and C2 are multi-domain plasma glycoproteins with a molecular weight of 92 and 100 kDa, respectively. The 5 domain proteins comprise three N-terminal Complement Control Protein domains (CCP) connected with a ~45 residue linker to a central von Willebrand factor type A domain (VWA), and a C-terminal Serine Protease (SP) domain (Figure 1.2B). Factor B and C2 consist of respectively 739 and 732 residues and display 39% identity in amino acid composition. The difference in molecular weight is due to the extent of glycosylation; C2 has 8 N-linked glycans (1 on CCP1 and CCP2, 2 on VWA, 4 on SP) whereas factor B has 4 (2 on CCP2 and 2 on VWA). During convertase formation C2 is cleaved in C2a and C2b. C2a, the larger of the two parts, comprises

the VWA and SP domains whereas C2b comprises the CCP domains and most of the linker. The a and b nomenclature is not consistent since the large and small factor B-cleavage products are called Bb and Ba, respectively.

CCP domains, also known as short consensus repeats (SCR) or Sushi domains, comprise ~60 residues and adopt a typical  $\beta$ -sandwich fold; a small and compact hydrophobic core enveloped by six  $\beta$ -strands and stabilized by two disulfide bridges. CCP domains are involved in many recognition processes. The VWA domain comprises ~200 residues and adopts the dinucleotide binding or Rossmann fold; a central mostly parallel  $\beta$ -sheet surrounded by amphiphathic  $\alpha$ -helices. The VWA domain is structurally homologous to integrin I domains in which the metal ion dependent adhesion site (MIDAS) conformation and position of the C-terminal  $\alpha 7$  helix determines ligand affinity (see paragraph 5). The SP domain accommodates the catalytic center of the C3 and C5 convertases and belongs to the family of proteins that adopt the chymotrypsin-like fold. This fold consists of two  $\beta$ -barrels surrounded by surface loops (see paragraph 6).

### **Interaction sites of factor B and C2**

During formation of the C3 convertases, pro-enzymes C2 and factor B associate with their cofactors via one  $Mg^{2+}$  independent and one  $Mg^{2+}$  dependent binding site. Because recombinant factor B – C2 chimeric proteins, in which complete or partial CCP domains are exchanged, display a reduced capacity to bind their cofactor (Hourcade et al., 1995; Xu and Volanakis 1997) and the reduced rate of C3 convertase formation (Pryzdial and Isenman 1987) in the presence of purified Ba, it is likely that a site of interaction is located within the three N-terminal CCP domains. Both effects are observed in the absence of divalent ions indicating this cofactor-binding site is the  $Mg^{2+}$  independent one. In analogy to integrin I domains, mutations in the MIDAS of C2 yields protein with a strongly reduced capacity to form the C3 convertase of the classical/lectin pathway (Horiuchi et al., 1991). These data indicate the MIDAS, located within VWA domain, is the  $Mg^{2+}$  dependent cofactor-binding site.

Regulators of complement activation interact with C3 convertases and enhance their dissociation. Point mutations in the VWA domain of factor B yields C3 convertases with reduced sensitivity to the regulatory proteins factor H, DAF and CR1 (Hourcade et al., 1999; Kuttner-Kondo et al., 2001; Hourcade et al., 2002). These data indicate the VWA domain, next to its role in cofactor binding, is involved in convertase dissociation.

## 5 Integrins

Integrins are a family of noncovalently associated heterodimers of  $\alpha$  and  $\beta$  subunits that mediate cell-cell and cell-extracellular matrix interactions. The  $\alpha$  and  $\beta$  subunits are composed of an extracellular, a transmembrane, and a cytoplasmic region. Together these transduce bidirectional signals between the cytoplasm and the extracellular matrix or other cells (Takagi et al., 2002). Outside-in signaling takes place in response to ligand binding to the extracellular domains whereas signals within the cell act on the cytoplasmic tail trigger inside-out signaling. Nineteen different integrin  $\alpha$ -subunits and eight different  $\beta$ -subunits have been reported. Which ligand the integrin binds mainly depends on the type of  $\alpha$  and  $\beta$  subunits.

### I domains

Nine of the  $\alpha$ -subunits contain an additional domain that is inserted in the extracellular region where it plays a central role in ligand binding (Shimaoka et al., 2002). This inserted (I) domain contains a metal ion dependent adhesion site (MIDAS) that coordinates a divalent ion, typically a  $Mg^{2+}$  ion, through five side chains; three located in loop  $\beta A\alpha 1$  forming the signature sequence  $DxSxS$ , a threonine in loop  $\alpha 3\alpha 4$ , and an aspartic acid in loop  $\beta D\alpha 5$ . Binding of a negatively charged residue from the ligand to the MIDAS triggers a change in metal coordination; the direct bond of the aspartate to the metal is replaced by a water-mediated bond, and the metal moves 2 Å towards the threonine, directly coordinating it (Figure 1.3A) (Emsley et al., 1997, 2000; Shimaoka et al., 2003).

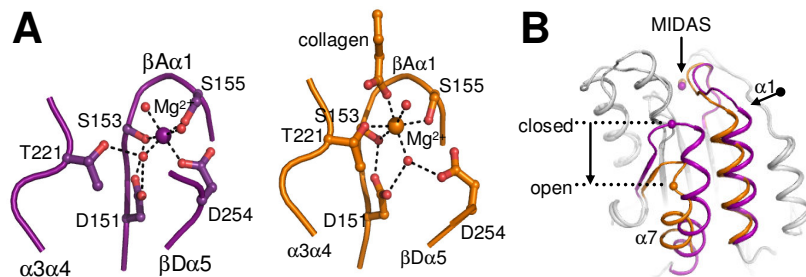


**Figure 1.3 Integrin I domain**

**A)** Metal ion dependent adhesion site of integrin  $\alpha_2\beta_1$ . The MIDAS residues (residue number and loop names are indicated), waters (small spheres), and  $Mg^{2+}$  ion (large sphere). Left panel – unliganded closed MIDAS (PDB 1aox), right panel – liganded open MIDAS (PDB 1dzi). **B)** Conformational changes of the I domain following ligand binding. I domain shown in ribbon representation, highlighted are the MIDAS, helix  $\alpha 1$  and the C-terminal helix  $\alpha 7$ .



The  $\beta A\alpha 1$  loop follows the movement of the metal in order to maintain its direct bonds via the two serines and thereby “pulls” helix  $\alpha 1$  towards the center of the I domain. These concerted movements squeeze out the C-terminal  $\alpha 7$  helix that moves 10 Å away from the ligand-binding surface (Figure 1.3B). This displacement of helix  $\alpha 7$  transduces the signal to other domains of the protein and is thought to convey the “outside-in” signaling to the intracellular part of the receptor. These two conformations are termed the “closed” unliganded state and the “open” liganded state. In the open state the metal ion is strongly electrophilic because its three coordinating residues (two serines and a threonine) lack a formal negative charge. This enables the metal ion to form a strong bond to the carboxylate moiety of an aspartate or glutamate residue of the ligand. Structure-based mutagenesis and biophysical studies of recombinant integrin I domains demonstrate the existence of a dynamic equilibrium between the two conformational states. For certain integrins, an intermediate state is observed which may be of physiological importance for precise regulation of ligand-binding affinity (Shimaoka et al., 2003; Jin et al., 2004).

### **Integrin conformational states**

The extracellular region of integrins comprises a globular headpiece connected to the transmembrane region by two long legs. Based on the bent conformation seen in the crystal structure of the integrin  $\alpha V\beta 3$  headpiece (Xiong et al., 2001) and the extended conformations seen in electron micrographs (Takagi et al., 2002) the switchblade-like extension model was proposed (for a review see Luo and Springer 2006). In this model the closed to open transition of the I domain, which is inserted in the headpiece, is coupled to separation of the integrin legs. The transmembrane and cytoplasmic regions follow the leg movements, transducing the outside-in signal. Likewise, inside-out signaling takes place by association of the transmembrane and cytoplasmic regions, which, via closure of the extracellular legs, stabilizes the I domain in the unliganded closed low-affinity state. These rearrangements of the extra- and intracellular domains underlie the bi-directional signaling across the membrane by integrins.

## **6 Serine proteases**

Serine proteases form a family of proteolytic enzymes that cleave peptide bonds in other proteins. In mammals, serine proteases perform many important functions, especially in digestion, blood clotting, and the complement system. The activity of these enzymes depends on a set of catalytic amino-acid residues; serine 195 (hence

the name “serine protease”), histidine 57 and aspartate 102. Together with the oxyanion hole these three residues form the catalytic center that is positioned at the interface of two six stranded anti-parallel  $\beta$ -barrels. This arrangement is referred to as the chymotrypsin-like fold (Figure 1.4A).

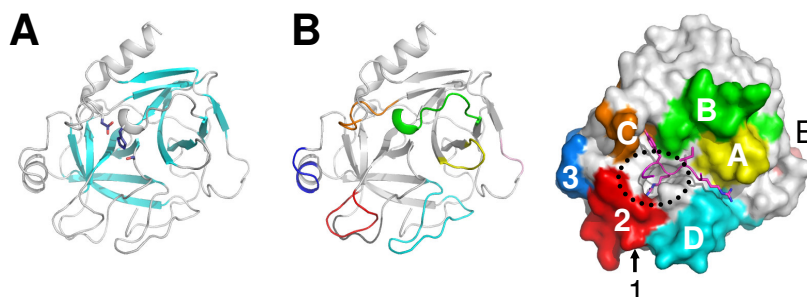


**Figure 1.4 Serine proteases; fold and substrate binding**

**A)** The chymotrypsin fold. The catalytic triad residues (dark blue) are positioned in between the two  $\beta$ -barrels (light blue). **B)** The 8 conserved substrate-binding loops surrounding the catalytic center shown in cartoon (left) and surface (right) representation (pdb 1aww). In the right panel a part of the soybean trypsin inhibitor is shown (purple), indicated are the P1-arginine (in sticks) that occupies the S1 pocket (dotted circle), and four adjacent residues interacting with the surface loops.

### Substrate specificity

The catalytic center of serine proteases is surrounded by eight conserved surface loops (Figure 1.4B); loops 1-3 and loops A-E (Perona and Craik 1997). The primary substrate-binding site, the S1-pocket, is formed by three  $\beta$ -strands connected via loops 1 and 2. This S1-pocket exactly positions the scissile peptide bond, between the P1 and P1' residue (Schechter and Berger 1968) for the nucleophilic attack by serine 195. Typically this pocket is complementary to the P1 residue, e.g. the deep and cylindrical S1 pocket of trypsin with an negatively charged aspartate (from loop 1) at its base specifically binds P1 arginines. To a large extent the nature of the S1-pocket determines the substrate specificity of serine proteases (Perona and Craik 1995). However, surface loops further away from the P1 residue are also important regarding specific interactions with substrate and form additional substrate-binding pockets for the residues positioned both N- and C-terminal from the scissile peptide (Figure 1.4B).

### Activation mechanism

To prevent unwanted protein degradation proteolytic enzymes are synthesized as inactive pro-enzymes, or “zymogens”. Chymotrypsin-like zymogens are characterized by an improperly formed oxyanion hole that cannot stabilize the negatively charged oxygen (i.e. the oxyanion) that arises during substrate conversion. A proteolytic cleavage in between residues 15 and 16 initiates zymogen activation (for a review see Khan and James 1998). The newly liberated  $\text{NH}_3^+$ -terminus (Ile-16) forms an ion-pair with the carboxylate side chain of aspartate 194 inducing conformational changes in and around the active site (Figure 1.5A); the backbone conformation of the loop (res. 190-194) preceding the catalytic serine (res. 195) moves from an “inwards” to an “outwards” orientation which results in the required maturation of the oxyanion hole (Figure 1.5B).

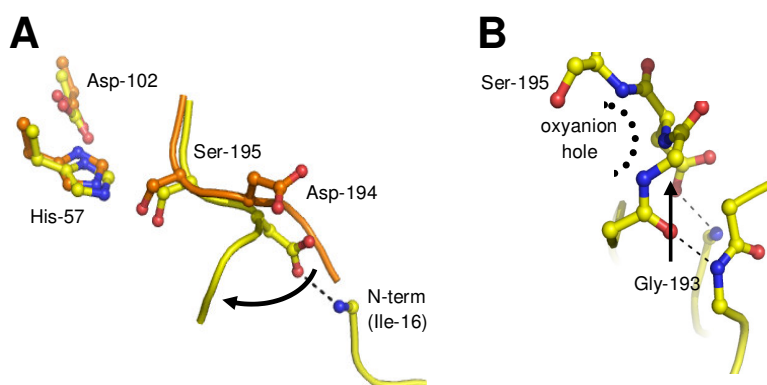


**Figure 1.5 The serine protease catalytic center**

**A)** Overlay of the catalytic center of chymotrypsinogen (orange; PDB 2cga) and chymotrypsin (yellow; 4cha). Shown in sticks are the catalytic triad (His-57, Asp-102, and Ser-195) and the Asp-194 interaction with the liberated N-terminus in the activate protease. **B)** The amides of the catalytic serine and glycine 193 pointing inwards form the oxyanionhole.

In some cases, activation of chymotrypsin-like zymogens requires specific protein-protein interactions such as enzyme-cofactor association, enzyme self-assembly, and enzyme-substrate interactions. The blood clotting (coagulation pathway) and the complement system are rich in such regulated serine proteases. Their pattern of sequential activation allows regulation on multiple levels.

## 7 Techniques used

The three-dimensional structures of proteins are a valuable tool in studying the function of and the interaction in between proteins. Protein crystallography, nuclear magnetic resonance spectroscopy (NMR) and electron microscopy (EM) are the main methods developed to determine the structure of macromolecules. Both protein crystallography and NMR may yield protein structures at an atomic level, whereas EM is mostly used to determining the overall shapes of proteins and large protein assemblies. In contrast to NMR that is limited to smaller proteins, protein crystallography can also be used to determine the structures of larger proteins.

The method of choice in this thesis is protein crystallography. This technique requires relatively large quantities of pure protein, which in most cases, are difficult or practically unfeasible to isolate in sufficient amounts from the host. This bottleneck in the structural biology is circumvented by the introduction of recombinant protein expression, a technique in which the transcription and translation machinery of an expression host is utilized to produce protein of interest.

### 7.1 Protein Crystallography

Crystallographic determination of protein structures involves several steps: (i) crystallization of the protein, (ii) measurement of diffraction data, (iii) determination of the phases, and (iv) building the protein model in the electron density.

#### Crystallization of proteins

A protein crystal is formed when a large number of protein molecules are aligned in a repeating series of “unit cells”. The most common used method to crystallize a protein is the hanging-drop vapor diffusion method. Typically a 1  $\mu$ l drop of a highly pure protein sample is mixed with an equal volume of precipitant solution containing buffer and precipitant, and is sealed above a reservoir containing a similar precipitant solution. Due to this set-up the precipitant concentration in the reservoir is twice as high as in the drop containing the protein. During the experiment the system will equilibrate; water transfers from the protein drop to the reservoir until the precipitant concentration is the same in both solutions. As such, the precipitant concentration in the drop gradually increases and the protein may precipitate in an ordered way, forming a crystal (Figure 1.6).

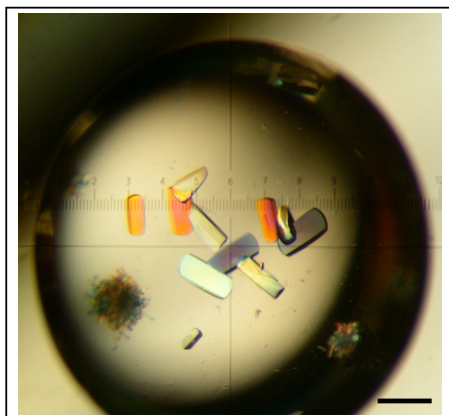


**Figure 1.6 SCIN crystals**

A drop containing SCIN crystals. Both clusters of small crystals and larger single crystals are present. Due to their birefringence, protein crystals are highlighted in different colors using polarized light. The bar indicates 100  $\mu\text{m}$ .

A priori it is impossible to predict the condition under which the protein will crystallize. Therefore many different combinations of protein concentration, precipitant solution, and temperature need to be tested.

### **Diffraction**

The electrons in a protein crystal scatter an incident X-ray beam. Because of the periodic lattice, a crystal can be described as composed of thousands of equivalent and parallel planes of atoms. The reflected X-ray waves will remain in phase if the difference in path length of each wave is equal to an integer multiple of the wavelength. This principle is described by Bragg's law:  $2d\sin\theta=n\lambda$ , where  $n$  is an integer,  $\lambda$  is the wavelength of the X-rays,  $d$  is the spacing between the planes in the atomic lattice, and  $\theta$  is the angle between the incident ray and the scattering planes. Thus, only at certain  $\theta$  angles the waves are successfully added up and reflection occurs. The enhanced waves form a distinct pattern of spots with different intensities and can be measured with a detector. The diffraction pattern is determined by the unit-cell parameters of the crystal (axes  $a$ ,  $b$ , and  $c$ , and angles  $\alpha$ ,  $\beta$ , and  $\gamma$ ), whereas the intensity of the spots depends on the distribution of the electrons in the unit cell.

### **Phasing**

The structure factor ( $F_{hkl}$ ) is a summation of all atomic scattering factors and thus describes how the incident X-rays are scattered by the crystal. The Fourier transform of the structure factors results in the three-dimensional distribution of the electron density. To calculate this Fourier transform, both the amplitude and

the phase of the diffracted waves are needed. The amplitudes of the waves are related to the intensity of the spots in the diffraction pattern. The phase, however, cannot be measured directly. This problem is referred to as the phase problem. In this thesis two different methods have been used to solve this problem: Molecular Replacement (MR) and Multiple wavelength Anomalous Dispersion (MAD).

With MR, the structure of a homologous protein (>40% amino acid identity) is used to calculate initial phase estimates. The idea is to find the rotation (three parameters) and translation (also three parameters) which position the model structure in the unit cell that gives the highest correlation between experimental diffraction measurements and those calculated from the model.

MAD phasing makes use of the changes in scattering power of heavy atoms near their absorption edge. The anomalous scattering heavy atoms cause two reflections that are normally equal to each other (i.e. Friedel pairs), to be slightly different. This difference is used to determine the position of the heavy atom and thus the initial phases. The anomalous scatterers may be naturally present in the protein or may be introduced by replacing methionine with seleno-methionine when producing the protein, or by soaking crystals in solutions containing heavy atoms.

### Atomic model

The final step in determining the three-dimensional structure of a protein crystal is to "fit" amino acids in the electron density map. Initially the electron density maps are of low quality due to errors in the determination of the phase. In an iterative process of rebuilding and recalculating the electron density map the protein model is improved (Figure 1.7).

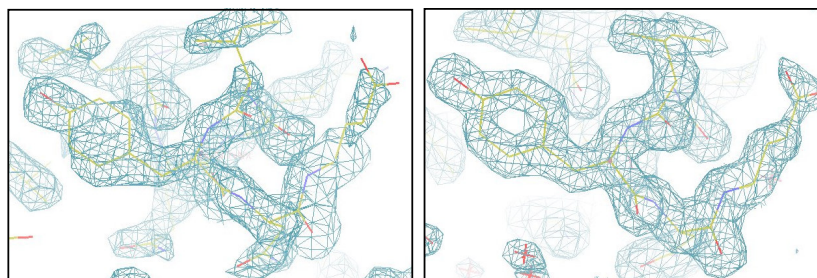


**Figure 1.7 Electron density**

A 1.8 Å resolution electron density map ( $1.4 \sigma$ ) before (left) and after (right) refinement of the model.

The residual between the protein model and the experimental data is expressed in the R-factor. This factor will decrease during successful cycles of refinement. To prevent over-fitting of the data, the quality of the model is validated by the so-called free R-factor, which is the R-factor of a set of reflections (5%) that was not used for refinement. Additionally, the geometry of the final protein model is compared with the geometry of very accurately determined protein structures.

## 7.2 Recombinant protein expression

Expression of eukaryotic proteins, e.g. complement proteins, in prokaryotic systems generally is not successful due to the lack of post-translational modification, limited disulfide-bond formation and the absence of various chaperones. To overcome these problems several eukaryotic expression systems have been developed, which can be categorized in three main groups i) yeast, ii) insect cells, and iii) mammalian cells (for a review see Aricescu et al. 2006). Mammalian expression is particularly successful for the production of secreted proteins such as many of the complement proteins. However, recombinant expression of proteins using mammalian cells is an expensive methodology that requires significant expertise in tissue culturing.

### Mammalian expression

The two mammalian expression systems used in this thesis are stable expression in Baby Hamster Kidney (BHK) cells and transient expression in Human Embryonic Kidney (HEK) cells.

BHK cells are cultured adherently in polystyrene flasks. Typically the expression vector is incorporated in the host genome following transfection (hence the name “stable expression”). Due to the presence of a selection marker in the culturing medium, cells that have not successfully incorporated the vector will die whereas positive cells survive and form colonies. The position in the genome at which the vector is incorporated is related to the level of protein expressed. Because the incorporation is random, the expression level of multiple colonies (10-20) is monitored. The highest expressor is selected for up scaling. The sequential steps of transfection, selection, and up scaling typically take one to two months. This time consuming property is the major drawback of stable expression in BHK cells.

HEK cells are grown in suspension. Since the expression vector is not incorporated in the host genome following transfection the expression is called transient. Clone selection is not needed due to efficient transfection methods (75% of positives). To ensure sufficient amounts of plasmid during the days following transfection genetic variants have been developed that express the Epstein-Barr virus nuclear

antigen 1 (EBNA1)(Durocher et al., 2002). These HEK cells allow episomal amplification of plasmids containing the viral EBV origins of amplification throughout the entire production phase. In contrast to the elaborate expression in BHK cells, the complete HEK expression experiment is finished within two weeks.

## 8 Scope of this thesis

The complement system plays a crucial role in mammalian immune defense. Activation of complement elicits a wide range of effector functions such as inflammatory responses, lysis, phagocytosis, and B-cell stimulation. However, activation of complement to an inappropriate extent is associated with various acute and chronic inflammatory diseases and is implicated in several autoimmune disorders. The three pathways activating complement all converge to the formation of active protease complexes (convertases) on the surface of invading pathogens or altered host cells. How the convertases are formed, activated and regulated is unclear. This thesis describes research performed on the proteins that provide the proteolytic activity to these complexes (factor B and C2) and addresses questions like; what is the role of their CCP domains, does their VWA domain act like integrin I domains, and how is the activity of the SP domain regulated. Additionally a protein secreted by the pathogen *S. aureus* that inhibits convertase activity is structurally and functionally characterized.

**Chapter 2** describes the crystal structure of recombinant human complement component C2a that harbors the catalytic center of the classical and lectin-binding activation pathways convertases. The C-terminal serine protease domain displays a near active catalytic center surrounded by substrate binding loops, which differ significantly from observed in trypsin. The N-terminal von Willebrand factor A (VWA) domain which contains the major ligand binding site, adopts an intermediate conformation that was previously only observed in engineered I domains.

Prior to activation C2a and its alternative pathway homologue Bb circulate in the blood stream as pro-enzymes C2 and factor B, respectively. In **Chapter 3** the structure of recombinant human factor B is described. The structure reveals how the five-domain protein factor B is kept inactive. The data derived from the factor B structure provide a basis for an allosteric activation model in which the VWA domain, that adopts a previously unknown “locked” conformation, plays a central role. This allosteric mechanism is crucial for the tight regulation of the complement-amplification step in the immune response.



The human pathogen *Staphylococcus aureus* blocks host defense mainly via secretion of small proteins that inhibit several steps of the immune response. **Chapter 4** describes the crystal structure and the identification of active sites of one of these molecules, the Staphylococcal Complement Inhibitor (SCIN), that inhibits convertase activity. These data provide insight in the modulation of convertase activity by SCIN and form a basis for the development of non-immunogenic complement inhibitors.

The obtained insights into the molecular mechanisms underlying convertase formation, activation and regulation described in this thesis, are summarized and discussed in **Chapter 5**.

## References

- Aricescu, A.R., Assenberg, R., Bill, R.M., Busso, D., Chang, V.T., Davis, S.J., Dubrovsky, A., Gustafsson L., Hedfalk, K., Heinemann, U., Jones, I.M., Ksiazek, D., Lang, C., Maskos, K., Messerschmidt, A., Macieira, S., Peleg, Y., Perrakis, A., Poterszman, A., Schneider, G., Sixma, T.K., Sussman, J.L., Sutton, G., Tarboureich, N., Zeev-Ben-Mordehai, T., and Jones, E.Y. (2006). Eukaryotic expression: developments for structural proteomics. *Acta Crystallogr. D Biol. Crystallogr.* *62*, 1114-1124.
- Donaldson, V.H. and Evans, R.R. (1963). A Biochemical Abnormality in Hereditary Angioneurotic Edema: Absence of Serum Inhibitor of C' 1-Esterase. *Am. J. Med.* *35*, 37-44.
- Durocher, Y., Perret, S., and Kamen, A. (2002). High-level and high-throughput recombinant protein production by transient transfection of suspension-growing human 293-EBNA1 cells. *Nucleic Acids Res.* *30*, E9.
- Edwards, A.O., Ritter, R. 3rd, Abel, K.J., Manning, A., Panhuysen, C., and Farrer, L.A. (2005). Complement factor H polymorphism and age-related macular degeneration. *Science* *308*, 421-424.
- Emsley, J., King, S.L., Bergelson, J.M., and Liddington, R.C. (1997). Crystal structure of the I domain from integrin alpha2beta1. *J. Biol. Chem.* *272*, 28512-28517.
- Emsley, J., Knight, C.G., Farndale, R.W., Barnes, M.J., and Liddington, R.C. (2000). Structural basis of collagen recognition by integrin alpha2beta1. *Cell* *101*, 47-56.
- Fishelson, Z. and Muller-Eberhard, H. J. (1984). Residual hemolytic and proteolytic activity expressed by Bb after decay-dissociation of C3b,Bb. *J. Immunol.* *132*, 1425-1429.
- Fishelson, Z., Pangburn, M.K., and Muller-Eberhard, H.J. (1984). Characterization of the initial C3 convertase of the alternative pathway of human complement. *J. Immunol.* *132*, 1430-1434.
- Goicoechea de Jorge, E., Harris, C.L., Esparza-Gordillo, J., Carreras, L., Arranz, E.A., Garrido, C.A., Lopez-Trascasa, M., Sanchez-Corral, P., Morgan, B.P., and Rodriguez de Cordoba, S. (2007). Gain-of-function mutations in complement factor B are associated with atypical hemolytic uremic syndrome. *Proc. Natl. Acad. Sci. U S A* *104*, 240-245.
- Gold, B., Merriam, J.E., Zernant, J., Hancox, L.S., Taiber, A.J., Gehrs, K., Cramer, K., Neel, J., Bergeron, J., Barile, G.R., Smith, R.T.; AMD Genetics Clinical Study Group, Hageman, G.S., Dean, M., and Allikmets, R. (2006). Variation in factor B (BF) and complement component 2 (C2) genes is associated with age-related macular degeneration. *Nat. Genet.* *38*, 458-462.
- Haines, J.L., Hauser, M.A., Schmidt, S., Scott, W.K., Olson, L.M., Gallins, P., Spencer, K.L., Kwan, S.Y., Noureddine, M., Gilbert, J.R., Schnetz-Boutaud, N., Agarwal, A., Postel, E.A., and Pericak-

- Vance, M.A. (2005). Complement factor H variant increases the risk of age-related macular degeneration. *Science* 308, 419-421.
- Horiuchi, T., Macon, K.J., Engler, J.A., and Volanakis, J.E. (1991). Site-directed mutagenesis of the region around Cys-241 of complement component C2. Evidence for a C4b binding site. *J. Immunol.* 147, 584-589.
- Hourcade, D.E., Mitchell, L., Kuttner-Kondo, L.A., Atkinson, J.P., and Medof, M.E. (2002). Decay-accelerating factor (DAF), complement receptor 1 (CR1), and factor H dissociate the complement AP C3 convertase (C3bBb) via sites on the type A domain of Bb. *J. Biol. Chem.* 277, 1107-1112.
- Hourcade, D.E., Mitchell, L.M., and Oglesby, T.J. (1999). Mutations of the type A domain of complement factor B that promote high-affinity C3b-binding. *J. Immunol.* 162, 2906-2911.
- Hourcade, D.E., Wagner, L.M., and Oglesby, T.J. (1995). Analysis of the short consensus repeats of human complement factor B by site-directed mutagenesis. *J. Biol. Chem.* 270, 19716-19722.
- Janssen, B.J., Christodoulidou, A., McCarthy, A., Lambris, J.D., and Gros, P. (2006). Structure of C3b reveals conformational changes that underlie complement activity. *Nature* 444, 213-216.
- Jin, M., Andricioaei, I., and Springer, T.A. (2004). Conversion between three conformational states of integrin I domains with a C-terminal pull spring studied with molecular dynamics. *Structure* 12, 2137-2147.
- Johnson, C.A., Densen, P., Wetsel, R.A., Cole, F.S., Goeken, N.E., and Colten, H. R. (1992). Molecular heterogeneity of C2 deficiency. *N. Engl. J. Med.* 326, 871-874.
- Kam, C.M., McRae, B.J., Harper, J.W., Niemann, M.A., Volanakis, J.E., and Powers, J.C. (1987). Human complement proteins D, C2, and B. Active site mapping with peptide thioester substrates. *J. Biol. Chem.* 262, 3444-3451.
- Kerr, M.A. and Parkes, C. (1984). The effects of iodine and thiol-blocking reagents on complement component C2 and on the assembly of the classical-pathway C3 convertase. *Biochem. J.* 219, 391-399.
- Khan, A.R. and James, M.N. (1998). Molecular mechanisms for the conversion of zymogens to active proteolytic enzymes. *Protein Sci.* 7, 815-836.
- Kirkitadze, M.D. and Barlow, P.N. (2001). Structure and flexibility of the multiple domain proteins that regulate complement activation. *Immunol. Rev.* 180, 146-161.
- Kuttner-Kondo, L.A., Mitchell, L., Hourcade, D.E., and Medof, M.E. (2001). Characterization of the active sites in decay-accelerating factor. *J. Immunol.* 167, 2164-2171.
- Lindahl, G., Sjobring, U., and Johnsson, E. (2000). Human complement regulators: a major target for pathogenic microorganisms. *Curr. Opin. Immunol.* 12, 44-51.
- Luo, B.H. and Springer, T.A. (2006). Integrin structures and conformational signaling. *Curr. Opin. Cell. Biol.* 18, 579-586.
- Perona, J.J. and Craik, C.S. (1995). Structural basis of substrate specificity in the serine proteases. *Protein Sci.* 4, 337-360.
- Perona, J.J. and Craik, C.S. (1997). Evolutionary divergence of substrate specificity within the chymotrypsin-like serine protease fold. *J. Biol. Chem.* 272, 29987-29990.
- Pichette, V., Quérin, S., Schürch, W., Brun, G., Lehner-Netsch, G., and Delâge, J.M. (1994). Familial hemolytic-uremic syndrome and homozygous factor H deficiency. *Am. J. Kidney. Dis.* 24, 936-941.
- Pryzdial, E.L. and Isenman, D.E. (1987). Alternative complement pathway activation fragment Ba binds to C3b. Evidence that formation of the factor B-C3b complex involves two discrete points of contact. *J. Biol. Chem.* 262, 1519-1525.
- Rawal, N. and Pangburn, M.K. (2001). Structure/function of C5 convertases of complement. *Int. Immunopharmacol.* 1, 415-422.

- Rooijackers, S.H.M., Ruyken, M., Roos, A., Daha, M.R., Presanis, J.S., Sim, R.B., van Wamel, W.J., van Kessel, K.P., and van Strijp, J.A. (2005). Immune evasion by a staphylococcal complement inhibitor that acts on C3 convertases. *Nat. Immunol.* 6, 920-927.
- Schechter, I. and Berger, A. (1968). On the active site of proteases. 3. Mapping the active site of papain; specific peptide inhibitors of papain. *Biochem. Biophys. Res. Commun.* 32, 898-902.
- Serraino, D., Piselli, P., Angeletti, C., Scuderi, M., Ippolito, G., and Capobianchi, M.R. (2005). Infection with Epstein-Barr virus and cancer: an epidemiological review. *J. Biol. Regul. Homeost. Agents* 19, 63-70.
- Shimaoka, M., Takagi, J., and Springer, T.A. (2002). Conformational regulation of integrin structure and function. *Annu. Rev. Biophys. Biomol. Struct.* 31, 485-516.
- Shimaoka, M., Xiao, T., Liu, J.H., Yang, Y., Dong, Y., Jun, C.D., McCormack, A., Zhang, R., Joachimiak, A., Takagi, J., Wang, J.H., and Springer, T.A. (2003). Structures of the alpha L I domain and its complex with ICAM-1 reveal a shape-shifting pathway for integrin regulation. *Cell* 112, 99-111.
- Takagi J, Petre B.M., Walz, T., and Springer, T.A. (2002). Global conformational rearrangements in integrin extracellular domains in outside-in and inside-out signaling. *Cell* 110, 599-511.
- Thern, A., Stenberg, L., Dahlbäck, B., and Lindahl, G. (1995). Ig-binding surface proteins of *Streptococcus pyogenes* also bind human C4b-binding protein (C4BP), a regulatory component of the complement system. *J. Immunol.* 154, 375-386.
- Walport, M. J. (2001a). Complement. First of two parts. *N. Engl. J. Med.* 344, 1058-1066.
- Walport, M. J. (2001b). Complement. Second of two parts. *N. Engl. J. Med.* 344, 1140-1144.
- Wiesmann, C., Katschke, K.J., Yin, J., Helmy, K.Y., Steffek, M., Fairbrother, W.J., McCallum, S.A., Embuscado, L., DeForge, L., Hass, P.E., and van Lookeren Campagne, M. (2006). Structure of C3b in complex with CRIg gives insights into regulation of complement activation. *Nature* 444, 217-220.
- Wurzner, R. (1999). Evasion of pathogens by avoiding recognition or eradication by complement, in part via molecular mimicry. *Mol. Immunol.* 36, 249-260.
- Xiong, J.P., Stehle, T., Diefenbach, B., Zhang, R., Dunker, R., Scott, D.L., Joachimiak, A., Goodman, S.L., and Arnaout, M.A. (2001). Crystal structure of the extracellular segment of integrin alpha Vbeta3. *Science* 294, 339-345.
- Xu, Y., Narayana, S.V., and Volanakis, J.E. (2001). Structural biology of the alternative pathway convertase. *Immunol. Rev.* 180, 123-135.
- Xu, Y. and Volanakis, J. E. (1997). Contribution of the complement control protein modules of C2 in C4b binding assessed by analysis of C2/factor B chimeras. *J. Immunol.* 158, 5958-5965.



# 2

## Structure of complement component C2a: implications for convertase formation and substrate binding

Fin J. Milder<sup>1</sup>, Hans C.A. Raaijmakers<sup>1,†</sup>, Mitja D.A.A. Vandeputte<sup>1,\*</sup>, Arie Schouten<sup>1</sup>, Eric G. Huizinga<sup>1</sup>, Roland A. Romijn<sup>2</sup>, Wieger Hemrika<sup>2</sup>, Anja Roos<sup>3</sup>, Mohamed R. Daha<sup>3</sup> and Piet Gros<sup>1</sup>

<sup>1</sup>Crystal and Structural Chemistry, Bijvoet Center for Biomolecular Research, Faculty of Science, Utrecht University, Padualaan 8, 3584 CH Utrecht, The Netherlands. <sup>2</sup>ABC Expression Center, Utrecht University, 3584 CH Utrecht, The Netherlands <sup>3</sup>Dept of Nephrology, Leiden University Medical Center, 2300 RC Leiden, The Netherlands <sup>†</sup>Present address: N.V. Organon, Molecular Design & Informatics, Molenstraat 110, 5342 CC Oss, The Netherlands <sup>\*</sup>Present address: Department of Neuroscience, Erasmus Medical Center, 3000 DR, Rotterdam, The Netherlands

Structure, 14, 1587-1597 (2006)

## Abstract

C2a provides the catalytic center to the convertase complexes of the classical and lectin-binding pathways of complement activation. We determined two crystal structures of full-length C2a, with and without a pseudo-ligand bound. Both structures reveal a near-active conformation of the catalytic center of the serine protease domains, while the von Willebrand factor A-type domains display an intermediate activation state of helix  $\alpha 7$  with an open, activated metal-ion dependent adhesion site. The open adhesion site likely serves to enhance the affinity for the ligand C4b, similar to “inside-out” signaling in integrins. Surprisingly, the N-terminal residues of C2a are buried in a crevice near helix  $\alpha 7$ , indicative of a structural switch between C2 and C2a. Extended loops on the protease domain possibly envelop the protruding anaphylatoxin domain of the substrate C3. Together with a putative substrate-induced completion of the oxyanion hole, this may contribute to the high substrate specificity of the convertases.

## Introduction

The complement system plays a crucial role in mammalian immune defense (for a review see e.g. Walport 2001a, 2001b). It consists of over 30 fluid phase and cell-surface proteins that recognize and kill invading pathogens, present them to the adaptive immune system and elicit inflammatory responses. Three pathways activate the complement system: the classical, the lectin and the alternative pathway. Complement protein C2 is critical to the classical and lectin pathways by providing the proteolytic center to their C3 and C5 convertases, which proteolytically activate C3 and C5 enabling amplification of the complement response, stimulation of inflammatory responses, opsonization of pathogenic particles and initiation of the terminal membrane-attack phase of complement.

Human C2 (732 amino-acid residues, MW of 100 kDa) is produced as an inactive, heavily glycosylated zymogen consisting of five domains: three N-terminal complement-control-protein (CCP) domains, a Von Willebrand factor A-type (VWA) domain and a C-terminal trypsin-like serine proteinase (SP) domain (Bentley, 1986); see Figure 2.1A. The last two domains, VWA and SP, form the C2a fragment (residues 224-732, 70 kDa) that is produced in the proteolytic activation cascade of the classical and lectin pathways. Activation starts by binding of the

zymogen C2 in a magnesium-dependent manner to activated pathogen-bound complement component C4b (193 kDa). Proteolysis at Arg-223 – Lys-224, by either C1s of the classical pathway or MASP2 of the lectin pathway, yields a complex of C4b and C2a. This complex is referred to as C4b2a and is the active C3 convertase of the classical and lectin pathways. The C3 convertase is unstable and dissociates with a half-life time of 60 seconds (Kerr, 1980). Once dissociated C2a loses proteolytic activity and cannot re-associate with C4b (Kerr and Parkes 1984). C2 and C2a are homologous to factor B and its fragment Bb of the alternative pathway (39% sequence identity between full-length proteins as well as protein fragments). Factor B associates with complement component C3b and after proteolysis yields the C3 convertase of the alternative pathway, C3bBb, which has a half-life time of 90 seconds (Pangburn and Muller-Eberhard 1986). The C3 convertases, C4b2a and C3bBb, cleave C3 into the anaphylatoxin C3a and C3b. Attachment of C3b to either C4b2a or C3bBb yields the C5 convertases, C4b2a3b and C3bBb, respectively, that cleave complement component C5 (reviewed by Rawal and Pangburn 2001).

C2 and factor B differ from chymotrypsinogens and trypsinogens in their mechanism of activation. In chymotrypsinogens and trypsinogens cleavage in the N-terminus generates a new N-terminus (Ile-16 in trypsin) that induces formation of the oxyanion hole (Bode, 1979; Khan and James 1998). In C2 and factor B, instead, proteolysis occurs between the third CCP and the VWA domain, leaving the VWA domain attached to the N-terminus of the SP domain after activation; and, thus no new N-terminus in the SP domain is provided that may induce oxyanion hole formation. The VWA domain is homologous to integrin-inserted (I) domains and contains a metal-ion dependent adhesion site (MIDAS) motif. Amino-acid residue mutations in the MIDAS motif abolish hemolytic activity (Horiuchi et al., 1991), indicating a critical role for the MIDAS motif in convertase formation, stability or activity. It was hypothesized that the VWA domain might play an activating role via a conformational change similar to that observed in I domains of integrins in outside-in signaling (Bhattacharya et al., 2004), where ligand binding at the MIDAS site induces a  $\sim 10$  Å movement of the C-terminal  $\alpha 7$  helix (Emsley et al., 1997; 2000). In analogy to disulphide-bridge engineered I domains, Ponnuraj *et al.* (Ponnuraj et al., 2004) made a Bb disulphide mutant (Cys-428 – Cys-435) enforcing the VWA domain in an artificial active conformation in the absence of ligand C3b. The structure of this engineered Bb, which also was truncated at the N-terminus by 7 residues, showed that the SP domain displays an active conformation of the catalytic Asp-His-Ser triad and a near-active conformation of the oxyanion hole, i.e. the loop 670-674 adopts a conformation similar to mature chymotrypsins and trypsin except that peptide bond 671-672 is flipped by  $\sim 180^\circ$

(Ponnuraj et al., 2004). In this conformation the negative charge of the oxyanion intermediate cannot be stabilized. The structure of Bb covalently inhibited by diisopropyl phosphate has this peptide plane in the active orientation, indicating that a fully active site may be induced by substrate binding (Ponnuraj et al., 2004). The role of VWA, however, in the molecular mechanisms of convertase formation, stability or activity remains unclear.

We have expressed human C2 and C2a in mammalian cells, crystallized C2a, and tested C2 and two C2 glycan-deletion mutants in hemolytic assays. Here we present crystal structures of native, glycosylated C2a, one unliganded and one with a pseudo ligand bound to the VWA domain. The N-terminal residues, absent in the truncated Bb fragment (Ponnuraj et al., 2004), play an important structural role. They interact with the C-terminal tail of VWA and partake in the VWA-SP interface. Comparison of the SP domains of C2a and Bb indicates a distinct binding groove for the scissile loop of C3. Placing the C3 structure (Janssen et al., 2005) onto the SP domains indicates putative interaction sites in the proteinase-substrate complex.

## Results and discussion

### Expression, purification and activity of recombinant C2, C2a and C2 mutants

Human C2a (residues 224-732) with an N-terminal His<sub>6</sub>-tag was stably expressed in baby-hamster kidney (BHK) cells. Stable BHK-cell lines secreted 10-15 mg C2a per liter medium. Purification yielded 10 mg C2a per liter medium. Purified C2a runs as a single band on SDS-PAGE at 70 kDa. The observed molecular weight is in agreement with the extent (10-15 w/w %) of glycosylation observed in human plasma (Tomana et al., 1985). Human C2 (residues 1-732) and two C2 single glycan-deletion mutants (N447D and N451D) and one C2 double glycan-deletion mutant (N447D/N451D) were transiently expressed in human embryonic kidney (HEK293E) cells. Native and mutant C2 gave comparable expression levels of 15-20 mg protein per liter medium. The harvested media from BHK and HEK293E cells were tested for complement activity in a hemolytic assay using sensitized sheep erythrocytes. Recombinant C2 in medium showed a hemolytic activity (normalized for concentration) that was comparable ( $98 \pm 31\%$ ) to native C2 in normal human serum. No hemolytic activity for the harvested C2a-containing medium was observed. This is in agreement with the observation that C2, and not C2a, associates with C4b to form an active convertase (Kerr, 1980).



### Structure determinations

Crystals of C2a were obtained by the hanging-drop vapor diffusion method. C2a was crystallized with 35% w/v polyethylene glycol 1000 (PEG-1000) and 0.1 M malonate-imidazol boric acid buffer (MIB-buffer) at pH 7.0. One crystal was grown in the presence of 20 mM LiCl and diffracted to a resolution of 2.7 Å. A second crystal was grown in the presence of 3% w/v xylitol. We soaked this crystal in a solution containing 10 mM MnCl<sub>2</sub>. This crystal diffracted to a resolution of 2.1 Å. We refer to the two diffraction data sets and structures as C2a-Li<sup>+</sup> (C2a in the presence of LiCl) and C2a-Mn<sup>2+</sup> (C2a soaked in MnCl<sub>2</sub>), respectively. Data collection and processing statistics for both crystals are given in Table 2.1.

**Table 2.1 Crystallographic data collection and refinement statistics.**

	Data collection statistics	
	C2a-Li <sup>+</sup>	C2a-Mn <sup>2+</sup>
Space group	<i>P</i> 2 <sub>1</sub>	<i>P</i> 2 <sub>1</sub>
Cell dimensions	a = 51.16 Å b = 75.08 c = 71.56 β = 110.32°	a = 51.48 Å b = 77.19 c = 70.86 β = 109.55°
Resolution (Å)	37.5-2.7	50.5-2.1
Completeness (%)	98.5	89.9
Multiplicity	3.6 (3.2)	3.6 (2.9)
R <sub>merge</sub> (%)	8.5 (42)	6.1 (52)
I/σI	13.7 (2.4)	15.1 (1.9)
	Refinement statistics	
# reflections (work/test)	13177/690	26081/1389
R/R <sub>free</sub> (%)	21.2/28.7	18.9/24.0
B-factor (Å <sup>2</sup> )	32.1	22.5
RMSD bond length (Å)	0.004	0.003
RMSD bond angle (°)	0.674	0.862
# protein atoms	3928	3994
# glycan atoms	144	91
# water molecules	38	133
# ions	-	1 (Mn <sup>2+</sup> )
# ligand atoms	-	7 (malonate)

Values between parentheses refer to a high-resolution shell.

First, we determined the structure of C2a-Li<sup>+</sup>. For molecular replacement we used the structures of the isolated VWA (protein databank entry 1q0p) and SP (1dle) domains of factor B as search models (Jing et al., 2000; Bhattacharya et al., 2004). The structures of Bb (Ponnuraj et al., 2004) containing both the VWA and the SP domain were not made available at that moment. A clear and correct solution in molecular replacement was obtained when using the program Phaser (Storoni et al., 2004). The model was rebuilt using the graphics program O (Jones et al., 1991) and refined using programs CNS (Brunger et al., 1998) and REFMAC (CCP4 1994; Murchudov et al., 1997). Electron density allowed modeling of the vector-derived N-terminal Ser, C2a residues 224-732 (except for residues 395-397, 408-413, and 691-694), partial glycans at Asn-270, Asn-313, Asn-447, Asn-451 and Asn-601; and 38 water molecules. No additional density was observed at the putative glycosylation site Asn-631. The final model had R and R<sub>free</sub>-factor of 21.2 and 28.7 % respectively, and displayed good stereochemistry. Statistics on the model quality are given in Table 2.1.

Second, we determined the structure of C2a soaked in MnCl<sub>2</sub> (C2a-Mn<sup>2+</sup>) by molecular replacement using the structure of C2a-Li<sup>+</sup>. The complete model of C2a-Li<sup>+</sup> was placed in the unit cell and the position of the domains optimized by rigid-body refinement using Phaser. Model building and refinement yielded a final model consisting of the vector derived Ser residue, C2a residues 224-732 except loop 687-693, partial glycans at Asn-313, Asn-447 and Asn-601; and 133 water molecules. Even though the C2a-Mn<sup>2+</sup> crystal diffracted to higher resolution than C2a-Li<sup>+</sup>, less electron-density was visible at the glycosylation sites. Final model had an R and R<sub>free</sub> of 18.9 and 24.0 % and good stereochemistry (see Table 2.1). An example of electron density is shown in Figure 2.1B.

The model of C2a-Mn<sup>2+</sup> was used to finalize the modeling of C2a-Li<sup>+</sup>. In the original C2a-Li<sup>+</sup> model VWA-helix  $\alpha_6$  (residues 398-407) was missing. Density at 0.5- $\sigma$  contour level correlated very well with the superimposed C2a-Mn<sup>2+</sup> structure in this region; therefore this helix was included in the model. As a consequence, the R and R<sub>free</sub>-factor dropped from 21.7/29.1 to 21.2/28.7 %. Continuous electron density was visible throughout the  $\alpha_6$  helix at 0.8  $\sigma$  and for the main chain of residues 401-406 at 1- $\sigma$  contour level. The final position of the helix in C2a-Li<sup>+</sup> model is very similar to that in C2a-Mn<sup>2+</sup>. SP-loop 687-694 is most likely disordered in both crystals. For C2a-Li<sup>+</sup> 4 residues and for C2a-Mn<sup>2+</sup> 7 residues of this loop were not modeled. The two models C2a-Li<sup>+</sup> and C2a-Mn<sup>2+</sup> differ 8° in domain-domain orientation, which is possibly due to small differences in crystallization

conditions and soaking of the C2a-Mn<sup>2+</sup> crystal. The separate VWA and SP domains show root-mean-square coordinate differences of respectively 0.54 and 0.59 Å for all C $\alpha$  positions.

For C2a-Mn<sup>2+</sup>, we observed a significant (12  $\sigma$ ) electron-density peak at the ion-binding position in the MIDAS site. We modeled a manganese ion at this position. The Mn<sup>2+</sup> ion displays an octahedral coordination provided by MIDAS residues Ser-240, Ser-242, Thr-317, two water molecules and one malonate molecule, originating from the crystallization buffer and acting as a pseudo ligand. In the case of C2a-Li<sup>+</sup>, no significant electron-density peak was present at the ion-binding site nor was density present for a pseudo ligand. Possibly, the ion-binding site was occupied by the weakly scattering Li<sup>+</sup> ion. However, the resolution (2.7 Å) of the diffraction data does not allow modeling of Li<sup>+</sup> binding and no ion was included at the MIDAS site for C2a-Li<sup>+</sup>.

### Overall structure of C2a

The overall structure of C2a is characterized by the VWA and SP domains that are in close contact (see Figure 2.1C). The overall fold of C2a is similar to that of its homolog Bb (Ponnuraj et al., 2004), but significant differences are apparent between the structures. In part this is expected given the amino-acid sequence identity of 39 % and the differences in glycosylation. C2a has six whereas Bb has two putative N-linked glycosylation sites. The orientation of the VWA-SP domains in C2a-Li<sup>+</sup> and C2a-Mn<sup>2+</sup> differ respectively by 16.5° and 21.5° from the orientation observed in Bb, see Figure 2.1D. Between C2a-Li<sup>+</sup> and C2a-Mn<sup>2+</sup> the VWA-SP orientation differs by only 8°. In part, these different domain-domain orientations in C2a and Bb may be due to crystal packing effects and may reflect flexibility in the domain-domain linkage. However, as we will argue below, differences in glycosylation, the introduced disulphide-bridge in Bb and, in particular, the N-terminal truncation in Bb affect the interface region. The absence of mutations and truncations in C2a allows the analysis of the unperturbed state of the MIDAS motif, the  $\alpha$ 7 helix of VWA and the VWA-SP interface.

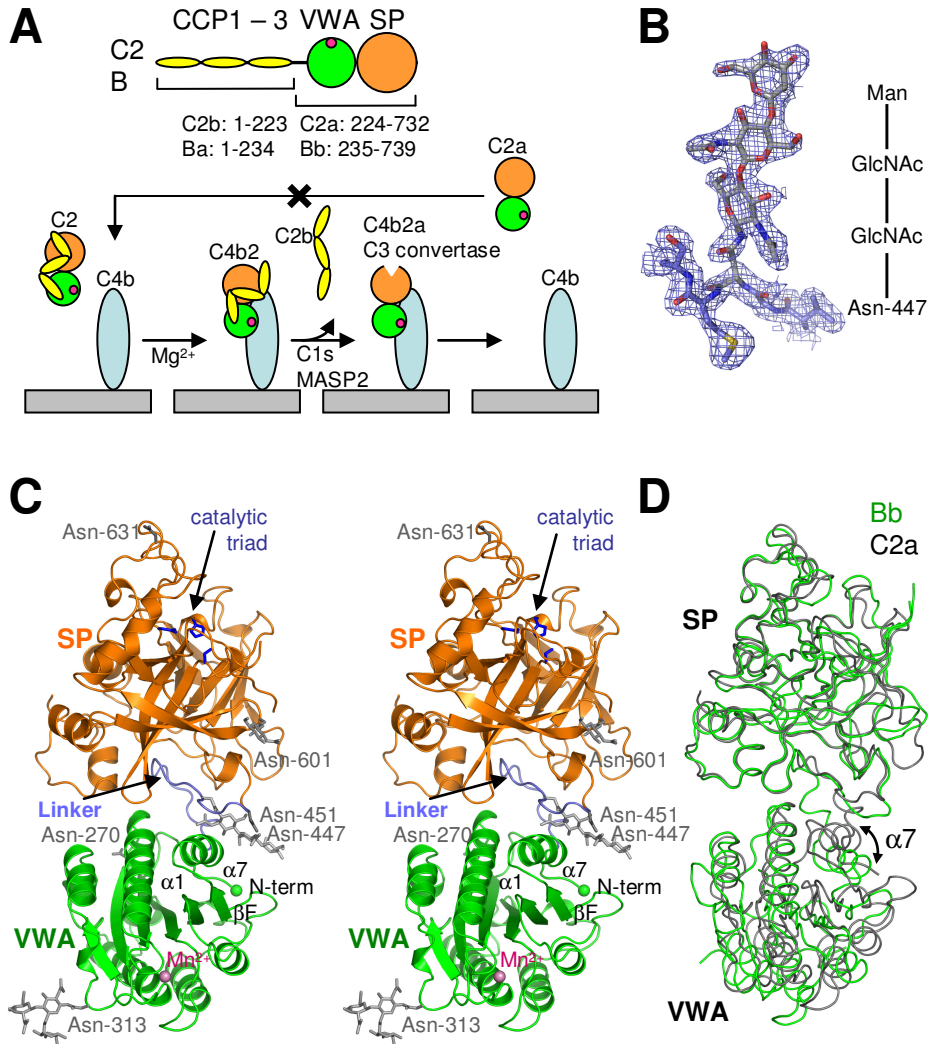


**Figure 2.1 Crystal structure of C2a.**

**A)** Schematic representation of domain topology of C2 and formation of the C3 convertase. **B)** Electron density ( $2mF_o - DF_c$ ,  $\phi_c$ ) of the glycan attached to Asn-447, shown are Asn-447-GlcNAc-GlcNAc-Man. **C)** Stereo ribbon representation of the C2a-Mn<sup>2+</sup> structure, indicated are the catalytic triad (blue) in the SP domain (orange), the linker region (light blue) between the SP and VWA domain (green with its N-terminal residue indicated by a green sphere), the manganese ion (pink) bound at the MIDAS motif; and, the six glycosylation sites (grey). **D)** Overlay of C2a (black) and Bb (1rrk, green) (Ponnuraj et al., 2004) superimposed on the SP domains, indicated is the different positions of the  $\alpha 7$  helix in the VWA domains.

### MIDAS motif

The MIDAS site in C2a is formed by Asp-240, Ser-242, and Ser-244 from loop  $\beta A\alpha 1$ , Thr-317 from loop  $\alpha 3\alpha 4$ , and Asp-356 from loop  $\beta D\alpha 5$  (Figure 2.2A). In C2a-Li<sup>+</sup> no ligand is bound and no ion can be observed, whereas a metal ion and pseudo ligand are clearly bound to the MIDAS motif in C2a-Mn<sup>2+</sup>. Putatively, the pseudo-ligand malonate, originating from the crystallization buffer, binds in a similar way as the carboxylate moiety of an aspartate or glutamate residue of the true ligand, C4b. In C2a-Mn<sup>2+</sup> the manganese ion is coordinated by hydroxyl groups from residues Ser-242, Ser-244, and Thr-317, and two waters, one of which mediates contacts with the two MIDAS aspartatic acids 240 and 356. The octahedral coordination is completed by carboxylate oxygen of the pseudo ligand, malonate (Figure 2A). This conformation of the MIDAS residues is virtually identical to that observed in the engineered Bb structure and other open and ligand-bound MIDAS sites (Emsley et al., 1997; 2000; Shimaoka et al., 2003); see Figure 2.2A. Superposition of the MIDAS sites of C2a-Li<sup>+</sup> and C2a-Mn<sup>2+</sup> shows that the side chain of Ser-244 in C2a-Li<sup>+</sup> is rotated by  $\sim 90^\circ$  and thus points its hydroxyl away from the metal-binding site and forms a hydrogen bond with the carboxylate group of Asp-356 (Figure 2.2A). All other residues in the MIDAS site show identical conformations in C2a-Li<sup>+</sup> and C2a-Mn<sup>2+</sup>. The minor rearrangement of Ser-244 may compensate for the loss of either a +1 or +2 charge when either a Li<sup>+</sup> ion or a water molecule replaces Mn<sup>2+</sup>, respectively. In contrast, in an ion-free and unliganded disulphide engineered  $\alpha$ -I domain Asp-239 (equivalent to Asp-356 in C2a) rotates away and hence compensates for the loss of a +2 charge (Shimaoka et al., 2003). Most surprisingly, the liganded C2a-Mn<sup>2+</sup> and unliganded C2a-Li<sup>+</sup> structures display essentially identical, both open, MIDAS motifs. Thus the open conformation of the MIDAS site in C2a occurs independently of ligand binding.

### VWA $\alpha 7$ helix

In integrin-I domains, ligand binding at the MIDAS site is coupled to a 10 Å displacement of the C-terminal helix  $\alpha 7$  from an inactive, closed, conformation to one that is activated and open (Emsley et al., 1997; 2000). Concerted movements of loop  $\beta A\alpha 1$  and helix  $\alpha 1$  and subsequent rearrangement of loops  $\beta D\alpha 5$  and  $\beta E\alpha 6$  transmits the signal from the MIDAS site to loop  $\beta F\alpha 7$  and helix  $\alpha 7$ . The conformation of these loops and helices is identical in the unliganded and pseudo-liganded C2a structures. Comparison of C2a with engineered, open, Bb shows that loop  $\beta A\alpha 1$  and  $\beta D\alpha 5$  and helix  $\alpha 1$  have similar conformations in the two structures (Figure 2.2B).

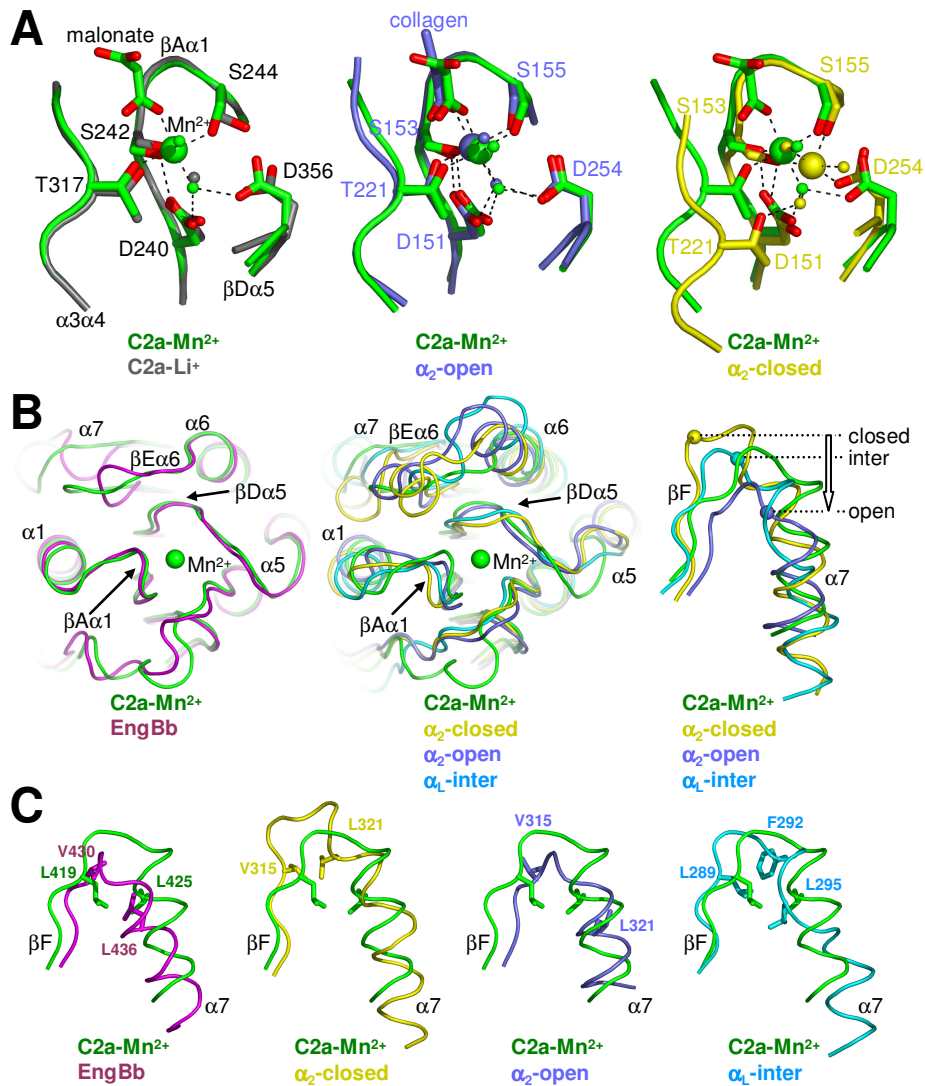


**Figure 2.2** Activation state of the VWA domain.

**A**) Left panel: the MIDAS motif of C2a as observed in the structures of C2a- $Li^+$  (grey) and C2a- $Mn^{2+}$  (green). Shown are the MIDAS residues (residue number and loop names as indicated), pseudo-ligand malonate, waters (small spheres), and  $Mn^{2+}$  (large sphere). Middle and right panel: the MIDAS motif of C2a- $Mn^{2+}$  and the  $\alpha_2$  I domain in an open (1dzi, blue) and closed (1aox, yellow) conformation (Emsley et al., 1997; 2000). **B**) View of the VWA domain. Left panel: C2a- $Mn^{2+}$  (green) and engineered open Bb (1rrk, magenta) (Ponnuraj et al., 2004); middle panel: C2a- $Mn^{2+}$  (green), closed (1aox, yellow) and open (1dzi, blue)  $\alpha_2$  (Emsley et al., 1997; 2000) and intermediate (1mjn, light blue)  $\alpha_4$  (Shimaoka et al., 2003) I domains; and, right panel: coil representation of the strand  $\beta F$  and helix  $\alpha 7$ , coloured as in the middle panel. Indicated is the conformation of loops  $\beta A\alpha 1$  and  $\beta D\alpha 5$  and helix  $\alpha 1$  transmitting structural changes between the MIDAS motif and helix  $\alpha 7$ . **C**) Position of hydrophobic 'ratchet' residues of loop  $\beta F\alpha 7$  and helix  $\alpha 7$ , coloured as in B. From left to right; C2a- $Mn^{2+}$  and engineered open Bb, C2a- $Mn^{2+}$  and closed  $\alpha_2$ , C2a- $Mn^{2+}$  and open  $\alpha_2$ ; and, C2a- $Mn^{2+}$  and intermediate  $\alpha_4$ .

Their conformation corresponds best to the open conformation of these loops and helix in  $\alpha$ -I domains (Emsley et al., 2000; Shimaoka et al., 2003); see Figure 2.2B. However, the  $\beta$ F $\alpha$ 7 loop and  $\alpha$ 7 helix differ between the C2a structures and Bb. The  $\alpha$ 7 helices differ 27-29° in orientation and are shifted approximately two-thirds of a helical turn towards the MIDAS site in C2a (Figure 2.2C). Superposition of C2a with closed and open  $\alpha$ <sub>2</sub> and intermediate  $\alpha$ <sub>L</sub> I-domain structures (Shimaoka et al., 2003) shows no evident similarities in backbone position of loop  $\beta$ F $\alpha$ 7 and helix  $\alpha$ 7. Although the C2a  $\alpha$ 7 helix is positioned in between the open and closed states of  $\alpha$ <sub>2</sub>-I domains, it differs from the intermediate position as observed in  $\alpha$ <sub>L</sub>-I domain due to a tilt of helix  $\alpha$ 7 in C2a (Figure 2.2C).

Based on structural data and molecular dynamic simulations Jin *et al.* (Jin et al., 2004) suggest that the position of the  $\alpha$ 7 helix in I domains is stabilized by hydrophobic “ratchet” residues that occupy underlying hydrophobic pockets. For the  $\alpha$ <sub>2</sub> and  $\alpha$ <sub>L</sub>-I domains respectively two (315-VxxxxxL-321) and three (289-LxxFxxL-295) ratchet residues have been identified. Alignment indicates that C2a and Bb may have two hydrophobic ratchet residues: 419-LxxxxxL-425 in C2a and 430-VxxxxxL-436 in Bb; suggesting that the two VWA domains may occur in an open and closed conformation similar to the  $\alpha$ <sub>2</sub>-I domain. So far, only an open-like conformation for Bb has been observed, and the 2 ratchet residues, Val-430 and Leu-436, are positioned in hydrophobic pockets according to the activated, open I domains. The situation in C2a, however, differs. The first ratchet residue of C2a, Leu-419, resembles most the situation observed for  $\alpha$ <sub>2</sub> in the closed conformation and  $\alpha$ <sub>L</sub> in either the closed or intermediate conformation (Figure 2.2C). The second putative ratchet residue of C2a, Leu-425, is located at an uncommon position: it sits in between the position that the second  $\alpha$ <sub>2</sub>-ratchet residue occupies in the closed and open conformation; and, it overlaps with the position of the third  $\alpha$ <sub>L</sub>-ratchet residue in the intermediate conformation (Figure 2.2C). These differences with Bb,  $\alpha$ <sub>2</sub> and  $\alpha$ <sub>L</sub> are possibly due to differences in loop  $\beta$ E $\alpha$ 6 (Figure 2.2B). This loop is one residue longer in C2a than in Bb and adopts a different conformation with the side chain of Val-393 occluding the ratchet pocket (for the second ratchet residue in the open conformation) as observed in Bb,  $\alpha$ <sub>2</sub> or  $\alpha$ <sub>L</sub>. In conclusion, C2a has 2 putative ratchet residues; and, their positions correspond best with those of an intermediate conformation of the  $\alpha$ 7 helix.

### C2a N-terminus

We expected the N-terminus of C2a, which is formed upon proteolysis of C2 in the C4bC2 complex, to be unstructured. Surprisingly however, the N-terminal residues (224 to 231) are well ordered and positioned in a groove near the VWA-SP interface region. Strands  $\beta$ A and  $\beta$ D, and the C-terminal end of the VWA domain form a crevice in which the N-terminal residues are bound via the side chains of Ile-225 and Ile-227 that are deeply buried in hydrophobic pockets (Figure 2.3A).

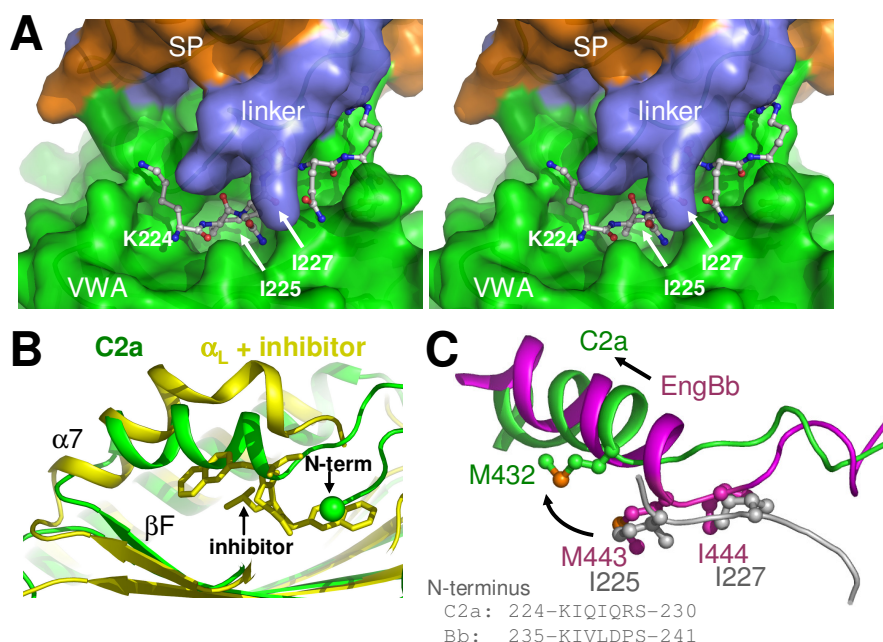


**Figure 2.3 N-terminal residues of C2a.**

**A)** Stereo figure showing the N-terminal residues (ball-and-stick) of C2a positioned in a crevice near the linker (blue) connecting the VWA (green) and SP (orange) domains. The C2a N-terminus is anchored via Ile-225 and Ile-227 that are buried in underlying hydrophobic pockets. **B)** Overlay of C2a-Mn<sup>2+</sup> (green) and the closed  $\alpha_L$  I domain (1xuo, yellow) in complex with a small molecule antagonist (Wattanasin et al., 2005). The binding site for the N-terminal segment in C2a and the antagonist partially overlap. **C)** Overlay of the N and C-terminal regions of the VWA domain of C2a (green) and engineered Bb (1rrk, magenta) (Ponnuraj et al., 2004). In C2a the N-terminal residues interact with  $\alpha_7$  and Ile-225 and Ile-227 occupy hydrophobic pockets. In engineered Bb residues of the C-terminal end of  $\alpha_7$  (Met-443 and Ile-444) occupy these hydrophobic pockets.



Furthermore, the main chain of residues 225-227 forms a small irregular parallel  $\beta$ -sheet with residues 432-434 C-terminal of helix  $\alpha 7$ . Residues 228-231 form a loop that connects to the first strand ( $\beta A$ ) of the VWA domain. Additional contacts of the N-terminal residues with the VWA-SP linker region involve a salt bridge, hydrogen bonds and hydrophobic contacts. Thus, the N-terminal residues of C2a interact extensively with the VWA domain and VWA-SP interface.

The observed interactions of the C2a N-terminal segment with residues in the C-terminal end of the VWA domain are absent in the models of the isolated VWA domain of factor B (Bhattacharya et al., 2004) and engineered Bb (Ponnuraj et al., 2004) due to disorder and truncation of the N-terminal residues, respectively. The conformation of the N-terminal segment in C2a is, however, consistent with the observation made by Hinshelwood and Perkins (Hinshelwood and Perkins 2000). Based on up-field methyl NMR spectra, these authors suggest that in Bb, and not in factor B or the isolated VWA domain, the N-terminus 235-KIVLD-239 is structurally incorporated in the proximity of an aromatic residue. Indeed, the homologous residues in C2a (224-KIQIQ-228) are within 4-6 Å distance of three aromatic residues (Tyr-389, Phe-429 and Phe-267), which are identical or homologous aromatic residues in factor B. Furthermore, the structure of the N-terminally truncated Bb shows a similar crevice, which may harbour the N-terminal residues in full-length Bb. However, binding of the N-terminus in this crevice requires the presence of the SP domain, because the N-terminal residues and helix  $\alpha 7$  are disordered in the isolated VWA structure of factor B. The fragments C2a and Bb arise after binding of respectively C2 and B to their cofactors and subsequent proteolysis between the third CCP and the VWA domain. For proteolysis the loop with the scissile bonds, Arg-223 – Lys-224 of C2 and Arg-234 – Lys-235 of B, must be exposed. In the structure of C2a however, the main-chain atoms of Lys-224 are buried and inaccessible to the C1s or MASP-2 proteases. Thus, the N-terminal residues of C2a and Bb must adopt a conformation in the C4bC2 and C3bB complexes that is drastically different from the conformation observed in C2a.

The binding site for the N-terminal segment in C2a partially overlaps with the small-molecule antagonist-binding site observed in the  $\alpha L$ -I domain (Kallen et al., 1999; Crump et al., 2004; Wattanasin et al., 2005); see Figure 2.3B. Binding of antagonists locks the  $\alpha L$ -I domains in an inactive, closed conformation of both the  $\alpha 7$  helix and the MIDAS site. In contrast, in C2a we observe an intermediate-like conformation for helix  $\alpha 7$  and an open conformation of the MIDAS site. This difference is perhaps correlated with the precise location of binding the antagonist

*vs.* binding the N-terminus; i.e. the antagonists bind adjacent to the helix whereas the N-terminus binds at the C-terminal end of the helix (Figure 2.3B). Comparison of C2a and Bb indicates that binding of the N-terminal segment likely dislocates the  $\alpha 7$  helix (see Figure 2.3C). A prominent aspect of binding the N-terminal segment in C2a is the positioning of Ile-225 and Ile-227 in well-defined hydrophobic pockets. In engineered, truncated Bb these two pockets are occupied by hydrophobic residues Met-443 and Ile-444 of the C-terminal end of helix  $\alpha 7$ . Thus, the position of the  $\alpha 7$  helix in Bb is incompatible with binding of the N-terminal segment. We assume that in native, full-length Bb the N-terminal segment, with Ile-236 and Leu-238, will dislocate the  $\alpha 7$  helix as in C2a (Figure 2.3C). The structure of C2a indicates that dislocation of the  $\alpha 7$  helix by the N-terminus causes rearrangements in the VWA-SP interface region.

### Domain-domain interface

The VWA-SP interface area is significantly larger in C2a than in Bb: 1,967 and 1,920 Å<sup>2</sup> buried surface area in C2a-Li<sup>+</sup> and C2a-Mn<sup>2+</sup>, respectively, *vs.* 1,320 Å<sup>2</sup> in Bb (computed using domain boundaries as defined by (Ponnuraj et al., 2004)). The linker region, residues 433-442, interacts intimately with both the VWA and SP domain. The contacts between the two domains involve numerous van der Waals interactions, hydrogen bonds and three salt bridges. Three aspects contribute to the difference in buried surface area. First, the domain-domain orientations differ by 16-21° between C2a and Bb and the  $\alpha 7$  helices take on different positions. Consequently, the interface has a more compact arrangement in C2a (Figure 2.1C). Second, the contribution of the  $\alpha 7$  helix to buried surface area increases from 191 Å<sup>2</sup> in Bb to 286 and 271 Å<sup>2</sup> in C2a-Li<sup>+</sup> and C2a-Mn<sup>2+</sup> respectively. Third, in addition, in C2a two N-linked glycans at asparagines 447 and 451 are located at or near the VWA-SP domain interface (Figure 2.1B; both glycosylation consensus sequences are conserved among the known C2 sequences). The glycan at Asn-447 contributes significantly (~250 Å<sup>2</sup>) to the buried surface area in both C2a structures. The glycan at Asn-451 contributes another 60 Å<sup>2</sup> in the C2a-Li<sup>+</sup> model (this glycan was not modeled in C2a-Mn<sup>2+</sup>). Carbohydrate units of the glycan at Asn-447 make multiple hydrogen bonds with residues of both the linker and VWA and SP domains. Hydrogen bonds are formed between the first GlcNAc-unit and residues from the VWA  $\alpha 7$  helix (Glu-430), the linker (Leu-433), and the first SP  $3_{10}$ -helix (Glu-456) and between the second GlcNAc-unit with the N-terminus (Lys-224), the VWA  $\alpha 7$ -helix (His-431), and the linker (Asp-434). To verify the role of these glycans we made native C2, two single-glycan-deletion mutants (N447D and N451D), and one double-glycan-deletion mutant (N447D/N451D) that were tested for hemolytic activity. Compared to native C2 the N451D mutant has enhanced activity ( $149 \pm 36$

%) indicating that this glycan is not required for activity. In contrast, the N447D mutant is almost hemolytic inactive ( $4.0 \pm 0.1$  % residual activity). In the double mutant N447D/N451D, however, the activity slightly recovers to  $22 \pm 8$  %. This indicates that the N447 interface glycan plays an important, but not critical, role in C4b2a convertase stability or activity.

### SP domain

The catalytic residues, His-487, Asp-541 and Ser-659, of C2a are in an active conformation. The oxyanion-hole loop, Lys-656 - Ser-659, adopts a conformation similar but not identical to that of mature trypsins and chymotrypsins (Figure 2.4A). As observed in the structure of Bb (Ponnuraj et al., 2004), one of the oxyanion-hole forming peptide planes in C2a (between Lys-656 and Gly-657) is flipped by  $\sim 180^\circ$  compared to trypsin. Although Arg-696 in loop 2 of C2a takes over the role of Ile-16, which induces oxyanion hole formation in trypsin, this does not suffice to establish a fully formed oxyanion hole. In C2a the carbonyl oxygen of Lys-656 points inwards and makes a hydrogen bond with the catalytic serine hydroxyl whereas in activated trypsin the amide group of Gly-193 points inwards to stabilize the oxyanion-reaction intermediate (Khan and James 1998). In trypsin the peptide plane is stabilized in a proper orientation by a hydrogen bond between Asn-143 of loop D and the carbonyl of Gln-192 (Figure 2.4A). Compared to trypsins and chymotrypsins, C2a and Bb have a very short loop D and a long loop 2. Nonetheless, a structural homolog of Asn-143 is not provided in either C2a or Bb. As suggested (Jing et al., 2000; Ponnuraj et al., 2004), the ill-formed oxyanion hole may explain the low proteolytic activity towards peptide substrates (Kam et al., 1987).

The substrate-binding grooves in C2a and Bb differ significantly from trypsin due to large insertions and deletions in surface loops (Figure 2.4B; with substrate-binding loops labeled according to (Perona and Craik 1997)). In comparison to trypsin, loops 2, 3 and C are respectively 15, 13 and 9 residues longer and loops D and E are respectively 12 and 4 residues shorter in C2a. Notably, the extended loops 3 and C enclose the left side of the putative substrate-binding groove (Figure 2.4B). Thus, the ordinary S2 and S3 binding pockets appear to be absent in C2a and Bb. Differences between C2a and Bb occur primarily in the putative substrate-binding loop E and loop 2. Loop E is positioned near the interface region of the VWA and SP domain and the observed differences may result from the differences in domain-domain orientation between C2a and Bb. Loop 2 is seven residues longer in C2a than in Bb. This loop is disordered in all structures of C2a and Bb; respectively 691-KNS-693 and 701-KNQ-703 are missing in all models.

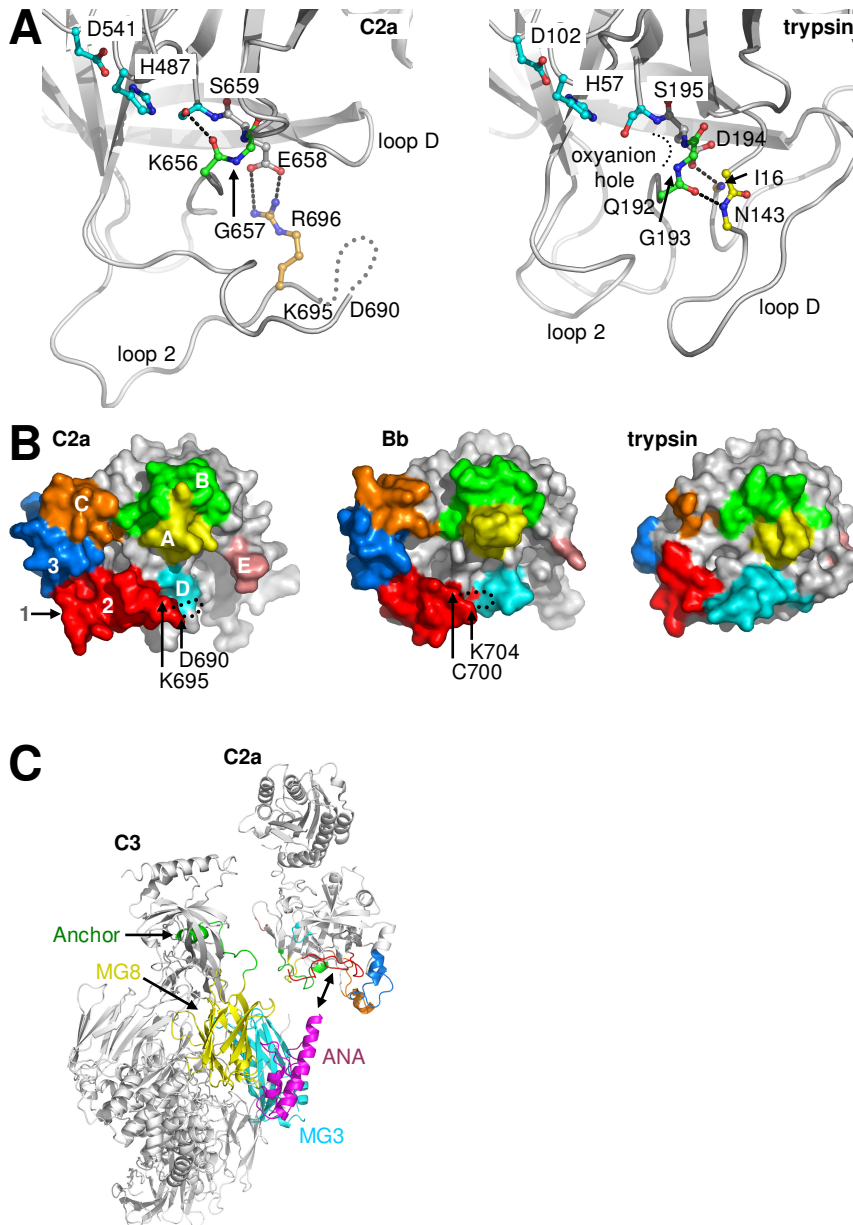


**Figure 2.4 The SP domain.**

**A** Catalytic center and oxyanion hole in C2a-Li<sup>+</sup> (left panel) and trypsin (1avw, right panel) (Song and Suh 1998); indicated are the catalytic triad Asp-His-Ser (light blue), the oxyanion hole (green) and Arg-696 (orange) in C2a replacing the N-terminal Ile-16 in trypsin. In trypsin the main-chain of Asn-143 (yellow) forms a hydrogen bond with the main chain of 192-193. A similar interaction is absent in C2a. Instead, the peptide plane of 656-657 is flipped and makes a hydrogen bond with the catalytic serine. **B** Surface representation of the putative substrate-binding grooves;

shown are C2a-Li<sup>+</sup> (left panel), Bb (1rrk, middle panel) (Ponnuraj et al., 2004) and trypsin (1avw, right panel) (Song and Suh 1998). Surface loops 1 (grey), 2 (red), 3 (blue), A (yellow), B (green), C (orange), D (light blue), and E (pink) are highlighted **C**) Hypothetical model of C2a placed onto C3 (2a73, (Janssen et al., 2005)); shown are the SP domain of C2a with substrate-binding loops coloured as in B; and, substrate C3 with the flexible scissile loop indicated by a dotted line; domains of C3 are labelled as defined in (Janssen et al., 2005).

These residues are part of a conserved positively charged stretch (692-698 in C2a and 701-707 in Bb; which include arginines 696 in C2a and 705 in Bb that interact with the oxyanion hole). This stretch may provide a specific electropositive patch for interactions with the substrate C3. Other surface charges conserved between C2a and Bb are located within loops A, B and C near the S1 binding pocket. As shown in Figure 2.4B, loops 2 and D on one side and loops A and B on the other side form a distinct binding groove, similar to the substrate binding groove in trypsin. In contrast, the substrate-binding grooves in C2a and Bb are delineated by an obstruction formed by the extended loops 3 and C, which is likely to play a part in the high substrate specificity of C2a and Bb.

The SP domains in C2a and Bb are in near-active conformations. Hence, we may assume that the SP domains do not undergo large structural changes in cofactor binding (i.e. in the formation of C4b2a and C3bBb) and substrate C3 binding. Figure 2.4C represents a simple model of the enzyme-substrate complex. This model is obtained by placing C3 (Janssen et al., 2005) onto C2a with the scissile loop oriented in a productive N to C direction in the primary substrate binding groove. In the structures of human and bovine C3 the scissile loop is disordered and exposed to the solvent (Janssen et al., 2005; Fredslund et al., 2006); in human C3 9 residues of the scissile loop (720-728) are absent in the model and the C $\alpha$  atoms of residues 719 and 729 are 11 Å apart in the structure of C3. The simple enzyme-substrate model identifies putative interactions between C2a, or Bb, and C3. Loops 2, 3 and C on the SP domain likely interact with the anaphylatoxin domain of C3. These extended loops may increase the contact area between the two proteins by positioning themselves around the protruding anaphylatoxin domain. Loops A and B possibly contact the residues following the scissile bond and macroglobulin (MG)-3 domain. Several complementary charges are present suggesting a significant contribution from electrostatic interactions. Putative interactions of the anchor and MG8 domain of C3 may stabilize the partially disordered loop 2 potentially aiding in the formation of a mature oxyanion hole. These latter interactions support a substrate-induced activation mechanism of the SP domain proposed by (Ponnuraj et al., 2004). Based on the observed VWA-SP orientation, the VWA domain is located in this enzyme-substrate model close to the C345C domain of C3. It may thus bridge interactions between the substrate C3

and the ligand, C4b or C3b, which is thought to bind at the MIDAS motif on the VWA domain. Of course, given the size of the molecules we may expect additional interaction sites that may be important in the substrate affinity and specificity of the C3 convertases. Modeling these interactions requires a structure of either C3b or C4b. Nonetheless, the enzyme-substrate model presented here identifies a series of potential interactions sites that will help direct mutagenesis studies.

## Concluding remarks

The two structures of C2a give insights into the possible roles of the VWA domain in convertase formation and indicate potential primary and secondary interaction sites between the SP domain and the substrate C3. The VWA domain of C2a does not require its ligand, C4b, to maintain an open conformation of the MIDAS motif. The open MIDAS conformation observed in unliganded C2a-Li<sup>+</sup> and pseudo-liganded C2a-Mn<sup>2+</sup> possibly serves to enhance the affinity for C4b. The N-terminal residues of C2a are buried in the VWA domain possibly stabilizing the observed intermediate conformation of the VWA- $\alpha$ 7 helix. The observed structure implies that the N-terminal residues undergo a conformational change from exposed and accessible to proteases in the C4bC2 complex to inaccessible in C2a. An extensive contact area is observed between the VWA and SP domains of C2a. Glycan N447 contributes significantly to the domain-domain interface. This glycan is important, but not critical, for hemolytic activity. As was previously observed in the structure of engineered Bb, the open VWA domain in C2a does not suffice to induce a fully active conformation of the SP domain. The proposed substrate-induced activation mechanism, forming a fully active oxyanion hole upon C3 binding, possibly involves loop 2 of the SP domain. In a simple substrate-enzyme (C3-C2a and C3-Bb) model, the negative charges of the anchor region and/or MG8 of C3 possibly interact with the positive charges of the extended, and unique, loop 2 of C2a and Bb. Extensions of substrate binding loops 2, 3 and C possibly serve to enhance the contact area by enveloping the protruding anaphylatoxin domain in C3, hence contributing to substrate affinity and specificity.

## Experimental procedures

### Cloning and expression of recombinant C2a and C2

The cDNA coding for human C2a was amplified by PCR from I.M.A.G.E. clone 2191586. Forward primer C2afor (5'-GGATCCGCTCCCTCCTG-3') introduced a BamHI restriction site. Reverse primer C2rev (5'-GCGGCCGCGAGGGGTAAAAA ATTCAGGA-3'), which anneals to the 3' untranslated region, introduced a NotI restriction site. The PCR product was cloned in the pCR4-TOPO vector (Invitrogen) and sequenced. Next, C2a was ligated as a BamHI-NotI fragment into a pNUT expression vector (Palmiter et al., 1987) that encodes the secretion signal peptide of human von Willebrand factor followed by a hexa-histidine tag. This construct was used for transfection of BHK cells according to the DNA-calcium phosphate method (Graham and van der Eb 1973). Colonies were selected on 100 µM methotrexate. For identification of highly expressing clones expression medium was diluted 50-100 fold in coating buffer (50 mM sodium carbonate, 0.02 % sodium azide, pH 9.6), coated in 96-well plates and probed with anti-polyhistidine monoclonal antibody his-1 (Sigma) followed by horseradish peroxidase coupled rabbit-anti-mouse antibodies (DAKO). For large-scale production cells were cultured in a cell factory (Nunc) using Ultrosor G (ITK Diagnostics) as serum replacement. Expression medium was stored at -20 °C until further use.

For construction of the human C2 expression vector a PCR was performed with forward primer C2for (5'-GCAGGATCCGCTCCCTCCTGCCCT-3') and reverse primer C2rev. The PCR product was cloned in pCR4-TOPO and sequenced. This plasmid served as template for the generation of glycosylation mutants C2-N447D and C2-N451D and the double glycosylation mutant C2-N447D/N451D. Mutagenesis was achieved by an "in house" variation of the QuikChange method. In the case of mutant C2-N447D a PCR was performed using limiting amounts (6 pmol) of forward mutagenesis primer N447D (5'-GGGGTGGGGGACATGTCAGC-3') and primer C2rev with 100 ng (~25 fmol) pCR4-C2 template and 1.7 units Pfu Turbo DNA polymerase (Stratagene). After a few PCR cycles both primers are exhausted. The PCR product then provides two complementary mega-primers that, in a QuikChange-like reaction, generate full-length mutated copies of the template vector. After completion of the reaction, template vector was destroyed by incubation with DpnI restriction enzyme (NewEngland Biolabs) for 2 hours at 37 °C and 5 µl of the reaction product was transformed into Top10 cells. For the construction of mutant C2-N451D a similar PCR reaction was performed using primer C2for and reverse mutagenesis primer N451Drev (5'-CAGAGGCGTCTGCTGACATG-3'). The double mutant was constructed using

mutation primers N447Dfor and N451Drev. Introduction of the respective mutations was confirmed by sequencing. C2 and C2 mutants were ligated in a modified pTT3 expression vector (Durocher et al., 2002) encoding a cystatin secretion signal peptide (Barash et al., 2002) followed by a hexa-histidine tag. Suspension growing HEK293-EBNA-1 (Epstein-Barr virus nuclear antigen 1) cells were transfected using polyethyleneimine (Durocher et al., 2002) and recombinant mutant C2 was transiently expressed at low serum concentration (~0.1 % fetal calf serum). Expression medium containing C2 was harvested 96 hours after transfection and stored at -20 °C until further use.

### **Hemolytic assay**

Hemolytic activity of recombinant C2 was assessed by a C2-dependent hemolytic assay, using C2-deficient guinea pig serum as a complement source. The method was similar to that previously described for a C1q-dependent hemolytic assay (Roos et al., 2001). In brief,  $1 \cdot 10^7$  antibody-coated sheep erythrocytes were incubated with 100-fold diluted C2-deficient serum in the presence or absence of culture supernatant containing human recombinant C2 or C2a, normal human serum, or mock culture supernatant, in various dilutions, for one hour at 37 °C. The assay was performed using dextrose gelatin Veronal buffer<sup>2+</sup> (DGVB<sup>2+</sup>) as a buffer, in a final volume of 200  $\mu$ l. DGVB<sup>2+</sup> consists of 0.05% gelatin, 167 mM glucose, 0.15 mM CaCl<sub>2</sub>, 0.5 mM MgCl<sub>2</sub> in veronal-buffered saline (1.8 mM Na-5,5-diethylbarbital, 0.2 mM 5,5-diethylbarbituric acid, 145 mM NaCl). Following addition of 1.5 ml phosphate-buffered saline and centrifugation, hemolysis was assessed by measuring OD at 414 nm. C2 hemolytic activity was calculated as a Z-value, as described (Roos et al., 2001), followed by calculation of hemolytic activity per ml and normalization for the concentration of C2 as determined by specific ELISA. The relative hemolytic activity of mutant C2 was calculated as a percentage of hemolytic activity of wildtype C2.

### **Purification of C2a**

C2a expression medium was concentrated 10-fold using a Quickstand bench top concentrator (GE Health Care) with a 10 kDa molecular weight cut off and the pH of the medium was adjusted to 8.0. Next, C2a was purified from concentrated medium using a HiTrap-chelating HP column (Amersham) charged with Ni<sup>2+</sup>. After loading, the column was extensively washed with buffer containing 20mM Tris, 300 mM NaCl, pH 8. Non-specifically bound proteins were eluted with 15 mM of imidazole in the same buffer. Next C2a was eluted at an imidazole concentration of 100 mM. Peak fractions were analyzed by SDS-PAGE and Western blotting using antibodies directed against the His-tag. The N-terminal



sequence was analyzed on an automated protein sequencer from Perkin Elmer Applied Biosystems 476A confirming the presence of the expected amino acids HHHHHHGSKI.

### **Crystallization and diffraction data collection**

For crystallization purified C2a was dialyzed against a solution containing 20 mM Tris, 50 mM NaCl at pH 7.5 and concentrated to 15 mg/ml. Crystallization experiments were performed at 20 °C using the hanging drop vapor-diffusion method and a 1:1 ratio of protein and reservoir solution. Initial crystals of poor quality were obtained with reservoir solution consisting of 35% w/v PEG 1000 and 0.1 M malonate-imidazole boric acid buffer, made by mixing 0.1 M sodium malonate, 0.1 M imidazol, and 0.1 M boric acid in a 2:3:3-ratio, at pH 7.0. A subsequent screen for additives identified two conditions that produced crystals suitable for data collection. In the presence of 20 mM LiCl triangular shaped crystals with dimensions 0.08 x 0.06 x 0.02 mm appeared after 4-5 days. We refer to these crystals as C2a-Li<sup>+</sup>. For data collection a C2a-Li<sup>+</sup> crystal was passed through a 2- $\mu$ l drop of reservoir solution and rapidly frozen by immersion in liquid nitrogen. In the presence of xylitol at a concentration of 3% w/v crystals of 0.1 x 0.1 x 0.1 mm in size appeared after 5 months. These crystals were soaked for 24 hrs in a 2- $\mu$ l drop of reservoir solution containing 20 mM NaCl and 10 mM MnCl<sub>2</sub> and then flash cooled in liquid nitrogen. We refer to these crystals as C2a-Mn<sup>2+</sup>. Diffraction data up to a resolution of 2.7 Å for C2a-Li<sup>+</sup> and 2.1 Å for C2a-Mn<sup>2+</sup> were collected at ESRF beam-lines ID14-EH2 and ID14-EH4 in Grenoble, France. The data were indexed and integrated with MOSFLM (Leslie, 2006) and scaled using SCALA (CCP4 1994). Data statistics are given in Table 2.1.

### **Structure determination and refinement**

The structure of C2a was determined by molecular replacement using Phaser (Storoni et al., 2004). As search models we used the coordinates of protein data bank entries 1DLE (Jing et al., 2000) and 1Q0P (Bhattacharya et al., 2004) representing the SP and VWA domain of factor B, respectively. Sequence identities between C2 and factor B are 39 % for these domains. Phaser yielded a clear answer, where attempts with other programs had failed, placing first the SP domain and subsequently the VWA domain. Reversing the order, i.e. starting with the smaller VWA domain, yielded the same solution.

The model of C2a-Li<sup>+</sup> was iteratively built using the program O (Jones et al., 1991) and refined to near completion using CNS (Brunger et al., 1998) and REFMAC (Winn et al., 2001). Subsequently, higher-resolution diffraction data of C2a soaked

with  $\text{MnCl}_2$  was obtained, and its structure was solved and refined, yielding a more complete model. The C2a- $\text{Mn}^{2+}$  model was then used to finalize the model of C2a- $\text{Li}^+$ . The final R and Rfree factors were 0.21/0.29 for all data out to 2.7 Å resolution for C2a- $\text{Li}^+$  and 0.19/0.24 for all data to 2.1 Å resolution for C2a- $\text{Mn}^{2+}$ . Both models display good geometry (see Table 2.1). The final model for C2a- $\text{Li}^+$  consists of 497 protein residues, 11 glycan units, and 38 water molecules. Due to poor electron density, residues 395-397, residues 408-413, and residues 691-694 were excluded from the model. The final model for C2a- $\text{Mn}^{2+}$  consists of 502 protein residues, 7 glycan units, 133 water molecules, and a  $\text{Mn}^{2+}$  ion. Residues 687-693 are missing due to unclear electron density.

Coordinates and structure factors are available in the Protein Data Bank under accession codes 2I6Q (C2a- $\text{Mn}^{2+}$ ) and 2I6S (C2a- $\text{Li}^+$ ).

## Acknowledgements

We thank the ID14-beam line scientists at the European Synchrotron Radiation Facility (EMBL/ESRF) in Grenoble, France, for their help with data collection. We thank Randy J. Read for solving the molecular replacement problem in minutes at the EMBO course “Automated Macromolecular Structure Solution” in Amsterdam. We acknowledge Shizuko Tsuji for her help with expression of C2a in BHK cells. Danielle J. van Gijlswijk-Janssen and Nicole Schlagwein (LUMC, Leiden) are acknowledged for technical assistance. We are indebted to one of the referees for very helpful criticisms. This work was supported by a ‘Pionier’ programme grant No. 700.99.402 (P.G.) of the Council for Chemical Sciences of the Netherlands Organization for Scientific Research (NWO-CW) and the Dutch Kidney Foundation (A.R.).

## References

- Barash, S., Wang, W., and Shi, Y. (2002). Human secretory signal peptide description by hidden Markov model and generation of a strong artificial signal peptide for secreted protein expression. *Biochem. Biophys. Res. Commun.* 294, 835-842.
- Bentley, D.R. (1986). Primary structure of human complement component C2. Homology to two unrelated protein families. *Biochem. J.* 239, 339-345.
- Bhattacharya, A.A., Lupher, M.L., Jr., Staunton, D.E., and Liddington, R.C. (2004). Crystal structure of the A domain from complement factor B reveals an integrin-like open conformation. *Structure (Camb)* 12, 371-378.
- Bode, W. (1979). The transition of bovine trypsinogen to a trypsin-like state upon strong ligand binding. II. The binding of the pancreatic trypsin inhibitor and of isoleucine-valine and of sequentially

- related peptides to trypsinogen and to p-guanidinobenzoate-trypsinogen. *J. Mol. Biol.* 127, 357-374.
- Brunger, A.T., Adams, P.D., Clore, G.M., DeLano, W.L., Gros, P., Grosse-Kunstleve, R.W., Jiang, J.S., Kuszewski, J., Nilges, M., Pannu, N.S., Read, R.J., Rice, L.M., Simonson, T., and Warren, G.L. (1998). Crystallography & NMR system: A new software suite for macromolecular structure determination. *Acta Crystallogr. D Biol. Crystallogr.* 54, 905-921.
- CCP4 (1994). The CCP4 suite: programs for protein crystallography. *Acta Crystallogr. D Biol. Crystallogr.* 50, 760-763.
- Crump, M.P., Ceska, T.A., Spyropoulos, L., Henry, A., Archibald, S.C., Alexander, R., Taylor, R.J., Findlow, S.C., O'Connell, J., Robinson, M.K., and Shock, A. (2004). Structure of an allosteric inhibitor of LFA-1 bound to the I-domain studied by crystallography, NMR, and calorimetry. *Biochemistry* 43, 2394-2404.
- Durocher, Y., Perret, S., and Kamen, A. (2002). High-level and high-throughput recombinant protein production by transient transfection of suspension-growing human 293-EBNA1 cells. *Nucleic Acids. Res.* 30, E9.
- Emsley, J., King, S.L., Bergelson, J.M., and Liddington, R.C. (1997). Crystal structure of the I domain from integrin alpha2beta1. *J. Biol. Chem.* 272, 28512-28517.
- Emsley, J., Knight, C.G., Farndale, R.W., Barnes, M.J., and Liddington, R.C. (2000). Structural basis of collagen recognition by integrin alpha2beta1. *Cell* 101, 47-56.
- Fredslund, F., Jenner, L., Husted, L.B., Nyborg, J., Andersen, G.R., and Sottrup-Jensen, L. (2006). The structure of bovine complement component 3 reveals the basis for thioester function. *J. Mol. Biol.* 361, 115-127.
- Graham, F.L., and van der Eb, A.J. (1973). A new technique for the assay of infectivity of human adenovirus 5 DNA. *Virology* 52, 456-467.
- Hinshelwood, J., and Perkins, S.J. (2000). Conformational changes during the assembly of factor B from its domains by <sup>1</sup>H NMR spectroscopy and molecular modelling: their relevance to the regulation of factor B activity. *J. Mol. Biol.* 301, 1267-1285.
- Horiuchi, T., Macon, K.J., Engler, J.A., and Volanakis, J.E. (1991). Site-directed mutagenesis of the region around Cys-241 of complement component C2. Evidence for a C4b binding site. *J. Immunol.* 147, 584-589.
- Janssen, B.J., Huizinga, E.G., Raaijmakers, H.C., Roos, A., Daha, M.R., Nilsson-Ekdahl, K., Nilsson, B., and Gros, P. (2005). Structures of complement component C3 provide insights into the function and evolution of immunity. *Nature* 437, 505-511.
- Jin, M., Andricioaei, I., and Springer, T.A. (2004). Conversion between three conformational states of integrin I domains with a C-terminal pull spring studied with molecular dynamics. *Structure* 12, 2137-2147.
- Jing, H., Xu, Y., Carson, M., Moore, D., Macon, K.J., Volanakis, J.E., and Narayana, S.V. (2000). New structural motifs on the chymotrypsin fold and their potential roles in complement factor B. *Embo J.* 19, 164-173.
- Jones, T.A., Zou, J.Y., Cowan, S.W., and Kjeldgaard (1991). Improved methods for building protein models in electron density maps and the location of errors in these models. *Acta Crystallogr. A* 47, 110-119.
- Kallen, J., Welzenbach, K., Ramage, P., Geyl, D., Kriwacki, R., Legge, G., Cottens, S., Weitz-Schmidt, G., and Hommel, U. (1999). Structural basis for LFA-1 inhibition upon lovastatin binding to the CD11a I-domain. *J. Mol. Biol.* 292, 1-9.
- Kam, C.M., McRae, B.J., Harper, J.W., Niemann, M.A., Volanakis, J.E., and Powers, J.C. (1987). Human complement proteins D, C2, and B. Active site mapping with peptide thioester substrates. *J. Biol. Chem.* 262, 3444-3451.

- Kerr, M.A. (1980). The human complement system: assembly of the classical pathway C3 convertase. *Biochem J* 189, 173-181.
- Kerr, M.A., and Parkes, C. (1984). The effects of iodine and thiol-blocking reagents on complement component C2 and on the assembly of the classical-pathway C3 convertase. *Biochem J* 219, 391-399.
- Khan, A.R., and James, M.N. (1998). Molecular mechanisms for the conversion of zymogens to active proteolytic enzymes. *Protein Sci.* 7, 815-836.
- Leslie, A.G. (2006). The integration of macromolecular diffraction data. *Acta Crystallogr. D Biol. Crystallogr.* 62, 48-57.
- Murshudov, G.N., Vagin, A.A., and Dodson, E.J. (1997). Refinement of macromolecular structures by the maximum-likelihood method. *Acta Crystallogr. D Biol. Crystallogr.* 53, 240-255.
- Palmiter, R.D., Behringer, R.R., Quaife, C.J., Maxwell, F., Maxwell, I.H., and Brinster, R.L. (1987). Cell lineage ablation in transgenic mice by cell-specific expression of a toxin gene. *Cell* 50, 435-443.
- Pangburn, M.K., and Muller-Eberhard, H.J. (1986). The C3 convertase of the alternative pathway of human complement. Enzymic properties of the bimolecular proteinase. *Biochem. J.* 235, 723-730.
- Perona, J.J., and Craik, C.S. (1997). Evolutionary divergence of substrate specificity within the chymotrypsin-like serine protease fold. *J. Biol. Chem.* 272, 29987-29990.
- Ponnuraj, K., Xu, Y., Macon, K., Moore, D., Volanakis, J.E., and Narayana, S.V. (2004). Structural analysis of engineered Bb fragment of complement factor B: insights into the activation mechanism of the alternative pathway C3-convertase. *Mol. Cell* 14, 17-28.
- Rawal, N., and Pangburn, M.K. (2001). Structure/function of C5 convertases of complement. *Int. Immunopharmacol.* 1, 415-422.
- Roos, A., Nauta, A.J., Broers, D., Faber-Krol, M.C., Trouw, L.A., Drijfhout, J.W., and Daha, M.R. (2001). Specific inhibition of the classical complement pathway by C1q-binding peptides. *J. Immunol.* 167, 7052-7059.
- Shimaoka, M., Xiao, T., Liu, J.H., Yang, Y., Dong, Y., Jun, C.D., McCormack, A., Zhang, R., Joachimiak, A., Takagi, J., Wang, J.H., and Springer, T.A. (2003). Structures of the alpha L I domain and its complex with ICAM-1 reveal a shape-shifting pathway for integrin regulation. *Cell* 112, 99-111.
- Song, H.K., and Suh, S.W. (1998). Kunitz-type soybean trypsin inhibitor revisited: refined structure of its complex with porcine trypsin reveals an insight into the interaction between a homologous inhibitor from *Erythrina caffra* and tissue-type plasminogen activator. *J. Mol. Biol.* 275, 347-363.
- Storoni, L.C., McCoy, A.J., and Read, R.J. (2004). Likelihood-enhanced fast rotation functions. *Acta Crystallogr. D Biol. Crystallogr.* 60, 432-438.
- Tomana, M., Niemann, M., Garner, C., and Volanakis, J.E. (1985). Carbohydrate composition of the second, third and fifth components and factors B and D of human complement. *Mol. Immunol.* 22, 107-111.
- Walport, M.J. (2001a). Complement. First of two parts. *N. Engl. J. Med.* 344, 1058-1066.
- Walport, M.J. (2001b). Complement. Second of two parts. *N. Engl. J. Med.* 344, 1140-1144.
- Wattanasin, S., Kallen, J., Myers, S., Guo, Q., Sabio, M., Ehrhardt, C., Albert, R., Hommel, U., Weckbecker, G., Welzenbach, K., and Weitz-Schmidt, G. (2005). 1,4-Diazepane-2,5-diones as novel inhibitors of LFA-1. *Bioorg. Med. Chem. Lett.* 15, 1217-1220.
- Winn, M.D., Isupov, M.N., and Murshudov, G.N. (2001). Use of TLS parameters to model anisotropic displacements in macromolecular refinement. *Acta Crystallogr. D Biol. Crystallogr.* 57, 122-133.

# 3

## **Factor B structure provides insights into activation of the central protease of the complement system**

**Fin J. Milder<sup>1</sup>, Lucio Gomes<sup>1</sup>, Arie Schouten<sup>1</sup>, Bert J.C. Janssen<sup>1</sup>, Eric G. Huizinga<sup>1</sup>, Roland A. Romijn<sup>2</sup>, Wieger Hemrika<sup>2</sup>, Anja Roos<sup>3</sup>, Mohamed R. Daha<sup>3</sup> and Piet Gros<sup>1</sup>**

<sup>1</sup>Crystal and Structural Chemistry, Bijvoet Center for Biomolecular Research, Faculty of Sciences; and, <sup>2</sup>ABC Expression Center, Utrecht University, Padualaan 8, 3584 CH Utrecht, The Netherlands. <sup>3</sup>Dept. of Nephrology, Leiden University Medical Center, 2300 RC Leiden, The Netherlands

Nature Structural and Molecular Biology, 3, 224-228 (2007)

## Abstract

Factor B is the central protease of the complement system of immune defense. Here, we present the crystal structure of human factor B at 2.3-Å resolution, which reveals how the five-domain pro-enzyme is kept securely inactive. The canonical activation helix of the Von Willebrand factor A (VWA) domain is displaced by a helix from the preceding domain linker. The two helices conformationally link the scissile-activation peptide and the metal-ion dependent adhesion site (MIDAS) required for binding of the ligand C3b. The data suggest that C3b binding displaces the three N-terminal complement-control-protein (CCP) domains and reshuffles the two central helices. Reshuffling of the helices releases the scissile bond for final proteolytic activation and generates a new interface between the VWA and serine protease (SP) domain. This allosteric mechanism is crucial for the tight regulation of the complement-amplification step in the immune response.

## Introduction

Factor B is a tightly regulated, highly specific serine protease. In its activated form it catalyzes the central amplification step of complement activation to initiate inflammatory responses, cell lysis, phagocytosis and B-cell stimulation (Carroll 2004; Walport 2001). Factor B is activated through an assembly process. Factor B binds to surface-bound C3b, or its fluid phase counterpart C3(H<sub>2</sub>O), after which it is cleaved by factor D into fragments Ba (res. 1-234) and Bb (res. 235-739) (Fishelson et al., 1984; Xu et al., 2001). Fragment Ba dissociates from the complex, leaving behind the alternative pathway C3-convertase complex C3b-Bb, which cleaves C3 into C3a and C3b (see Figure. 3.1A). This protease complex is intrinsically instable. Once dissociated from the complex Bb cannot re-associate with C3b (Pangburn and Muller-Eberhard 1986). A similar C3-convertase complex is formed upon activation of the classical (antibody-mediated) and lectin-binding pathways, comprised of C4 and C2, which are homologous to C3 and factor B respectively. The pro-enzyme factor B consists of three N-terminal CCP domains, connected by a 45-residue linker to a VWA domain and a C-terminal SP domain, which carries the catalytic center (Figure. 3.1A). Domains VWA and SP form fragment Bb; and, CCP1-3 and the linker form fragment Ba. Binding of factor B to C3b depends on elements in the Ba fragment (Prydzial and Isenman 1987) and the Mg<sup>2+</sup>-dependent MIDAS motif in the VWA domain of Bb (Horiuchi et al., 1991). The VWA domain is structurally homologous to inserted (I) domains in integrins. In I domains ligand binding to the MIDAS is coupled to a ~10-Å shift of the  $\alpha$ 7-activation helix with

concomitant domain rearrangements that activate the integrins (Emsley et al., 2000; Springer 2006). Structures of a truncated Bb fragment (Ponnuraj et al., 2004) and its full-length homolog C2a (Milder et al., 2006) show variable positions of the  $\alpha$ 7-activation helix affecting the orientation of the VWA and SP domains, which indicates that a related mechanism may occur in convertase formation and dissociation. These structures, however, do not reveal the regulation of the proteolytic activity of factor B. In particular, it is unclear how factor B is maintained in its inactive, zymogen state and how C3b binding makes factor B susceptible to proteolytic activation by factor D. To gain insights into the regulatory mechanisms underlying complement activation we set out to determine the structure of human pro-enzyme factor B.

## Results

### Overall structure of factor B

Here we present the crystal structure of human, pro-enzyme factor B at 2.3-Å resolution (see Methods and Supplementary Figure. 1). The overall structure (Figure. 3.1B) consists of three lobes, which is in agreement with electron micrographs (Smith et al., 1984). One lobe represents the trypsin-like SP domain with the catalytic site in a fully exposed position. The other two lobes represent the VWA domain with its  $\alpha/\beta/\alpha$  fold and the CCP1-3 domains with their typical  $\beta$ -sandwich fold stabilized by pairs of disulphide bonds. The long CCP3-VWA linker, containing the Arg234 – Lys235 scissile bond, forms a short loop (res. 198-201), a  $\alpha$  helix (res. 202-213) and a long loop (res. 214-242), which is partially disordered (res. 219-232 are not observed in the electron density). Unexpectedly the observed linker helix, denoted  $\alpha$ L, is integrated in the VWA domain and occupies the position of the  $\alpha$ 7-activation helix in Bb (Ponnuraj et al., 2004) (Figure. 3.2A). The displaced  $\alpha$ 7 helix lies adjacent to  $\alpha$ L on the surface of the VWA domain. These two helices lie at the center of the five-domain molecule and affect the domain-domain arrangement (Figure 3.1B). They provide a conformational link between two key regulatory sites of the molecule: the Mg<sup>2+</sup>-dependent C3b-binding MIDAS on one side and the activation scissile bond Arg234 – Lys235 on the opposite side of the molecule.

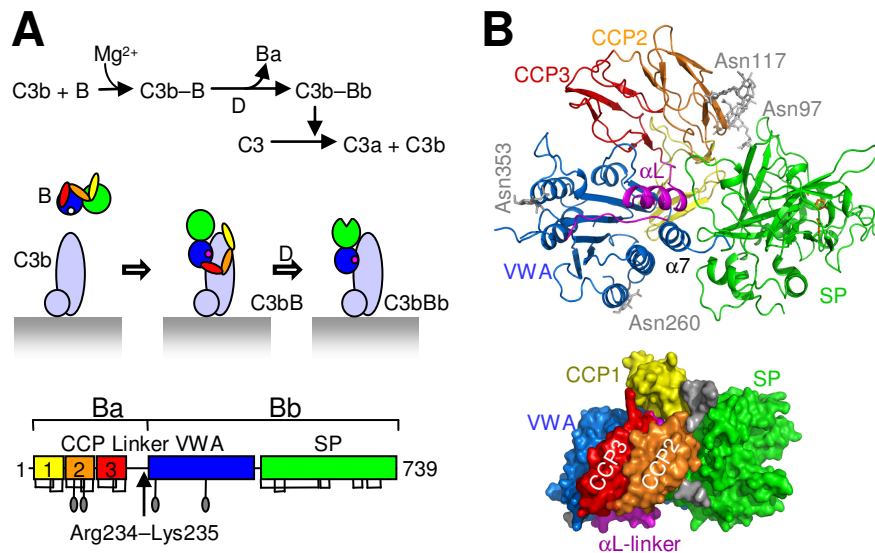


**Figure 3.1 C3-convertase formation and crystal structure of complement factor B.**

**A)** Schematic and cartoon representation of C3-convertase formation (top and middle panel; cartoon of C3b is based on crystal structure (Janssen et al., 2006; Wiesmann et al., 2006)); and, domain topology of factor B, indicated are the N-linked glycans, the disulphide bridges and the Arg234-Lys235 scissile bond (lower panel). **B)** Structure of factor B shown in ribbon representation colored by domains as in **a** (top panel). The linker connecting CCP3 and VWA is colored purple. The N-linked glycans (grey) and the catalytic triad Asp-His-Ser (brown) are presented in stick model. Labels indicate the centrally positioned helices  $\alpha L$  and  $\alpha 7$ . Bottom panel – factor B shown in surface representation, domains colored as indicated and glycans shown in grey (rotated by  $90^\circ$  with respect to figure in top panel).

### VWA domain adopts locked conformation

The VWA domain in factor B adopts an inactive conformation with a displaced helix  $\alpha 7$  and distorted MIDAS, which we refer to as a “locked” conformation. The inactive-closed and active-open conformational states of VWA and I domains are characterized predominantly by the conformation of loop  $\beta F\alpha 7$ , helix  $\alpha 7$  and the neighbouring helix  $\alpha 1$  (Figure 3.2B) (Emsley et al., 2000; Shimaoka et al., 2003). In factor B helix  $\alpha 7$  is displaced from its normal binding groove by helix  $\alpha L$  (Figure 3.2A). The preceding loop  $\beta F\alpha 7$  adopts a canonical closed conformation as shown by the positions of its hydrophobic ratchet residues (Val430, Leu436; see Figure 3.2B and Supplementary Figure 3.2). Also helix  $\alpha 1$  is positioned according to the inactive-closed conformation. Thus, the unliganded VWA domain displays an inactive conformation, as would be expected for the pro-enzyme state of factor B. Moreover, helix  $\alpha L$  obstructs the  $\alpha 7$ -activation helix from taking its normal position as observed in VWA and I domains (Bhattacharya et al., 2004; Emsley et al., 1997; 2000; Milder et al., 2006; Ponnuraj et al., 2004; Shimaoka et al., 2003),



thereby locking the VWA domain in its inactive conformation. Typically a closed-inactive domain conformation is coupled to a MIDAS conformation with a low affinity for ligands. In factor B, compared to Bb, displacements up to 5.5 Å in loops  $\beta A\alpha 1$  and  $\beta D\alpha 5$  distort the MIDAS (Figure 3.2C and Supplementary Figure 3.2). The distorted conformation indicates reduced divalent-ion binding. Moreover, we do not observe electron density for an ion bound to the MIDAS in factor B. The absence of an ion is consistent with the notion that Bb, but not factor B, has high affinity for divalent ions (Fishelson et al., 1983). The neighbouring CCP1 domain possibly affects the MIDAS conformation. First, Gln28 of loop  $\beta 2\beta 3$  in CCP1 makes a hydrogen bond to Asp254 located in the displaced VWA  $\beta A\alpha 1$  loop. Second, CCP1 possibly prevents loop  $\beta A\alpha 1$  from assuming the conformation seen in Bb by obstructing the glycan at Asn260. Instead, in factor B helix  $\alpha 1$  is shifted and partially unwound pointing the glycan on Asn260 away from the neighbouring CCP1 domain (Figure 3.2C). Factor B with D254G and N260D single and double mutations (where N260D deletes the N-glycosylation site) forms convertases more readily and more stably than wild-type factor B (Hourcade et al., 2002; Hourcade et al., 1999), indicating that these mutations promote the transition from an inactive to an active conformation of the VWA domain.

### Central role for linker region

The CCP3-VWA linker helix  $\alpha L$  occupies the position of helix  $\alpha 7$  of the VWA domain; and, binds Arg234 of the scissile bond preventing proteolytic activation. By virtue of its short-chain hydrophobic residues, helix  $\alpha L$  is squeezed in between helix  $\alpha 7$  and the VWA core, effectively blocking helix  $\alpha 7$  (Figure 3.2A). Following the helix  $\alpha L$  the CCP3-VWA linker forms a long loop and folds back to the C-terminal end of helix  $\alpha L$  (Figure 3.2D). Here, the scissile bond Arg234 – Lys235 is located and is being buried by the preceding, flexible loop. The side chain of Arg234, critical for substrate binding at the S1 pocket (Schechter and Berger notation) of factor D, is bound to both helix  $\alpha L$  (Glu207) and helix  $\alpha 7$  (Glu446) by salt bridges (Figure 3.2D). Thus, the scissile bond is protected in factor B from proteolysis by factor D and is conformationally linked to helices  $\alpha L$  and  $\alpha 7$ . In contrast, the scissile bond in isolated VWA domains is susceptible to factor D cleavage (Williams et al., 1999), because they lack the  $\alpha L$ - $\alpha 7$  arrangement that locks the P1 residue (Arg234). In the formation of the convertase, binding of C3b to factor B likely induces reshuffling of helices  $\alpha L$  and  $\alpha 7$  that liberates the P1-Arg residue and makes the scissile bond accessible for proteolysis by factor D.

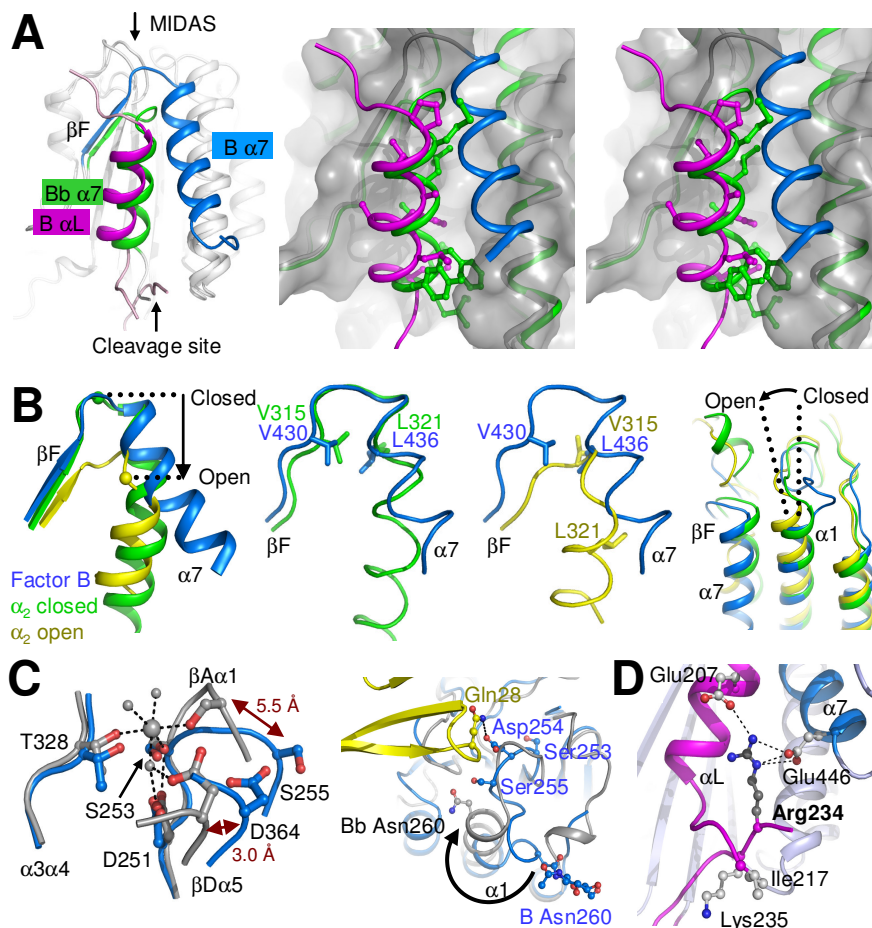


**Figure 3.2** Regulatory elements in the VWA domain.

**A** Dislocation of helix  $\alpha 7$  by helix  $\alpha L$ . Overlay of the VWA domains of factor B and Bb (PDB entry 1rrk) showing the displacement of helix  $\alpha 7$  (blue in factor B, green in Bb) by linker helix  $\alpha L$  (purple); and, stereo figure showing the packing of helices  $\alpha 7$  and  $\alpha L$  against the body of the VWA domain of factor B (grey, surface representation). Factor B (white) and Bb (green) are shown in ribbon representation with factor B helices  $\alpha L$  and  $\alpha 7$  colored purple and blue respectively. Hydrophobic residues of helices  $\alpha L$  (B) and  $\alpha 7$  (Bb) are shown in ball-and-stick. **B** Conformation of loop  $\beta F\alpha 7$  and helices  $\alpha 7$  and  $\alpha 1$ . Overlay of VWA domains of factor B (blue) with closed (green) and open (yellow) conformations of the  $\alpha 2$  I-domain (PDB entries 1aox and 1dzi respectively), showing strand  $\beta F$  and helix  $\alpha 7$  (left panel), positions of hydrophobic 'ratchet' residues (sticks) of loop  $\beta F\alpha 7$  and helix  $\alpha 7$  (middle two panels) and position of helix  $\alpha 1$  (right-panel). **C** Distortion of the  $Mg^{2+}$ -dependent MIDAS C3b binding site. Superposition of the MIDAS motif in factor B (blue) and Bb (grey) in stick model (left panel). Grey spheres represent water molecules (small spheres) and the bound ion (large sphere) as observed in Bb. Orientation of CCP1 (yellow) and VWA (blue) in factor B with the VWA domain of Bb (grey) superposed (right panel). Shown in ball-and-stick representation are the adjoining residues Gln28 and Asp254 and the glycosylation site Asn260. **D** The P1 residue of the buried scissile bond (Arg234 – Lys235) interacts with helices  $\alpha 7$  (blue) and linker helix  $\alpha L$  (purple) via salt-bridges.

### Conformation of the catalytic SP domain

In both factor B and Bb (Ponnuraj et al., 2004) the SP domain is exposed with the catalytic site freely accessible to small substrates (Kam et al., 1987). The two structures differ markedly in the VWA-SP domain orientation (Figure 3.3A). In factor B the VWA-SP interface is dominated by the helices  $\alpha_L$  and  $\alpha_7$ , with the N-terminal loop of SP folding over helix  $\alpha_L$ ; furthermore, contacts are observed between SP and domains CCP1 and 2. In Bb, where  $\alpha_L$  and the CCP1-3 domains are absent, SP rotates  $68^\circ$  and contacts helices  $\alpha_7$ ,  $\alpha_1$  and  $\alpha_3$  of the VWA domain. In addition to the interface loops, loop 2 of the SP domain shows marked differences between factor B and Bb. Putatively, Arg705 of this loop (similar to Arg696 in C2a (Milder et al., 2006)) induces formation of the oxyanion hole, similar to the N-terminus in trypsin after proteolytic activation of trypsinogen (Khan and James 1998). Consistent with this model, the guanidinium group of the arginine interacts with an aspartate of the oxyanion-hole loop in Bb and C2a (Supplementary Figure 3.3). In factor B loop 2 folds back towards the N-glycosylated Asn97 on CCP2 (weak electron density for the side chains indicates disorder in loop 2). Concomitant, the guanidinium group of Arg705 is displaced by 11 Å, as would be expected for the zymogen state. Nevertheless, the conformation of the oxyanion hole is identical between factor B and Bb, i.e. in factor B the oxyanion-hole loop does not adopt the zymogen state. This indicates that proteolytic activity of factor B is probably not controlled directly as in trypsinogens, but rather through quaternary rearrangement of the domains in the assembly process.

### Triad of CCP domains

The three CCP domains of Ba adopt an unexpected triad arrangement, with domains CCP2 and 3 packed tightly (Supplementary Table 3.1) into an anti-parallel dimer capped by CCP1. This arrangement produces a small hydrophobic core at the triad center (Figure 3.3B). Changes in the CCP2-3 interface reduce C3b binding and hemolytic activity (Hourcade et al., 1995; Xu and Volanakis 1997); and, antibodies directed against CCP1 and CCP3 block hemolytic activity (Hourcade et al., 1995; Thurman et al., 2005) (Supplementary Figure 4.4), indicating that the triad of CCP domains provides an important binding site for C3b. Domain CCP1 likely hinders access of the ligand C3b to the Mg<sup>2+</sup>-dependent MIDAS of the VWA domain (Supplementary Figure 3.5).

Because the triad of CCP domains appears to be only weakly associated with the VWA and SP domains (Supplementary Figure 3.4 and Supplementary Table 3.2), we hypothesize that binding of the CCP domains to C3b will dislocate the CCP triad from the VWA and SP domains. Concomitantly, dislocation of the CCP triad may be coupled, through the short CCP3- $\alpha$ L connecting loop (Figure 3.3B), to displacement of the helix  $\alpha$ L from its binding groove in the VWA domain.

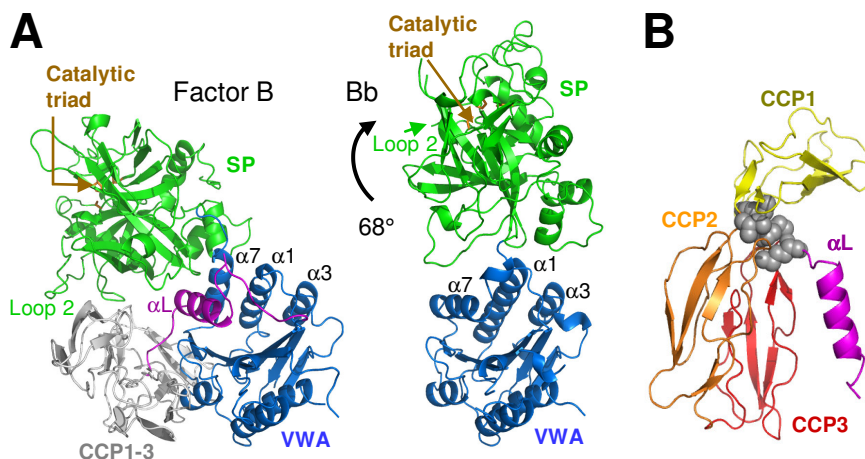


**Figure 3.3 Domain orientations in factor B and Bb.**

**A)** Orientation of VWA (blue) and SP (green) in factor B with linker and linker helix  $\alpha$ L shown in purple and CCP1-3 domains in grey (left panel); and orientation of VWA and SP in Bb (PDB entry 1rrk). Indicated are helices  $\alpha$ L,  $\alpha$ 1,  $\alpha$ 3 and  $\alpha$ 7, which are involved in the VWA-SP interfaces. **B)** The CCP triad arrangement in ribbon representation with CCP1 (yellow), CCP2 (orange) and CCP3 (red). Grey spheres indicate the four residues (Tyr42, Ile76, Phe197 and Met198) forming the hydrophobic triad center. The adjoining linker containing helix  $\alpha$ L is colored purple.

## Discussion

Factor B is activated by binding surface-bound C3b and subsequent cleavage by factor D. Our data reveal the conformation that keeps factor B locked in its proenzyme state. The structure adds this locked conformation to the open and closed conformations described in past studies of the VWA and I domains (Emsley et al., 2000; Springer 2006) and provides insights into a previously uncharacterized mechanism for regulating serine protease activity (Khan and James 1998). Assembly of an active protease complex likely proceeds through a number of steps. We hypothesize that initial binding of C3b dislocates the CCP triad.

In turn, dislocation of the CCPs likely induces formation of an active MIDAS and allows access of the large C3b ligand. Concomitantly, the blocking helix  $\alpha$ L will be displaced from its position in the VWA domain, thereby allowing the activation helix  $\alpha$ 7 to take its normal location. Rearrangement of helices  $\alpha$ L and  $\alpha$ 7 will liberate the bound scissile peptide, making it accessible for proteolytic cleavage by factor D. Cleavage of the scissile bond results in dissociation of the Ba fragment yielding the active, short-lived protease complex that cleaves C3 into C3a and C3b. Thus, the tight regulation of complement activation is determined by a series of conformational changes that establish the C3 convertase activity required for amplification, which is crucial for the biological functions of the complement system.

## Methods

### Protein expression, purification and crystallization

Human factor B fused to a N-terminal GlySer-(His)<sub>6</sub>-GlySer-tag was expressed in human embryonic kidney 293S GnT<sup>-</sup> cells to prevent complex and heterogeneous N-linked glycosylation (Reeves et al., 2002). Secreted factor B was purified from the expression medium via immobilized metal affinity chromatography followed by size exclusion chromatography. The purified protein showed a single band of 90 kDa on coomassie stained SDS-PAGE gels and on Western blots probed with an  $\alpha$ His<sub>6</sub>-antibody. Details of factor B expression and purification are given in the Supplementary Methods. Crystals were grown by hanging drop vapor diffusion by mixing 1  $\mu$ l factor B (13 mg/ml) in 10 mM tris(hydroxymethyl)-aminomethane (pH 7.4), 25 mM arginine, 25 mM glutamic acid and 1  $\mu$ l well solution (50 mM malic-acid 2-(N-morpholino)ethanesulfonic acid tris(hydroxymethyl)-aminomethane buffer (pH 6.5), and 12% (w/v) PEG 1500) at 20 °C. Glycerol (20% v/v) was added to the well solution before flash cooling of the crystal in liquid nitrogen. The crystal diffracted to 2.3 Å resolution at the ESRF beam line ID14-EH4. The space group of the crystal was identified as *P*3<sub>1</sub>21 ( $a = b = 104.0$  and  $c = 151.1$  Å). Data were processed by MOSFLM and CCP4 (CCP4 1994). Crystallographic data collection and refinement statistics are given in Table 3.1.

### Structure determination

The SP and VWA domain were placed by molecular replacement using Phaser (Storoni et al., 2004) with structures of the isolated SP (Jing et al., 2000) (pdb code 1dle) and VWA (Bhattacharya et al., 2004) (pdb code 1q0p) domains of factor B as search models. Subsequent placement of the three CCP domains using various

homologous structures, as well as model completion by automated model building using ARP/wARP (Perrakis et al., 1999), failed at this stage.

**Table 1 Data collection and refinement statistics**

Data collection statistics	
	Factor B
Space group	$P3_121$
Cell dimensions	
<i>a</i> , <i>b</i> , <i>c</i> (Å)	104.0, 104.0, 151.1
$\alpha$ , $\beta$ , $\gamma$ (°)	90, 90, 120
Resolution (Å)	60.0-2.3 (2.42-2.30)*
$R_{\text{merge}}$	10.8 (56.1)
$I / \sigma I$	10.4 (2.6)
Completeness (%)	99.8 (100)
Redundancy	4.1 (4.1)
Refinement statistics	
Resolution (Å)	60.0-2.30
No. reflections	40,409
$R_{\text{work}} / R_{\text{free}}$	0.195 / 0.241
No. atoms	
Protein	5,745
Ligand/ion	78
Water	295
<i>B</i> -factors (Å <sup>2</sup> )	
Protein	33.5
Ligand/ion	58.1
Water	31.6
R.m.s. deviations	
Bond lengths (Å)	0.010
Bond angles (°)	1.30

\*Values in parentheses are for highest-resolution shell.

The VWA helix  $\alpha 7$  and SP domain loops C and D were rebuilt and the partial model was refined using COOT (Emsley and Cowtan 2004), RESOLVE (Terwilliger 2003) and REFMAC5 (Winn et al., 2001). Using this partial model ARP/wARP now successfully completed the model to ~80%. Iterative cycles of refinement with REFMAC5 and model building in COOT were used to finalize the model. The refined model of factor B contains 710 residues; residues 1-8, 218-232, 321-326, and 344-346 were excluded from the model due to poor electron density.  $R$  and  $R_{\text{free}}$  values were 19.5 and 24.1%, respectively (see Table 3.1 for refinement statistics). All molecular graphic figures were generated with pymol (W. Delano; <http://pymol.sourceforge.net>).

## Coordinates

Protein Data Bank: Coordinates and structure factors have been deposited with accession code 2OK5.

## Acknowledgements

We acknowledge the European Synchrotron Radiation Facility for provision of synchrotron radiation facilities and we would like to thank the beamline scientists at ID-14-EH4 for their help with data collection. This work was supported by a “Pionier” programme grant (P.G.) of the Council for Chemical Sciences of the Netherlands Organization for Scientific Research (NWO-CW).

## Author Information

Reprints and permissions information is available at [www.nature.com/reprintsandpermissions](http://www.nature.com/reprintsandpermissions). The authors declare no competing financial interests. Correspondence and requests for materials should be addressed to P.G. (p.gros@chem.uu.nl).

## References

- Bhattacharya, A.A., Lupper, M.L., Jr., Staunton, D.E., and Liddington, R.C. (2004). Crystal structure of the A domain from complement factor B reveals an integrin-like open conformation. *Structure (Camb)* *12*, 371-378.
- Carroll, M.C. (2004). The complement system in regulation of adaptive immunity. *Nat. Immunol.* *5*, 981-986.
- CCP4 (1994). The CCP4 suite: programs for protein crystallography. *Acta Crystallogr. D Biol. Crystallogr.* *50*, 760-763.
- Emsley, J., King, S.L., Bergelson, J.M., and Liddington, R.C. (1997). Crystal structure of the I domain from integrin alpha2beta1. *J. Biol. Chem.* *272*, 28512-28517.
- Emsley, J., Knight, C.G., Farndale, R.W., Barnes, M.J., and Liddington, R.C. (2000). Structural basis of collagen recognition by integrin alpha2beta1. *Cell* *101*, 47-56.
- Emsley, P., and Cowtan, K. (2004). Coot: model-building tools for molecular graphics. *Acta Crystallogr. D Biol. Crystallogr.* *60*, 2126-2132.
- Fishelson, Z., Pangburn, M.K., and Muller-Eberhard, H.J. (1983). C3 convertase of the alternative complement pathway. Demonstration of an active, stable C3b, Bb (Ni) complex. *J. Biol. Chem.* *258*, 7411-7415.
- Fishelson, Z., Pangburn, M.K., and Muller-Eberhard, H.J. (1984). Characterization of the initial C3 convertase of the alternative pathway of human complement. *J. Immunol.* *132*, 1430-1434.

- Horiuchi, T., Macon, K.J., Engler, J.A., and Volanakis, J.E. (1991). Site-directed mutagenesis of the region around Cys-241 of complement component C2. Evidence for a C4b binding site. *J. Immunol.* *147*, 584-589.
- Hourcade, D.E., Mitchell, L., Kuttner-Kondo, L.A., Atkinson, J.P., and Medof, M.E. (2002). Decay-accelerating factor (DAF), complement receptor 1 (CR1), and factor H dissociate the complement AP C3 convertase (C3bBb) via sites on the type A domain of Bb. *J. Biol. Chem.* *277*, 1107-1112.
- Hourcade, D.E., Mitchell, L.M., and Oglesby, T.J. (1999). Mutations of the type A domain of complement factor B that promote high-affinity C3b-binding. *J. Immunol.* *162*, 2906-2911.
- Hourcade, D.E., Wagner, L.M., and Oglesby, T.J. (1995). Analysis of the short consensus repeats of human complement factor B by site-directed mutagenesis. *J. Biol. Chem.* *270*, 19716-19722.
- Janssen, B.J., Christodoulidou, A., McCarthy, A., Lambris, J.D., and Gros, P. (2006). Structure of C3b reveals conformational changes that underlie complement activity. *Nature* *444*, 213-216.
- Jing, H., Xu, Y., Carson, M., Moore, D., Macon, K.J., Volanakis, J.E., and Narayana, S.V. (2000). New structural motifs on the chymotrypsin fold and their potential roles in complement factor B. *Embo J.* *19*, 164-173.
- Kam, C.M., McRae, B.J., Harper, J.W., Niemann, M.A., Volanakis, J.E., and Powers, J.C. (1987). Human complement proteins D, C2, and B. Active site mapping with peptide thioester substrates. *J. Biol. Chem.* *262*, 3444-3451.
- Khan, A.R., and James, M.N. (1998). Molecular mechanisms for the conversion of zymogens to active proteolytic enzymes. *Protein Sci.* *7*, 815-836.
- Milder, F.J., Raaijmakers, H.C., Vandeputte, M.D., Schouten, A., Huizinga, E.G., Romijn, R.A., Hemrika, W., Roos, A., Daha, M.R., and Gros, P. (2006). Structure of complement component c2a: implications for convertase formation and substrate binding. *Structure* *14*, 1587-1597.
- Pangburn, M.K., and Muller-Eberhard, H.J. (1986). The C3 convertase of the alternative pathway of human complement. Enzymic properties of the bimolecular proteinase. *Biochem. J.* *235*, 723-730.
- Perrakis, A., Morris, R., and Lamzin, V.S. (1999). Automated protein model building combined with iterative structure refinement. *Nat. Struct. Biol.* *6*, 458-463.
- Ponnuraj, K., Xu, Y., Macon, K., Moore, D., Volanakis, J.E., and Narayana, S.V. (2004). Structural analysis of engineered Bb fragment of complement factor B: insights into the activation mechanism of the alternative pathway C3-convertase. *Mol. Cell* *14*, 17-28.
- Pryzdial, E.L., and Isenman, D.E. (1987). Alternative complement pathway activation fragment Ba binds to C3b. Evidence that formation of the factor B-C3b complex involves two discrete points of contact. *J. Biol. Chem.* *262*, 1519-1525.
- Reeves, P.J., Callewaert, N., Contreras, R., and Khorana, H.G. (2002). Structure and function in rhodopsin: high-level expression of rhodopsin with restricted and homogeneous N-glycosylation by a tetracycline-inducible N-acetylglucosaminyltransferase I-negative HEK293S stable mammalian cell line. *Proc. Natl. Acad. Sci. U S A* *99*, 13419-13424.
- Shimaoka, M., Xiao, T., Liu, J.H., Yang, Y., Dong, Y., Jun, C.D., McCormack, A., Zhang, R., Joachimiak, A., Takagi, J., Wang, J.H., and Springer, T.A. (2003). Structures of the alpha L I domain and its complex with ICAM-1 reveal a shape-shifting pathway for integrin regulation. *Cell* *112*, 99-111.
- Smith, C.A., Vogel, C.W., and Muller-Eberhard, H.J. (1984). MHC Class III products: an electron microscopic study of the C3 convertases of human complement. *J. Exp. Med.* *159*, 324-329.
- Springer, T.A. (2006). Complement and the Multifaceted Functions of VWA and Integrin I Domains. *Structure* *14*, 1611-1616.
- Storoni, L.C., McCoy, A.J., and Read, R.J. (2004). Likelihood-enhanced fast rotation functions. *Acta Crystallogr. D Biol. Crystallogr.* *60*, 432-438.



- Terwilliger, T.C. (2003). Automated main-chain model building by template matching and iterative fragment extension. *Acta Crystallogr. D Biol. Crystallogr.* *59*, 38-44.
- Thurman, J.M., Kraus, D.M., Girardi, G., Hourcade, D., Kang, H.J., Royer, P.A., Mitchell, L.M., Giclas, P.C., Salmon, J., Gilkeson, G., and Holers, V.M. (2005). A novel inhibitor of the alternative complement pathway prevents antiphospholipid antibody-induced pregnancy loss in mice. *Mol. Immunol.* *42*, 87-97.
- Walport, M.J. (2001). Complement. First of two parts. *N. Engl. J. Med.* *344*, 1058-1066.
- Wiesmann, C., Katschke, K.J., Yin, J., Helmy, K.Y., Steffek, M., Fairbrother, W.J., McCallum, S.A., Embuscado, L., DeForge, L., Hass, P.E., and van Lookeren Campagne, M. (2006). Structure of C3b in complex with CRIg gives insights into regulation of complement activation. *Nature* *444*, 217-220.
- Williams, S.C., Hinshelwood, J., Perkins, S.J., and Sim, R.B. (1999). Production and functional activity of a recombinant von Willebrand factor-A domain from human complement factor B. *Biochem. J.* *342 Pt 3*, 625-632.
- Winn, M.D., Isupov, M.N., and Murshudov, G.N. (2001). Use of TLS parameters to model anisotropic displacements in macromolecular refinement. *Acta Crystallogr. D Biol. Crystallogr.* *57*, 122-133.
- Xu, Y., Narayana, S.V., and Volanakis, J.E. (2001). Structural biology of the alternative pathway convertase. *Immunol. Rev.* *180*, 123-135.
- Xu, Y., and Volanakis, J.E. (1997). Contribution of the complement control protein modules of C2 in C4b binding assessed by analysis of C2/factor B chimeras. *J. Immunol.* *158*, 5958-5965.

## Supplementary information

### Methods

#### Cloning and expression of recombinant human factor B

The cDNA coding for human factor B was amplified by PCR from I.M.A.G.E. clone 2959706 (Open Biosystems). Forward primer (5'- GGATCCACTCCAT GGTCTTTGGCCCCGCCCCAGGGCTCCTGCTCTCTG-GAGGG-3') introduced a BamHI restriction site and reverse primer (5'-GCGGCCGCTAGAA AACCCAAATCCTCATCTTGGAGTTTCTCC-3') introduced a NotI re-striction site. The PCR product was cloned in the pCR4-TOPO vector (Invitrogen) and its sequence was verified. Subsequently, the factor B coding DNA was ligated in a modified pTT3 expression vector (Durocher et al., 2002) encoding a cystatin secretion signal (Barash et al., 2002) followed by a hexa-histidine tag. Suspension growing human embryonic kidney 293 GnTI<sup>-</sup> cells (Reeves et al., 2002) were transfected with polyethyleneimine at a density of 500,000 cells per ml, and recombinant factor B was transiently expressed at low serum concentration (~0.1% (v/v) fetal calf serum). To maximize expression of factor B the cells were co-transfected with a plasmid coding for the Epstein-Barr virus nuclear antigen 1 (EBNA-1) in a 3 to 1 ratio (factor B : EBNA-1). Medium was harvested 6 days post-transfection by centrifugation (30 minutes at 1,000 x g), concentrated (10-fold) and subsequently diafiltrated to 25 mM TRIS-HCl, 300 mM NaCl (pH 8.2), 5 mM benzamidine in a Quickstand bench top concentrator (GE Healthcare) with a 30 kDa molecular weight cut off filter. The concentrated material was stored at -20 °C until further use.

#### Purification of recombinant factor B

Frozen unpurified factor B was thawed and imidazole was added to a final concentration of 15 mM. Following removal of precipitates by centrifugation (20 minutes at 3,200 x g) the material was incubated overnight at 4 °C with Ni-NTA superflow (Qiagen) beads equilibrated in starting buffer (25 mM TRIS, 300 mM NaCl, pH 8.2) in a 1 to 25 v/v ratio. The beads were collected by centrifugation for 5 minutes at 400 x g and transferred to an empty XK-16 column (GE Healthcare). The column was connected to an Äkta FPLC (GE Healthcare) and extensively washed with starting buffer. Non-specifically bound proteins and recombinant factor B were eluted using 15 mM imidazole and 200 mM imidazole in starting buffer, respectively. Eluted fractions were collected and analyzed by coomassie stained SDS-PAGE gels. Factor B containing fractions were pooled and concentrated using a spin filter with a 5 kDa molecular weight cut off (Millipore) to a final volume of 1

ml. During concentration the buffer was exchanged to 10 mM TRIS-HCl, 150 mM NaCl, pH 7.4. Factor B was further purified by size exclusion chromatography using a superdex-200 column pre-equilibrated in 25 mM TRIS-HCl, 150 mM NaCl, pH 7.4. Fractions containing factor B were pooled and concentrated once more using a spin filter with a 5 kDa molecular-weight cut off (Millipore) to a final concentration of 13 mg/ml. During concentration the buffer was exchanged to 10 mM TRIS-HCl (pH 7.4), 25 mM NaCl, 25 mM arginine, 25 mM glutamic acid and stored at -80 °C until further use.

### **Completion of Bb model**

In the deposited structure of Bb (Ponnuraj et al., 2004), protein databank entry 1rrk, residue 705 (arginine) was not modeled. Electron density maps calculated from the deposited diffraction data indicated weak but significant density for this residue. The Bb model including this arginine was obtained by automated model building using ArpWarp (Perrakis et al., 1999) with the deposited Bb structure as starting model.

### **Hemolytic assay**

Hemolytic activity of recombinant factor B was determined by a B-dependent hemolytic assay, using B-depleted human serum (from Quidel) as a complement source. The method was analogous to that previously described for a hemolytic assay of the alternative pathway (AP50) (Roos et al., 2001). Rabbit erythrocytes ( $1 \cdot 10^7$ ) were incubated with 1/15 diluted B-deficient serum in the presence or absence of purified human recombinant B, normal human serum, or mock culture supernatant, in various dilutions, for one hour at 37 °C. The assay was performed using dextrose gelatin Veronal buffer<sup>2+</sup> containing MgEGTA (DGVB<sup>2+</sup>-MgEGTA) as a buffer, in a final volume of 200  $\mu$ l. DGVB<sup>2+</sup>-MgEGTA consists of 0.05% (w/v) gelatin, 167 mM glucose, 0.15 mM CaCl<sub>2</sub>, 5 mM MgCl<sub>2</sub> and 10 mM EGTA in veronal-buffered saline (1.8 mM Na-5,5-diethylbarbital, 0.2 mM 5,5-diethylbarbituric acid, 145 mM NaCl). Subsequent to addition of 1.5 ml phosphate-buffered saline and centrifugation, hemolysis was assessed by measuring the OD at 414 nm. Factor B hemolytic activity was calculated as a Z-value followed by calculation of hemolytic activity per ml and normalization for the concentration of B as determined by specific ELISA. The relative hemolytic activity of mutant B was calculated as a percentage of hemolytic activity of wild type B. With 70% hemolytic activity, recombinant human factor B is about as active as factor B from normal human serum.

## Tables

**Table S3.1 Analysis of CCP domains 1 to 3**

		CCP1	CCP2	CCP3
BSA (Å <sup>2</sup> )	CCP1	-	340	200
	CCP2	340	-	1340
	CCP3	200	1340	-
RMSD	CCP1	-	2.3	1.7
	CCP2	2.3	-	1.2
	CCP3	1.7	1.2	-

**Table S3.2 Contacts between domains CCP1-3 and the VWA and SP domains (Krissinel et al., 2005)**

CCP1-3			VWA			CCP1-3			SP		
residue	BSA	Δ <sup>l</sup> G	residue	BSA	Δ <sup>l</sup> G	residue	BSA	Δ <sup>l</sup> G	residue	BSA	Δ <sup>l</sup> G
R25	36.2	-0.77	D254	29.7	-0.31	G21	19.4	0.20	R460	37.2	-0.31
L27	26.1	0.42	R390	73.8	-0.94	G22	12.8	0.11	K461	14.7	-0.54
Q28	52.3	-0.08	G406	0.17	0.00	S23	17.8	0.01	K614	11.3	-0.07
A32	7.68	0.12	P407	83.6	1.29	V36	0.73	-0.01	E619	51.8	-0.18
E34	18.3	-0.06	L408	80.0	1.28	C37	0.95	0.02	Y621	9.50	-0.02
Q47	5.79	0.09	Q411	71.1	-0.42	P38	57.8	0.91	P663	6.25	-0.07
T48	30.4	0.36	V412	23.4	0.37	S39	35.9	0.41	Y664	89.3	0.73
T50	1.82	0.03	I414	2.01	0.03	F41	1.4	0.02	A665	3.67	-0.01
Q129	11.5	-0.13	N415	55.1	-0.35	V98	0.37	-0.00	K704	20.1	0.32
L158	9.20	0.15	S419	0.86	-0.01	S99	18.0	-0.21			
E159	17.3	0.12	K420	71.2	0.81	D100	2.94	-0.05			
T171	61.3	0.83	K421	10.3	-0.01	E101	11.1	-0.06			
L172	14.3	-0.16	D422	49.5	-0.16	G128	2.50	0.04			
R173	113	-1.14	N423	16.0	-0.18	Q129	49.0	0.04			
G174	36.7	-0.14	E424	12.1	-0.14						
S175	10.3	0.01	E425	23.4	-0.07						
R178	21.0	-0.30	V427	25.5	0.26						
Q181	0.33	0.01	F428	2.60	0.04						
E182	34.1	0.05	K429	19.2	-0.02						
W186	5.52	-0.06	K431	8.66	-0.10						
G188	34.9	0.12	D432	21.7	-0.30						
T189	64.2	0.39									
E190	3.46	-0.01									
Q194	21.5	0.22									
D195	12.2	-0.05									

BSA: The solvent-accessible surface area of the corresponding residue that is buried upon interface formation, in Å<sup>2</sup>

Δ<sup>l</sup>G: The solvation energy gain of the corresponding residue upon formation of the interface, in kcal/M

## Figures

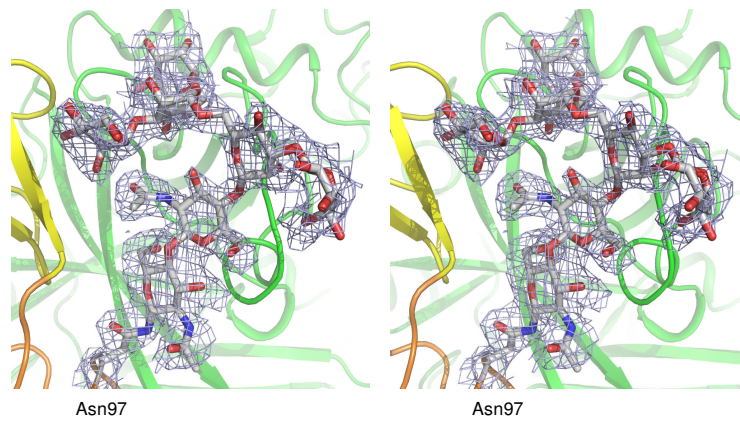


**Figure S3.1 Stereo figure showing the electron density for the N-linked glycan at Asn97.**

Electron density (2mFobs-DFcalc,  $\phi$ calc) contoured at 1  $\sigma$  of Man5-GlcNac2-Asn97 (shown in stick model), domains are shown in ribbon representation with CCP1 in yellow, CCP2 in orange, and the SP domain in green

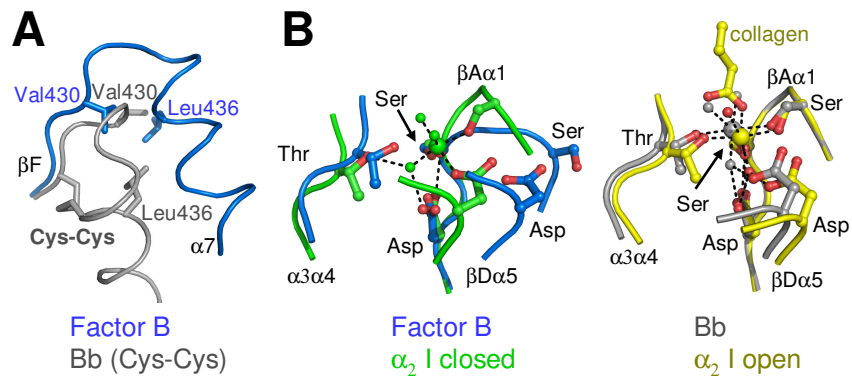


**Figure S3.2 Activation state of the VWA domain.**

**A)** Overlay of the VWA domain from factor B (blue) with Bb (1rrk, grey); position of hydrophobic 'ratchet' residues (stick) of loop  $\beta F\alpha 7$  and helix  $\alpha 7$ . **B)** Distortion of the MIDAS. Left panel – Superposition of the MIDAS motif in factor B (blue) and the closed  $\alpha 2$  I-domain (1aox, green). Right panel – Superposition of the MIDAS motif in Bb (1rrk, grey) and the open collagen bound  $\alpha 2$  I-domain (1dzi, yellow).

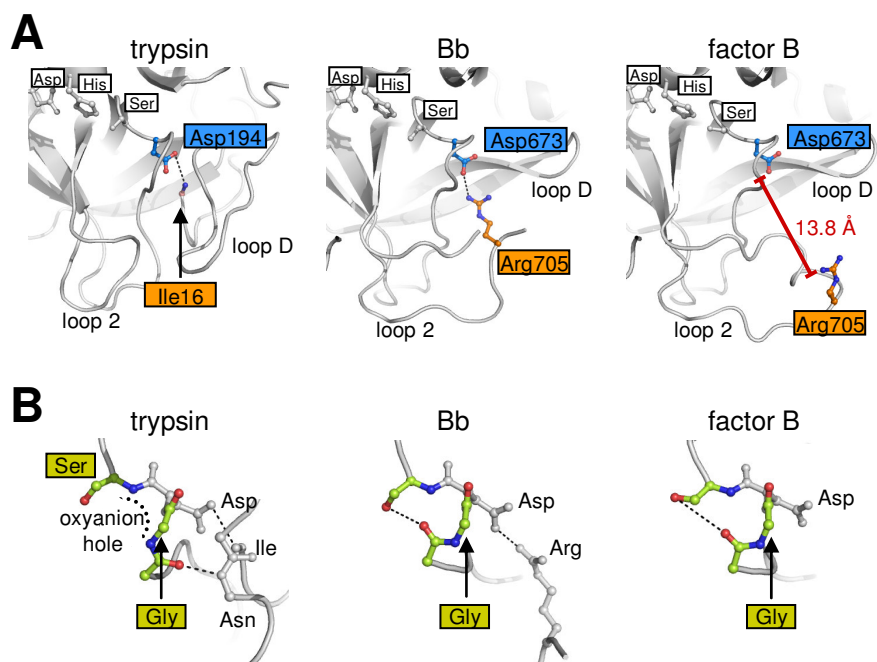


**Figure S3.3 The serine protease domain catalytic center.**

**A** The catalytic center of trypsin (Song and Suh 1998) (1aww), Bb (Ponnuraj et al., 2004) (1rrk) and factor B. Indicated is the interaction between the N-terminal Ile16 (orange) and Asp194 (blue), which is characteristic for activated trypsins. In Bb Arg705 replaces Ile-16. In factor B this arginine is positioned away from Asp-673. **B** The oxyanion holes of Bb (1rrk) and factor B are in an identical, near-active conformation with to an outward orientation of the glycine amide.

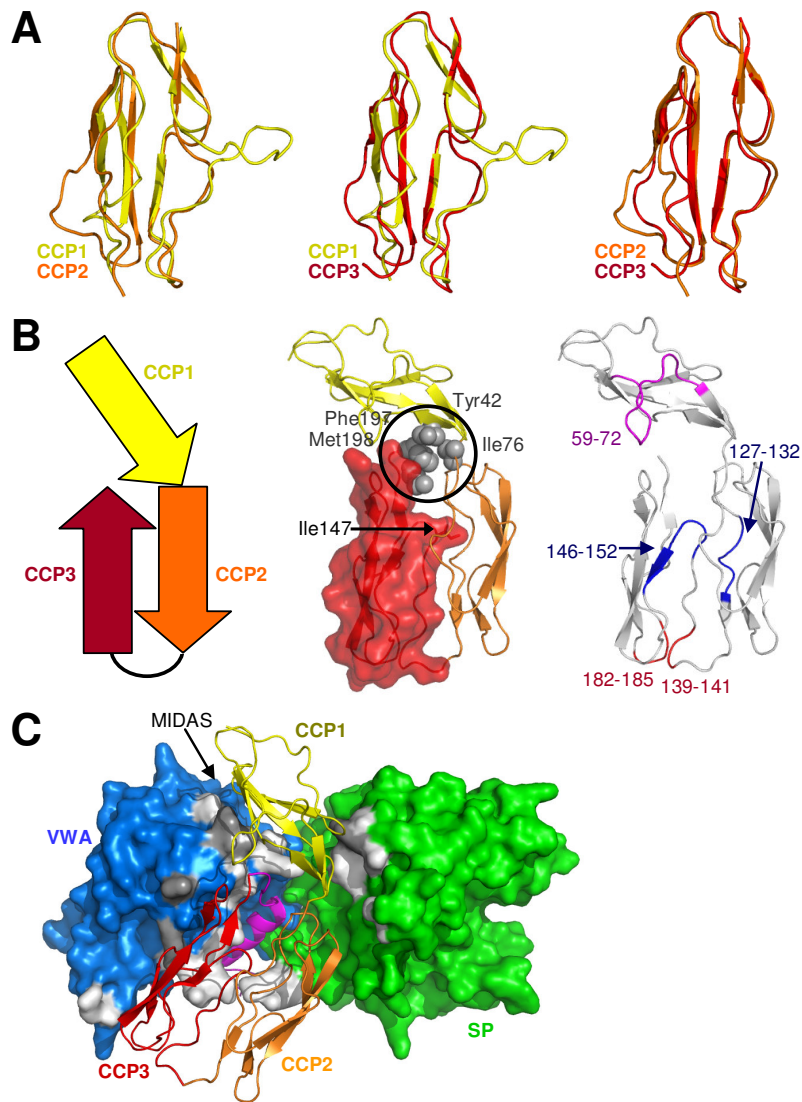


**Figure S3.4 The CCP triad arrangement.**

**A)** Overlays of the CCP domains shown in ribbon representation. **B)** Left panel - Schematic representation of the orientation of CCP domains 1 to 3. Middle panel - The CCP triad arrangement with CCP1 (yellow ribbons), CCP2 (orange ribbons) and CCP3 (red ribbon and transparent surface representation). Indicated are the four hydrophobic residues of the triad center and Ile147 of CCP3 that packs tightly into CCP2. Additional information is given in Supplemental Table S1. Right panel - Ribbon representation of CCP1-3; highlighted are segments (blue) in the CCP2-3 interface crucial for the factor B function (Hourcade et al., 1995; Xu and Volanakis 1997) and epitopes for monoclonal antibodies that reduce hemolytic activity upon binding; residues 59-728 and residues 138-141 with 182-185 (Thurman et al., 2005). **C)** Packing of CCP1-3 onto the VWA and SP domains. Shown are VWA (blue) and SP (green) in surface representation and CCP1-3 (yellow, orange and red) in ribbon representation. Grey areas represent contact area with dark grey indicating residues that yield gain in solvation energy upon formation of the interface (see Supplemental Table S2).

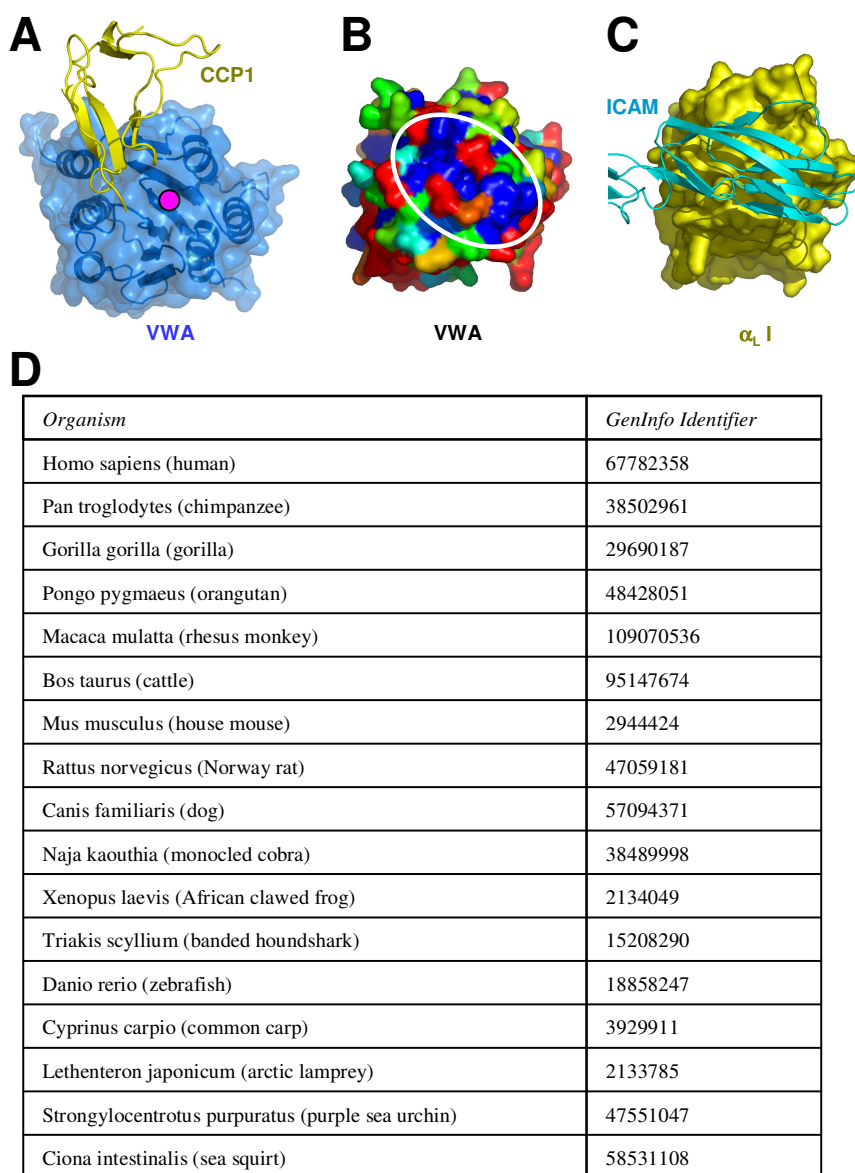


**Figure S3.5 The  $Mg^{2+}$ -dependent C3b binding site.**

**A** VWA domain in surface (transparent blue) and ribbon representation (green) with the position of CCP1 indicated in ribbon representation (yellow). The position of  $Mg^{2+}$  binding is indicated by a pink sphere. **B** Sequence conservation of the VWA domain based on a factor B alignment. In surface representation the VWA domain of Bb (Ponnuraj et al., 2004) (1rrk) colored from red (not conserved) to blue (conserved) (Landau et al., 2005). The white oval indicates the putative C3b contact site. **C** Shown for comparison is ICAM binding (light blue ribbons) to the same site of the I domain of integrin  $\alpha_L$  (Shimaoka et al., 2003) (1mq8, yellow surface representation). **D**) List of sequences used for the alignment in b.



## References

- Barash, S., Wang, W., and Shi, Y. (2002). Human secretory signal peptide description by hidden Markov model and generation of a strong artificial signal peptide for secreted protein expression. *Biochem. Biophys. Res. Commun.* 294, 835-842.
- Durocher, Y., Perret, S., and Kamen, A. (2002). High-level and high-throughput recombinant protein production by transient transfection of suspension-growing human 293-EBNA1 cells. *Nucleic Acids Res.* 30, E9.
- Hourcade, D.E., Wagner, L.M., and Oglesby, T.J. (1995). Analysis of the short consensus repeats of human complement factor B by site-directed mutagenesis. *J. Biol. Chem.* 270, 19716-19722.
- Krissinel, E. and Henrick, K. (2005). Detection of protein assemblies in crystals. Springer-Verlag Berlin Heidelberg M.R. Berthold *et.al.* (Eds.): *CompLife*, LNBI 3695, 163-174.
- Landau, M., Mayrose, I., Rosenberg, Y., Glaser, F., Martz, E., Pupko, T., and Ben-Tal N. (2005). ConSurf 2005: the projection of evolutionary conservation scores of residues on protein structures. *Nucl. Acids. Res.* 33, W299-302.
- Perrakis, A., Morris, R., and Lamzin, V.S. (1999). Automated protein model building combined with iterative structure refinement. *Nat. Struct. Biol.* 6, 458-463.
- Ponnuraj, K., Xu, Y., Macon, K., Moore, D., Volanakis, J.E., and Narayana, S.V. (2004). Structural analysis of engineered Bb fragment of complement factor B: insights into the activation mechanism of the alternative pathway C3-convertase. *Mol. Cell* 14, 17-28.
- Reeves, P.J., Callewaert, N., Contreras, R., and Khorana, H.G. (2002). Structure and function in rhodopsin: high-level expression of rhodopsin with restricted and homogeneous N-glycosylation by a tetracycline-inducible N-acetylglucosaminyltransferase I-negative HEK293S stable mammalian cell line. *Proc. Natl. Acad. Sci. U S A* 99, 13419-13424.
- Roos, A., Nauta, A.J., Broers, D., Faber-Krol, M.C., Trouw, L.A., Drijfhout, J.W., and Daha, M.R. (2001). Specific inhibition of the classical complement pathway by C1q-binding peptides. *J. Immunol.* 167, 7052-7059.
- Shimaoka, M., Xiao, T., Liu, J.H., Yang, Y., Dong, Y., Jun, C.D., McCormack, A., Zhang, R., Joachimiak, A., Takagi, J., Wang, J.H., and Springer, T.A. (2003). Structures of the alpha L I domain and its complex with ICAM-1 reveal a shape-shifting pathway for integrin regulation. *Cell* 112, 99-111.
- Song, H.K., and Suh, S.W. (1998). Kunitz-type soybean trypsin inhibitor revisited: refined structure of its complex with porcine trypsin reveals an insight into the interaction between a homologous inhibitor from *Erythrina caffra* and tissue-type plasminogen activator. *J. Mol. Biol.* 275, 347-363.
- Thurman, J.M., Kraus, D.M., Girardi, G., Hourcade, D., Kang, H.J., Royer, P.A., Mitchell, L.M., Giclas, P.C., Salmon, J., Gilkeson, G., and Holers, V.M. (2005). A novel inhibitor of the alternative complement pathway prevents antiphospholipid antibody-induced pregnancy loss in mice. *Mol. Immunol.* 42, 87-97.
- Xu, Y., and Volanakis, J.E. (1997). Contribution of the complement control protein modules of C2 in C4b binding assessed by analysis of C2/factor B chimeras. *J. Immunol.* 158, 5958-5965.



# 4

## **Staphylococcal complement inhibitor: Structure and active sites**

**Fin J. Milder<sup>1\*</sup>, Suzan H.M. Rooijackers<sup>2\*</sup>, Bart W. Bardoel<sup>2</sup>, Maartje Ruyken<sup>2</sup>,  
Jos A.G. van Strijp<sup>2</sup> and Piet Gros<sup>1</sup>.**

<sup>1</sup>Crystal and Structural Chemistry, Bijvoet Center for Biomolecular Research, Faculty of Science, Utrecht University, 3584 CH Utrecht, The Netherlands. <sup>2</sup>Experimental Microbiology, University Medical Center Utrecht, 3584 CX Utrecht, The Netherlands.

\*these authors contributed equally to this work

Accepted for publication in The Journal of Immunology

## Abstract

The pathogenic bacterium *Staphylococcus aureus* counteracts the host immune defense by excretion of the 85 residue Staphylococcal Complement Inhibitor (SCIN). SCIN inhibits the central complement convertases; thereby it reduces phagocytosis following opsonization and efficiently blocks all downstream effector functions. Here we present the crystal structure of SCIN at 1.8 Å resolution and the identification of its active site. Functional characterization of structure based chimeric proteins, consisting of SCIN and the structurally but non-functional homolog ORF-D, indicate an 18 residue segment (Leu31-Gly48) crucial for SCIN activity. In all complement activation pathways chimeras lacking these SCIN residues completely fail to inhibit production of the potent mediator of inflammation C5a. Inhibition of Alternative Pathway mediated opsonization (C3b deposition), and formation of the lytic membrane attack complex (C5b-9 deposition) is strongly reduced for these chimeras as well. For inhibition of the Classical/Lectin Pathway mediated C3b and C5b-9 deposition the same residues are critical although additional sites are involved. These chimeras also display reduced capacity to stabilize the C3-convertases of both the Alternative and the Classical/Lectin Pathway indicating the stabilizing effect is pivotal for the complement inhibitory activity of SCIN. Because SCIN specifically and efficiently inhibits complement, it has a high potential in anti-inflammatory therapy. Our data are a first step towards the development of a second-generation molecule suitable for such therapeutic complement intervention.

## Introduction

The complement system fulfills a critical role in our host defense against invading pathogens. As a key part of the innate immune system complement activation triggers acute inflammatory and cytolytic reactions, but also participates in regulation of adaptive immunity (Carroll 2004; Walport, 2001a; 2001b). On the other hand, unregulated complement activation is related to many unwanted inflammatory reactions associated with various acute and chronic inflammatory diseases (Seelen et al., 2005; Trouw et al., 2003). The complement system is activated via two specific recognition pathways, the Classical Pathway (CP) and Lectin Pathway (LP), that are amplified by the Alternative Pathway (AP) (Fujita et al., 2004). All three pathways converge to the formation of an active protease complex on the pathogenic surface, the C3 convertase. The CP and LP convertases are formed when a C4b molecule covalently binds to the cell surface and is

recognized by C2. Binding and subsequent cleavage of C2 results in the active convertase C4b2a. The AP convertase is formed in a similar manner by the proteins C3b and B which are homologous to C4b and C2, respectively. Both bimolecular complexes (C3bBb and C4b2a) have a short life time ( $t_{1/2}$  of 1-2 min.) and their dissociation is irreversible (Xu et al., 2001). The C3 convertases cleave large amounts of complement protein C3 into C3a and C3b, thus, providing amplification. Convertase action results in labeling of antigens with a large number of C3b molecules and their inactive derivatives iC3b (Lambris, 1988; Janssen et al., 2005; 2006). This so-called opsonization is essential for effective phagocytic uptake via complement receptors (Helmy et al., 2006; Gasque, 2004). Furthermore high local concentrations of C3b induce formation of C5 convertases (Pangburn and Rawal 2002). Cleavage of C5 by these convertases results in the release of C5a, an important chemo-attractant, and C5b, the initiator of the Membrane Attack Complexes (MAC, C5b-9) that directly lyses gram-negative bacteria.

A bacterium must counteract immune responses in order to survive within its host. Increasing evidence points out the human pathogen *Staphylococcus aureus* (*S. aureus*) is very successful in evading the innate immune defenses (Foster, 2005; Rooijakkers et al., 2005). *S. aureus* blocks host defenses mainly by excretion of small molecules that inhibit several steps of the immune response. Neutrophil responses are inhibited by Staphylococcal Superantigen Like (SSL) 5 and the Chemotaxis Inhibitory Protein of *S. aureus* (CHIPS) (Bestebroer et al., 2007; de Haas et al., 2004; Postma et al., 2004). SSL5 prevents neutrophil adhesion to the endothelial lining by binding P-selectin Glycoprotein Ligand 1 (PSGL-1), while CHIPS blocks neutrophil activation and chemotaxis by binding the C5a Receptor (C5aR) and the Formylated Peptide Receptor (FPR). Complement modulation was described for Extracellular Fibrinogen Binding protein (Efb) that binds C3 (fragments) and SSL7 that binds to C5 (Lee et al., 2004; Langley et al., 2005).

Recently we discovered a highly specific and unique complement modulator termed Staphylococcal Complement Inhibitor (SCIN). SCIN is a 9.8 kD protein excreted by *S. aureus* that specifically binds to and inhibits the activity of the C3 convertases on the bacterial surface (Rooijakkers et al., 2005). As such SCIN prevents phagocytosis following opsonization of *S. aureus* by C3b deposition on its surface. Furthermore, since C5 convertases are no longer formed SCIN strongly attenuates C5a-induced neutrophil responses and formation of the Membrane Attack complex (MAC) (Rooijakkers et al., 2006). Remarkably, SCIN does not enhance dissociation of the C3 convertase as observed for other regulators. In the presence of SCIN large amounts of surface-bound C2a and Bb were found,

indicating that SCIN prevents decay acceleration of the C3 convertases. Possibly this stabilizing effect is part of the mechanism of complement inhibition by SCIN

Because the C3 convertases initiate all downstream effector functions, modulation of these complexes is highly efficient to inhibit complement (Wang, 2006). SCIN has evolved to a highly specific complement inhibitor acting on the C3 convertases and for that reason has a high potential in anti-inflammatory therapy. Given that C3 convertases are localized at the cell surface, low concentrations of the inhibitor may suffice for complete inhibition. Furthermore, SCIN is a soluble and non-toxic molecule, thus, can easily be used as a therapeutic agent. However, due to the presence of pre-existing antibodies directed to this bacterial exoproduct, SCIN cannot be used in its present form.

A search in the *S. aureus* genome identified three proteins homologous to SCIN; SCIN-B, SCIN-C and ORF-D. Characterization of these proteins indicates SCIN-B and C inhibit complement whereas ORF-D displays no inhibitory activity. Based on the crystal structure presented in this paper we constructed chimeric proteins of SCIN and its non-functional homologue ORF-D to identify the active site of SCIN. This information provides insights in convertase modulation by SCIN, and forms a basis for development of small non-immunogenic convertase inhibitors.

## Materials and methods

### Cloning of SCIN and SCIN homologs

DNA sequences encoding the excreted SCIN, SCIN-B, SCIN-C and ORF-D proteins were amplified by PCR on chromosomal DNA of clinical *S. aureus* strains using primers listed in table 4.1. Pfu Turbo polymerase (Stratagene, Cedar Creek, TX) was used to create 5' blunt ends and reverse primers included an EcoRI cleavage site downstream of the stop codon. PCR products were digested with EcoRI (Invitrogen Life Technologies, Paisley, UK) and cloned into a prSETB vector (Invitrogen) to enable expression of recombinant proteins with a cleavable N-terminal Histidine (His) tag. In this study we used the prSETB-pshAI vector, a prSETB vector in which the BamHI site was modified into a pshAI site to enable blunt-end cloning of genes directly downstream of the enterokinase cleavage site (Haas et al., 2004). An extra guanine at the 5' end of the primers was used to complement the enterokinase cleavage site.

Table 4.1 Primers used in this study.

Protein	Primer name	Primer sequence
SCIN	SCIN For	5'-GAGCACAAGCTTGCCAACATCG-3'
	SCIN Rev	5'-GGAATTCCTTAATATTTACTTTTT-3'
SCIN-B	SCIN-B For	5'-GAGTAGTCTGGACAAATATTTA-3'
	SCIN-B Rev	5'-GGAATTCCTTATCTATTTATAA-3'
SCIN-C	SCIN-C For	5'-GAGTAGTAAGAAAGACTATAT-3'
	SCIN-C Rev	5'-GGAATTCCTTATCTATTTATAATTTCA-3'
ORF-D	ORF-D For	5'-GAGCAAATCTGAAACTACATCACAT-3'
	ORF-D Rev	5'-GGAATTCCTTAATGTTTTGTGAATGC-3'
CH-N	CH-N Rev	5'-AACGATTTTAATTCATTAGCTAACTTTTGATGTTGATACGTATGTGA-3'
	CH-C Rev	5'-CTACATCACATACGTATCAACATCAAAGTTAGCTAATGAATTAATAATC-3'
CH-C	CH-C Rev	5'-GGAATTCCTTAATGTTTTGACTTTTTAGTGCTTCGTCAAT-3'
CH- $\alpha$ 1N	CH- $\alpha$ 1 <sub>N</sub> Rev	5'-CAGTAGCTAATTCATTAACATTTAGGTTTGCTATTAATTCATGTA-3'
	CH- $\alpha$ 1 <sub>N</sub> For	5'-TCAATTACATGAATTAATAGCAAACCTAAATGTTAATGAATTAGC-3'
CH- $\alpha$ 1C	CH- $\alpha$ 1 <sub>C</sub> Rev	5'-GGTACGATAATTTATTTAAGTCAGTTTCATCTAATAACGATTTTA-3'
	CH- $\alpha$ 1 <sub>C</sub> For	5'-TGAATTAATAATCGTTATTAGATGAAACTGACTTAAATAAAT-3'
	CH- $\alpha$ 1 <sub>C</sub> Rev1	5'-TTATAGTTCGCTTATAATAAGTGTTTAAATTTAGGTACG-3'
CH- $\alpha$ 1C	CH- $\alpha$ 1 <sub>C</sub> For1	5'-AAATAAATTCGTACCTAAATTTAAACACTTATTATAAGCGAAC-3'
	CH- $\alpha$ 2 <sub>N</sub> Rev	5'-AAATACGCGTTTTTGAACGCATCTAACTCCAGTAGCTAATT-3'
	CH- $\alpha$ 2 <sub>N</sub> For	5'-TAATGAATTAGCTACTGGAAGTTTAGATGCGTTTCAAAAA-3'
CH- $\alpha$ 2 <sub>N</sub>	CH- $\alpha$ 2 <sub>N</sub> Rev1	5'-ACTTAAGAGCATACATTGCTTTTTAGTGCGCAGCTAAAAATCG-3'
	CH- $\alpha$ 2 <sub>N</sub> For1	5'-AAAACGCGATTTTTAGTGGCACCTAAAAGCAATGTATGCTCT-3'
	CH- $\alpha$ 2 <sub>C</sub> Rev	5'-TGCGTATAGCGATTTTGAATATAACCTGAAATTTTTATAGTTC-3'
CH- $\alpha$ 2 <sub>C</sub>	CH- $\alpha$ 2 <sub>C</sub> For	5'-TAAGCGAACTATAAAAAATTCAGGTTATATTGCAAATC-3'
	CH- $\alpha$ 2 <sub>C</sub> Rev1	5'-TTGCTTCTGACATTTTCTTAAAGTCTTTAGTGCGTATAG-3'
	CH- $\alpha$ 2 <sub>C</sub> For1	5'-TGCAAAATCCGCTATACGCACTAAAGACTTTAAGAAAATGTCAGA-3'
CH- $\alpha$ 3N	CH- $\alpha$ 3 <sub>N</sub> Rev	5'-TCGCTTTAGTCATTTGATCCAAATTTTTGACTTAAGAGCATACA-3'
CH- $\alpha$ 3 <sub>N</sub>	CH- $\alpha$ 3 <sub>N</sub> For	5'-AGCAATGTATGCTCTTAAGTCAAAAAATTTGGATCAAATGACTAA-3'
	CH- $\alpha$ 3 <sub>N</sub> Rev1	5'-GTGCTTCGTCAATTCGTTATAAATACTTTCTAATCTTTGTTTCG-3'
	CH- $\alpha$ 3 <sub>N</sub> For1	5'-TAAAGCGAAACAAAGATTAGAAAGTATTTATAACGAAATGACGA-3'
CH- $\alpha$ 3C	CH- $\alpha$ 3 <sub>C</sub> Rev	5'-AAGGGTTAGAAATGAATTGTAATCTTTGAAAGTTGATATTTG-3'
	CH- $\alpha$ 3 <sub>C</sub> For	5'-AGAAGCAAATATCAACTTCAAAGATTACAATCAATTTCTAA-3'
CH- $\alpha$ 1CA	CH- $\alpha$ 1 <sub>CA</sub> Rev	5'-TTTATTTAAGTCAGTTTCATCTAATAACGATTTTAATTC-3'
	CH- $\alpha$ 1 <sub>CA</sub> For	5'-ACTGACTTAAATAAATTAGCTACTGGAAGTTTAAACACT-3'
CH- $\alpha$ 1CB	CH- $\alpha$ 1 <sub>CB</sub> Rev	5'-TAAATTTAGGTACGATAATTCATTAACATTTAGTTCATCTAA-3'
	CH- $\alpha$ 1 <sub>CB</sub> For	5'-TTATCGTACCTAAATTTAAACACTTATTATAAGCGAACTATA-3'
CH- $\alpha$ 2NA	CH- $\alpha$ 2 <sub>NA</sub> Rev	5'-GCGTTTTTGAACGCATCTAACTCCAGTAGCTAATTCATT-3'
	CH- $\alpha$ 2 <sub>NA</sub> For	5'-GATGCGTTTCAAAAACGCACTATAAAAAATTTGAGTCAAAC-3'
CH- $\alpha$ 2NB	CH- $\alpha$ 2 <sub>NB</sub> Rev	5'-GTGCGCAGCTAAAAATATCTCGCTTATAATAAGTGTTTAACT-3'
	CH- $\alpha$ 2 <sub>NB</sub> For	5'-GATATTTAGCTGCGCACCAAAAAGCAATGTATGCTCTTAAG-3'
	XbaI For	5'-GCTCTAGAAATAATTTTGTTTAACTTTAAGGAGGAG-3'

The prSETB-pshAI vector was digested with EcoRI and pshAI (Westburg, Leusden, The Netherlands) before ligation. Ligation products were transformed into TOP10F' *E. coli* (Invitrogen) and plasmids of positive clones were analyzed by DNA sequencing. The sequences of cloned genes can be found in the genome databases using the following accession numbers: SCIN (YP\_041408/ SAR2035 in *S.*

*aureus* MRSA252), SCIN-B (NP\_374275, SA1004 in *S. aureus* N315), SCIN-C (YP\_040544, SAR1131 in *S. aureus* MRSA252), ORF-D (YP\_039686, SAR0221 in *S. aureus* MRSA252).

### **Cloning of chimeric proteins**

Chimeric proteins of SCIN and ORF-D were constructed by overlap extension PCR (Postma et al., 2005; Ho et al., 1989). XbaI-digested SCIN and ORF-D pRSETB vectors were used as templates for amplification of DNA fragments having overlapping ends using complementary primers (table 4.1) and PCR. For example, to create the SCIN chimera in which the 13 N-terminal residues were replaced with homologous residues of ORF-D, chimera N (CH-N), we designed a sense primer (CH-N Forward) and antisense (CH-N Reverse) primer containing codon 7-13 of ORF-D combined with codon 14-20 of SCIN. One PCR product was created using pRSETB-ORFD as a template and XbaI Forward (anneals at the XbaI restriction site, upstream of the translation initiation site) and CH-N Reverse as primers. Another PCR was performed with pRSETB-SCIN as a template and CH-N Forward and SCIN Reverse (containing an EcoRI site) as primers. The purified PCR products were then diluted, mixed with XbaI Forward and SCIN Reverse primers and amplified in a third PCR reaction. Because the strands of input PCR products have matching sequences at their 3'-ends, they overlap and act as primers for each other. Simultaneous addition of XbaI Forward and SCIN Reverse resulted in amplification of the full-length PCR product. Some chimeric constructs required annealing of 3 PCR products and therefore 4 different primers were designed. All final PCR products spanned from the XbaI site on the pRSETB vector to the EcoRI site at the 3'-end of the gene. Both PCR products and pRSETB vectors were digested with XbaI and EcoRI before ligation. Ligation products were transformed into TOP10F' *E. coli* (Invitrogen) and positive clones were analyzed by DNA sequencing.

### **Protein expression**

For expression, recombinant plasmids of both wild-type and chimeric proteins were transformed into *E. coli* Rosetta Gami (DE3) pLysS (Novagen; Merck Biosciences) and expression was carried out according to the manufacturer's instructions. For selenomethionine-labeling of SCIN, pRSETB-SCIN was transformed into strain JG301, a methionine-auxotrophic derivative *E. coli* BL21 Star (DE3) (Rutten et al., 2006). Transformants were grown until mid-exponential phase in minimal medium supplemented with 0.5% (w/v) glucose and 50 µg/ml selenomethionine (Rutten et al., 2006). Expression of selenomethionine-labeled SCIN was performed by incubation with 1 mM isopropyl-1-thio-β-D-



galactopyranoside (IPTG, Roche Applied Science, Indianapolis, USA) for 16 hours at 37 °C. After expression, bacteria were collected by centrifugation and stored at –20 °C.

### **Purification of recombinant proteins**

Bacterial pellets were lysed by incubation with 6 M guanidine, 500 mM NaCl and 20 mM sodium phosphate pH 7.8 for 30 min at 37 °C and subsequent sonication. After centrifugation, His-tagged proteins were purified on a His-Trap Nickel column (Amersham Biosciences, Piscataway, NJ) which was equilibrated in 8 M Urea buffer (containing 1 M NaCl, 10 mM Imidazole, 20 mM sodium phosphate, pH 6). His-tagged SCIN, SCIN-B, SCIN-C, ORF-D and selenomethionine-SCIN were refolded on the column by gradual lowering urea concentrations during wash steps until the final washing buffer contained 20 mM sodium phosphate, 1 M NaCl, 10 mM Imidazole, pH 6. Refolded proteins were then eluted in 50 mM EDTA in Phosphate Buffered Saline (PBS). After dialysis to PBS, the His-tag was cleaved off by a 2-hour incubation with Enterokinase (3.3 U/ml, Invitrogen) at 37 °C. The His-tag was subsequently separated by a second column passage. His-tagged chimeras were not refolded on the column but eluted under denaturing conditions using 0.5 M Imidazole in 8 M Urea, 1 M NaCl, 20 mM sodium phosphate, pH6. Proteins were then refolded by rapid dilution into PPBS and subsequently dialyzed against PBS. Since the N-terminal His-tag did not influence SCIN activity (Figure 4.1A-C), the tag was not removed for functional screening of chimeric proteins. All recombinant proteins were >95% pure as determined by SDS-PAGE and Coomassie staining. Protein concentrations were assessed by measuring absorbance at 280 nm using the calculated absorbance coefficients.

### **Crystallization**

Purified recombinant selenomethionine-labeled SCIN was dialyzed against 50 mM NaCl, 20 mM Tris pH 8.0 and concentrated to 24 mg/ml using a Centricon plus-20 filter with a 5 kDa molecular-weight cut off (Milipore). Initial crystallization experiments were performed at 20 °C by using the sitting drop vapor-diffusion method. A Mosquito robot (TTP labtech) was used to set up 200 nl drops with a 1:1 ratio of protein and reservoir solution. Initial crystals, stacked crystalline plates, were obtained with reservoir solution containing 25% (w/v) PEG 1500, 0.1 M propionic acid-cacodylate bis-tris propane (PCB) buffer, made by mixing 0.1 M sodium propionate, 0.1 M sodium cacodylate, and 0.1 M bis-tris propane in a 2:1:2 ratio at pH 9.0. The initial crystals were reproduced and optimized by hand using 2 µl hanging drops. Large amounts of rectangular plate like crystals with dimensions 0.2 x 0.1 x 0.08 mm were obtained using reservoir solution consisting of 35% (w/v)

PEG 1000 in 0.1 M PCB-buffer pH 8.5. Crystals were harvested from the drops and briefly washed in a 2  $\mu$ l drop of mother liquor prior to flash cooling by immersion in liquid nitrogen.

### **X-ray diffraction and analysis**

Diffraction data were collected at ESRF beam-line ID14-EH4 in Grenoble, France. A multiwavelength anomalous dispersion (MAD) dataset to a resolution of 1.8 Å was collected using a selenomethionine-labeled SCIN crystal. The dataset comprises 400 images in total; 100 images inflection ( $\lambda = 0.9795$  Å) data, 200 images peak ( $\lambda = 0.9793$  Å) data, and 100 images remote ( $\lambda = 0.9763$  Å) data. SCIN crystals displayed the orthorhombic space group P2<sub>1</sub>2<sub>1</sub>2<sub>1</sub>, with unit cell parameters a = 23.02 Å, b = 42.78 Å, and c = 63.91 Å and  $\alpha=\beta=\gamma=90^\circ$ . The crystal had a solvent content of 25% with one SCIN molecule per asymmetric unit. Diffraction data were indexed and further processed using the programs MOSFLM (Leslie, 2006) and SCALA from the CCP4 program suite, respectively. A summary of the data collection and processing statistics is provided in table 4.2.

### **Structure determination and refinement**

The structure of SCIN was solved by a three-wavelength (inflection, peak, and remote) selenomethionine MAD experiment with crystals diffracting to 1.8 Å resolution. Initial phases were derived from the position of the selenium atoms. One of the two selenium sites was identified with the SOLVE/RESOLVE package (Terwilliger 2003) whereas no clear solution was obtained for the second selenium site. An initial model was obtained by iterative model-building using RESOLVE (Terwilliger 2003). This model was completed to ~85% by automated model building using ARP/wARP (Perrakis et al., 1999). The model of SCIN was finalized by cycles of model building with COOT (Emsley and Cowtan 2004) and refinement using REFMAC5 (Winn et al., 2001). Because of radiation damage the automated model building and subsequent iterative refinement was performed using only 200 images of the peak data. The final model has R and R<sub>free</sub> factors of 20.1 and 22.6%, respectively, and displays good geometry. The model contains 74 protein residues, including 2 selenium methionines, and 43 water molecules. For the side chain of tyrosine 53 a double conformation was modeled. Residues 1-8 are missing from the model due to poor electron density, whereas the 3 C-terminal residues (res. 83-85) are not present in the crystal. Coordinates and structure factors have been deposited in the Protein Data Bank (PDB code 2qff). All molecular graphic figures were generated with pymol (W. Delano; <http://pymol.sourceforge.net>).

### Mass spectrometry

The mass of the protein used for crystallization was determined by recording positive-ion matrix-assisted laser desorption ionization time of flight (MALDI-TOF) mass spectra using a Voyager-DE PRO mass spectrometer (Applied Biosystems). SCIN was spotted on a MALDI plate via successive deposition and drying of 1 µl matrix-solution, 1 µl analyte, and again 1 µl matrix-solution. The matrix and analyte solutions used to prepare these sandwich spots consisted of 10 mg/ml 3,5-dimethoxy-4-hydroxycinnamic acid (sinapinic acid) in water:acetonitrile (1:1) and 1 mg/ml SCIN in 10 mM Tris, 10 mM NaCl, pH 7.5, respectively.

### ELISAs

Monoclonal and polyclonal antibodies against SCIN were produced and analyzed as described earlier (Rooijackers et al., 2005; Haas et al., 2004). Antibodies are specific for SCIN since they did not react with SCIN-B, SCIN-C or ORF-D. Monoclonal antibodies did not react with 15-mer linear peptides spanning the sequence of SCIN, initiating a new peptide every fifth amino acid (Dr. R. van der Zee, Institute of Infectious Diseases and Immunology, Utrecht University, The Netherlands).

Functional activity of complement was screened as described previously (Rooijackers et al., 2005; Roos et al., 2003) with minor modifications. C3b and C5b-9 deposition were detected using anti-C3c WM1 (ATCC, Rockville, MD (Veldkamp et al., 1997) and anti-C5b-9 (Abcam, UK) antibodies respectively. Antibody binding was detected using peroxidase-conjugated goat anti-mouse IgG (Southern Biotechnology Associates Inc, Birmingham) and visualized using TMB (Rooijackers et al., 2005).

### Complement activation on *S. aureus*

Laboratory strain *S. aureus* Cowan EMS was used for phagocytosis and complement activation assays. For phagocytosis experiments, FITC-labeled bacteria were incubated with human sera and freshly isolated human neutrophils for 15 minutes at 37 °C (Rooijackers et al., 2005). Reactions were stopped in 1% paraformaldehyde and bacterial uptake by 10.000 gated neutrophils was analyzed by flow cytometry. The formation of C5a during opsonization of heat-killed *S. aureus* was measured in a calcium flux assay with Fluo-3-AM (Molecular Probes) labeled neutrophils (Rooijackers et al., 2006). Supernatant-induced calcium responses are solely triggered by C5a, since pre-incubation of neutrophils with the C5a receptor antagonist CHIPS<sup>30</sup> (CHIPS, lacking the first 30 N-terminal residues) completely blocked supernatant-induced neutrophil activation (Rooijackers et al., 2006; Haas et al., 2004). For detection of bacterium-bound Bb and C2a, *S. aureus*

Cowan EMS ( $5 \cdot 10^6$ ) was incubated with serum for 20 min at 37 °C in Hepes-buffered (20 mM Hepes, 140 mM NaCl, 5 mM CaCl<sub>2</sub>, 2.5 mM MgCl<sub>2</sub>, pH 7.4, HBS<sup>++</sup>), washed and surface-associated proteins were subjected to SDS-PAGE and analyzed by immunoblotting (Rooijackers et al., 2005). Factor D deficient serum was prepared by size exclusion chromatography and functionally tested by AP50 (Rooijackers et al., 2005). Binding of FITC-labeled SCIN (labeled as described for CHIPS (de Haas et al., 2004)) to *S. aureus* was studied by incubation of *S. aureus* Cowan EMS ( $3 \cdot 10^7$ ) with 1 µg/ml SCIN-FITC in the presence of non-labeled SCIN molecules and serum for 20 min. We used 20% factor D deficient serum in HBS<sup>++</sup> for analyses of the CP/LP and 20% normal serum in HBS-2 mM MgCl<sub>2</sub>-2mM EGTA for the AP. Bacteria were washed and mean fluorescence of 10,000 particles was determined by flow cytometry.

## Results

### Structure determination

The SCIN protein crystallized in space group P2<sub>1</sub>2<sub>1</sub>2<sub>1</sub> with one molecule per asymmetric unit and a solvent content of 25%. The structure of SCIN was solved by multiwavelength anomalous dispersion (MAD) with data collected from a single selenomethionine-labeled crystal that diffracted to 1.8 Å resolution. The structure of SCIN was refined to an R and R<sub>free</sub> of 20.1 and 22.6%, respectively, with no outliers in the Ramachandran plot. Poor electron density was observed for the N-terminal region indicating flexibility; accordingly residues 1-8 were not modeled. In contrast the C-terminal region is well defined and is involved in multiple crystal contacts. However, no electron density is observed for the 3 C-terminal residues. MALDI-TOF mass spectrometry analysis of the sample used in the crystallization experiments confirmed the absence of residues 83-85 and consequently a carboxy terminus was modeled on Lys-82. Absence of residues 83-85 was only found in the concentrated samples (>25 mg/ml) specifically prepared for crystallization experiments. Likely the three C-terminal residues were cleaved off by the still present and co-concentrated Enterokinase used for the removal of the His-tag. Figure 1 indicates that SeMet-SCIN without residues 83-85 still had a specific SCIN activity (Figure 4.1A-C). The final model contains 74 residues and 43 water molecules. Data collection and refinement statistics are given in table 4.2.

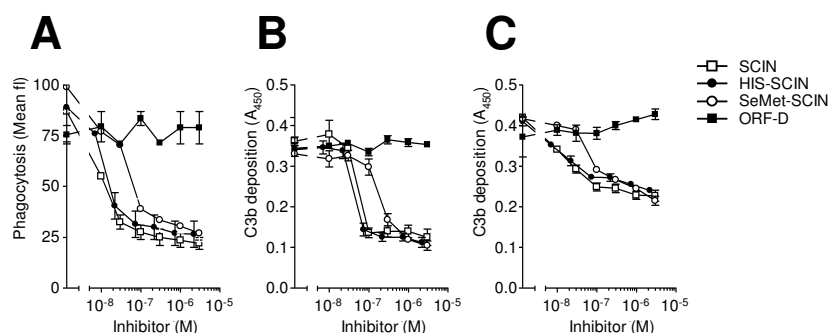


**Figure 4.1 Functional analyses of labeled SCIN molecules.**

Analyses of SCIN, His-tagged SCIN and selenomethionine-labeled SCIN. **A)** SCIN, His-SCIN and SeMet-SCIN show a dose-dependent inhibition of *S. aureus* uptake by human neutrophils in 10% human sera. **B)** Dose-dependent inhibition of AP-mediated C3b deposition by SCIN, His-SCIN and SeMet-SCIN in 30% human serum measured by ELISA. **C)** Dose-dependent inhibition of CP-mediated C3b deposition by SCIN, His-SCIN and SeMet-SCIN in 5% human serum measured by ELISA. ORF-D was used as a negative control in all three experiments. Data are mean  $\pm$  SEM of two independent experiments.

**Table 4.2 Crystallographic data collection and refinement statistics**

Data collection statistics			
Space group	P2 <sub>1</sub> 2 <sub>1</sub> 2 <sub>1</sub>		
Cell dimensions (Å)	a = 23.02, b = 42.78, c = 63.91		
Wavelength (Å)	0.9793	0.9795	0.9763
Resolution (Å)	40.0-1.80 (1.90-1.80)	40.0-1.8	40.0-1.80
Completeness (%)	99.9 (100)	99.8 (100)	99.8 (100)
Multiplicity	7.1 (7.4)	3.6 (3.8)	3.6 (3.8)
Rmerge (%)	6.0 (38.7)	5.2 (38.1)	5.4 (43.9)
I/ $\sigma$ I	22.8 (4.3)	16.3 (2.5)	15.4 (2.0)
Refinement statistics			
# reflections	5952/294		
R/R <sub>free</sub> (%)	20.1/22.6		
B-factor (Å <sup>2</sup> )	21.8		
rmsd bond length (Å)	0.060		
rmsd bond angle (°)	0.790		
# protein atoms	624		
# water molecules	43		

Values between parentheses refer to the highest-resolution

### Structure of SCIN

SCIN displays a triple  $\alpha$ -helical bundle structure. The three helices are connected via 2 short loops and adopt a compact arrangement with overall dimensions of approximately 45 x 25 x 25 Å (Figure 4.2a). The middle helix, helix  $\alpha 2$  (res. Thr-38 to Ser-57), is positioned anti-parallel with respect to both the N and C-terminal helices  $\alpha 1$  (res. Glu-9 to Ser-35) and  $\alpha 3$  (res. Phe-60 to Leu-81) respectively. The long helix  $\alpha 1$  extends from the N-terminal part of helix 3 to the N-terminal part of helix 2 and is kinked halfway (res. 25-26). The kink distorts the typical  $\alpha$ -helical hydrogen bonding pattern and a partial  $3_{10}$ -helix conformation is observed. A second  $3_{10}$ -helix conformation is present at the C-terminal part of helix  $\alpha 1$  (Ala-32 to Ser-35). The core of the protein is formed by hydrophobic residues whereas charged residues face the solvent (Figure 4.2a). In addition to the hydrophobic interactions, the three helices interact via 7 hydrogen bonds and 1 salt-bridge (Glu-18 to Lys-67). Altogether the structure of SCIN is characterized by three helices packed in a coiled coil.

### Identification and characterization of SCIN homologs

In search for structurally and functionally SCIN homologs the Protein Data Bank was screened using the Dali server. This yields over 500 proteins from various organisms with very different functions. To the contrary a BLAST search in the genome database revealed only a few proteins with homology in sequence. Present in the six available *S. aureus* genomes are the unknown proteins SCIN-B (46% amino acid identity), SCIN-C (48%) and open reading frame-D (ORF-D, 33%) (Figure 4.2B). Like SCIN, these proteins have a mass of 9.8 kD and are excreted via a signal peptide. Secondary structure predictions using the Predict Protein server indicate SCIN-B, SCIN-C and ORF-D have the same  $\alpha$ -helical distribution as present in SCIN. Following recombinant production, analyses of these SCIN homologs shows that SCIN-B and SCIN-C are effective complement inhibitors while ORF-D has no complement blocking activity (Jongerius et al, Submitted, manuscript added). Figure 4.2C indicates that phagocytosis of fluorescence-labeled *S. aureus* by human neutrophils is strongly inhibited by SCIN, SCIN-B and SCIN-C (10  $\mu$ g/ml) at serum concentration of 3% and higher whereas ORF-D does not inhibit phagocytosis.

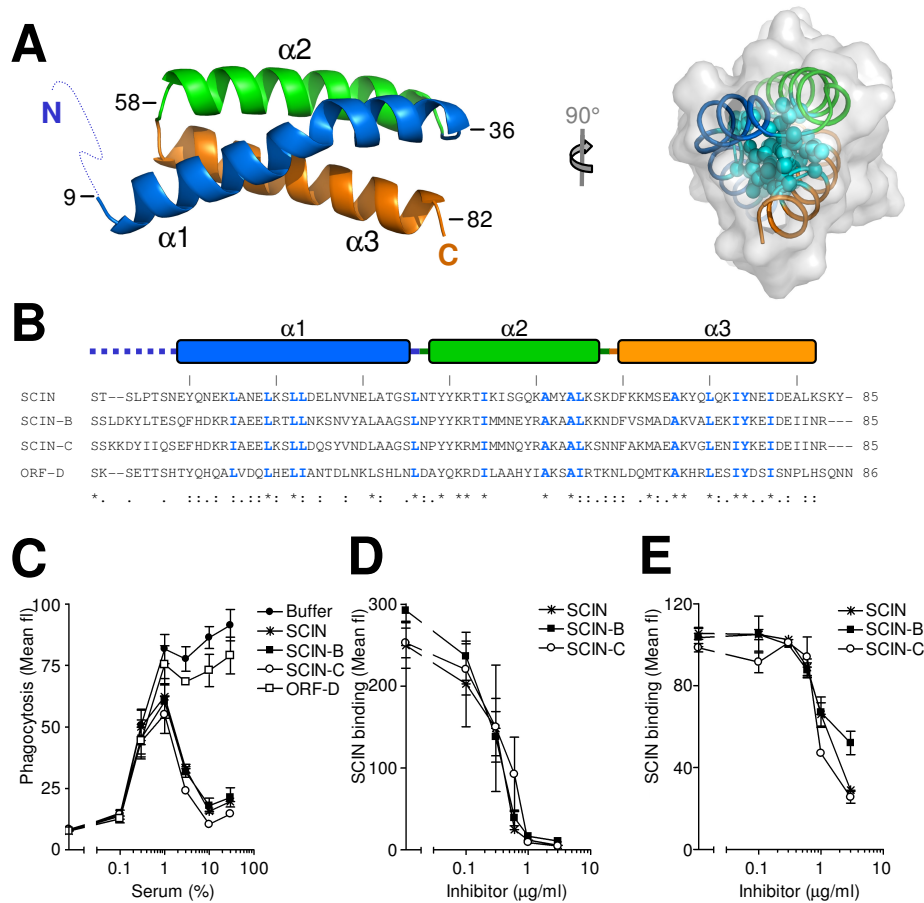


**Figure 4.2 Structure of SCIN and characterization of SCIN homologs.**

**A** left panel - Structure of SCIN shown in ribbon representation. Helices are colored blue (helix 1), green (helix 2), and orange (helix 3), the dotted line represents the flexible N-terminus. right panel - SCIN structure in ribbon and surface representation with side chains forming the conserved hydrophobic core in ball-and-stick (light blue) representation, helical coloring as in left panel. **B** Alignment of SCIN, SCIN B, SCIN C, and ORF-D. "\*" indicate identical residues, ":" indicate conserved substitutions and "." indicate semi-conserved substitutions (CLUSTAL W (1.83)). Highlighted in light blue are the conserved residues that form the hydrophobic core. **C** SCIN-B and SCIN-C (10  $\mu\text{g/ml}$ ) strongly reduce phagocytosis of *S. aureus* at different serum concentrations. ORF-D does not reduce phagocytic uptake. **D,E** Binding of SCIN-FITC (1  $\mu\text{g/ml}$ ) to *S. aureus* in 20% human sera in the presence of non-labeled SCIN, SCIN-B or SCIN-C. SCIN binding was analyzed by flow cytometry and is expressed as mean fluorescence of 10,000 bacteria. **D**, Non-labeled SCIN, SCIN-B and SCIN-C compete with SCIN-FITC for binding to surface-bound C3bBb. Binding to C3bBb was performed in the presence of MgEGTA. **E**, Non-labeled SCIN, SCIN-B and SCIN-C compete with SCIN-FITC for binding to surface-bound C4b2a. Binding to C4b2a was analyzed using factor D-deficient serum. All panels - data are mean  $\pm$  SEM of three independent experiments.

Further analyses of SCIN-B and SCIN-C showed they inhibit the complement system similar to SCIN (Jongerijs et al, Submitted, manuscript added). Although SCIN-B is less efficient in inhibition of C3b deposition via the CP and LP, both SCIN homologs block all complement pathways in ELISA. Additionally, SCIN-B and SCIN-C also reduce C4b2a and C3bBb dissociation. To investigate whether the three SCIN molecules bind to similar epitopes, competition-binding experiments were performed. First, we analyzed AP-mediated binding of fluorescence-labeled SCIN (SCIN-FITC) to *S. aureus* in the presence of 10% human serum and Mg-EGTA. Earlier we showed that binding of SCIN to bacterial surfaces occurs when C3bB is activated into C3bBb (21). Figure 4.2C illustrates that binding of SCIN-FITC (1 µg/ml) to C3bBb is completely blocked in the presence of equal concentrations of non-labeled SCIN, SCIN-B or SCIN-C indicating the homologs bind with equal affinity to a similar site within C3bBb. Second, we analyzed CP and LP mediated binding of SCIN to *S. aureus* in 10% factor D-deficient serum (to prevent AP activation). SCIN-C prevents binding of SCIN-FITC to C4b2a at identical concentrations as SCIN (Figure 4.2C). In agreement with the ELISA data, SCIN-B blocks SCIN-FITC binding less efficient indicating this protein has a lower affinity towards C4b2a compared to SCIN and SCIN-C.

Summarizing, characterization of SCIN and the three SCIN homologs indicates that SCIN-B and C are also convertase inhibitors that bind to similar epitopes on C3bBb. The 33% homolog ORF-D displays no complement inhibitory activity.

#### Preparation of chimeric proteins

To gain insight into the active site of SCIN 15-mer linear peptides spanning the molecule (initiating a new peptide every fifth amino acid) were tested for complement inhibitory activity. None of the peptides was active, indicating the tertiary structure is of importance for SCIN activity. The similarity in molecular weight and predicted secondary structure, and the conservation of hydrophobic residues (Figure 4.2) forming the protein core, indicates the structures of SCIN and its non-functional homologue ORF-D are alike. Based on these observations eight chimeric proteins (Figure 4.3) were designed to localize sites crucial for SCIN function. In chimera's CH-N and CH-C, SCIN residues 1-13 (the flexible N-terminus and the first part of helix  $\alpha$ 1) and 83-85 (missing in the structure), respectively, are replaced by homologous residues of ORF-D. In the six other chimera's half helices are replaced; CH- $\alpha$ 1N (res. 1-25, N-terminal half of helix  $\alpha$ 1 and flexible N-terminus), CH- $\alpha$ 1C (res. 26-36, C-terminal half of helix  $\alpha$ 1), CH- $\alpha$ 2N (res. 37-48), CH- $\alpha$ 2C (res. 49-58), CH- $\alpha$ 3N (res. 59-72), and CH- $\alpha$ 3C (res. 73-86).



The constructs coding for the chimeric proteins were prepared using the PCR-based overlap extension methodology (25, 26). The proteins were expressed in *E. coli* and purified as Histidine tagged proteins.

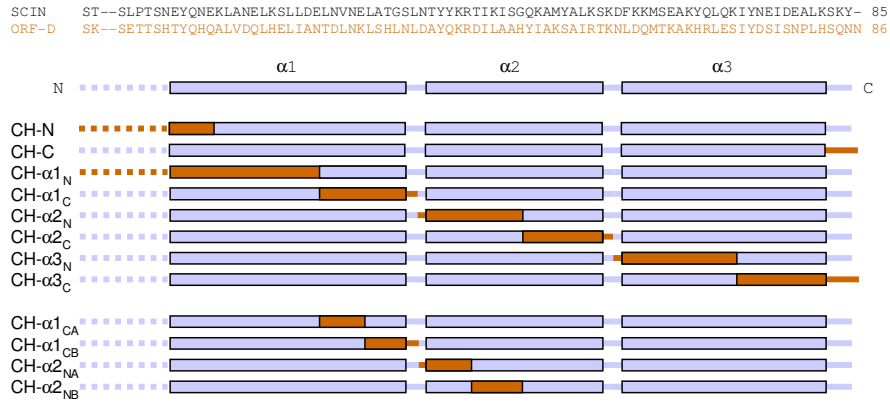


**Figure 4.3 Schematic representation of chimeric constructs used in this study.**

SCIN residues (grey) were exchanged with corresponding residues in ORF-D (orange). Exchanged residues: CH-N (res. 1-13), CH-C (res. 83-85), CH-α1<sub>N</sub> (res. 1-25), CH-α1<sub>C</sub> (res. 26-36), CH-α2<sub>N</sub> (res. 37-48), CH-α2<sub>C</sub> (res. 49-58), CH-α3<sub>N</sub> (res. 59-72), and CH-α3<sub>C</sub> (res. 73-86). CH-α1<sub>CA</sub> (res. 26-30), CH-α1<sub>CB</sub> (res. 31-36), CH-α2<sub>NA</sub> (res. 37-42) and CH-α2<sub>NB</sub> (res. 43-48).

The presence of the His-tag does not affect the activity of SCIN (Figure 4.1A-C). To demonstrate preservation of secondary structures we tested binding of 10 different antibodies that recognize conformational epitopes of SCIN since they do not react with the 15-mer linear peptides. Each of the chimeras proteins are recognized by multiple antibodies indicating the protein structure remained intact (Table 4.3).

**Table 4.3 Recognition of chimeric proteins by monoclonal antibodies against SCIN**

	Rabbit	Anti-His	2F4	2B12	3G3	3F1	1C9	6C2	6B4	7E3	3G1	1G10
ORF-D		Δ										
SCIN	Δ	Δ	Δ	Δ	Δ	Δ	Δ	Δ	Δ	Δ	Δ	Δ
N	Δ	Δ	Δ	Δ	Δ	Δ	Δ	Δ	Δ	Δ	Δ	Δ
C	Δ	Δ	Δ	Δ	Δ	Δ	Δ	Δ	Δ	Δ	Δ	Δ
α1 <sub>N</sub>	Δ	Δ	Δ	Δ	Δ	Δ	Δ	Δ	Δ	Δ	Δ	
α1 <sub>C</sub>	Δ	Δ		Δ	Δ		Δ	Δ	Δ		Δ	
α2 <sub>N</sub>	Δ	Δ			Δ		Δ		Δ		Δ	Δ
α2 <sub>C</sub>	Δ	Δ	Δ	Δ	Δ	Δ	Δ	Δ	Δ		Δ	Δ
α3 <sub>N</sub>	Δ	Δ	Δ	Δ		Δ		Δ		Δ		
α3 <sub>C</sub>	Δ	Δ	Δ	Δ	Δ	Δ	Δ	Δ		Δ	Δ	

### SCIN residues 26-48 are crucial for Alternative Pathway inhibition

To determine the residues involved in modulation of the AP, SCIN and the chimeric proteins were tested in an AP-mediated ELISA. Microtiter wells were coated with LPS and incubated with 30% human serum in the presence of Mg-EGTA. Subsequently, deposition of C3b and C5b-9 was measured in the presence of SCIN and the chimeras (10  $\mu\text{g}/\text{ml}$ ). The termini of SCIN are not involved in AP inhibition since chimeric proteins CH-N and CH-C had similar complement inhibitory activities as SCIN (Figure 4.4A). To the contrary, chimeras CH- $\alpha_{1C}$  (res. 26-36) and CH- $\alpha_{2N}$  (res. 37-48) had a markedly reduced capacity to inhibit C3b deposition while inhibition by other chimeras was equal to SCIN. Similarly, C5b-9 formation was inhibited by all chimeras, except by CH- $\alpha_{1C}$  and CH- $\alpha_{2N}$ . Chimeras of which the N-terminal His-tag was removed by enterokinase inhibited complement in a similar degree, confirming the tag does not alter the functional activity.

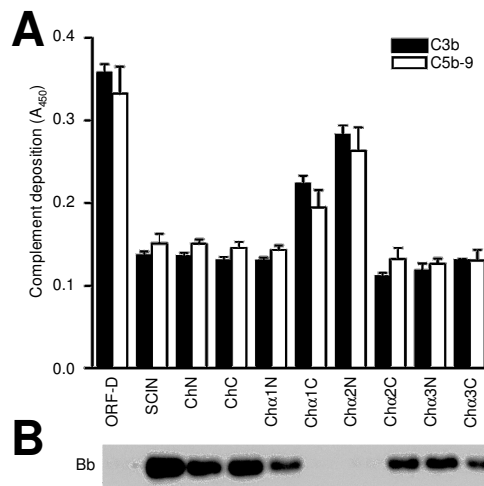


**Figure 4.4 SCIN residues 26-48 are crucial for inhibition and stabilization of C3bBb.**

**A)** Effect of chimeric proteins (10  $\mu\text{g}/\text{ml}$ ) on AP-mediated complement activation in 30% human sera. CH- $\alpha_{1C}$  and CH- $\alpha_{2N}$  show reduced complement inhibition, both at the level of C3b and C5b-9 deposition. Data are mean  $\pm$  SEM of three independent experiments. **B)** CH- $\alpha_{1C}$  and CH- $\alpha_{2N}$  do not stabilize C3bBb on bacterial surfaces. Surface detection of Bb on *S. aureus* after opsonization with 20% human serum in the presence of chimeras (10  $\mu\text{g}/\text{ml}$ ). Blot is a representative of three separate experiments.

Previous studies have shown that surface stabilization of the instable C3 convertases is a hallmark of SCIN activity. To determine the residues involved, the convertase-stabilizing capacity of the chimeras was examined. Following incubation of *S. aureus* with 20% serum in the presence of SCIN and SCIN chimeras (10 µg/ml), surface-bound Bb was detected by immunoblotting. Figure 4.4B clearly indicates that all chimeras, except for CH- $\alpha$ 1c and CH- $\alpha$ 2N, stabilize the AP C3 convertase (C3bBb) formed on the bacterial surface. This implicates that, next to their role in AP inhibition, SCIN residues 26-48 are also crucial for the observed stabilization effect. This indicates for the first time that stabilization of surface-bound AP convertase by SCIN is directly linked to inhibition of complement deposition. Taken together, these data indicate that residues 26-48 are crucial for SCIN activity.

### Inhibition of the Classical/Lectin Pathway requires additional regions

To study which residues are involved in inhibition of the CP and LP C3 convertase C4b2a, chimeric proteins were analyzed in a CP ELISA. IgM-coated microtiter wells were incubated with 5% human serum in the presence of SCIN and the chimeras (10 µg/ml) and deposition of C3b and C5b-9 was monitored. In contrast to the AP where only two chimeras show reduced complement inhibition, all chimeras, except CH-C, display a reduced ability to prevent C3b deposition in the CP (Figure 4.5A). This indicates a significant role for regions additional to residues 26-48 in CP inhibition. However, at the level of C5b-9 deposition only CH- $\alpha$ 2N displays reduced CP inhibition (Figure 4.5A).

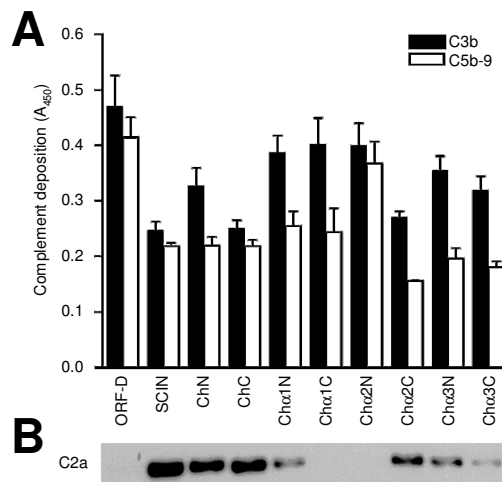


**Figure 4.5 SCIN residues 26-48 are crucial for inhibition and stabilization of C4b2a, but additional domains are required.**

**A)** Effect of chimeric proteins (10 µg/ml) on CP-mediated complement activation in 5% human sera. C3b deposition was inhibited by SCIN and CH-C, while all other chimera had a reduced ability to block C3b deposition. At the level of C5b-9, only CH- $\alpha$ <sub>2N</sub> was reduced in its ability to block complement. Data are mean  $\pm$  SEM of three independent experiments. **B)** CH- $\alpha$ <sub>1C</sub> and CH- $\alpha$ <sub>2N</sub> do not stabilize C4b2a on bacterial surfaces, while other chimeras also show reduced stabilization. Surface detection of C2a on *S. aureus* after opsonization with 20% human serum in the presence of chimeras (10 µg/ml). Blot is a representative of three separate experiments.

As expected, analyses of the chimeric proteins in a LP ELISA revealed similar results (data not shown). To identify SCIN residues involved in stabilization of C4b2a, we determined the amount of C2a molecules at the bacterial surface after opsonization in 20% serum. In correspondence with stabilization of C3bBb, CH- $\alpha$ <sub>1C</sub> and CH- $\alpha$ <sub>2N</sub> could also not stabilize C4b2a (Figure 4.5B). However, similar to the observed inhibition of the CP ELISA, other chimeras are also less efficient in stabilizing C4b2a. These data indicate that for the CP/LP additional regions to residues 26-48 are involved in both inhibition of C3b deposition and stabilization of the C3 convertase C4b2a.

**Inhibition of C5a responses depends on SCIN residues 26-48**

The anaphylatoxin C5a is one of the most potent mediators of inflammation. C5a is formed when C5 is cleaved by the C5 convertase that arises due to high local concentrations of C3b. To determine the residues that inhibit C5a production, SCIN and SCIN chimeras were tested in a system in which all complement pathways are active. *S. aureus* was incubated with 10% human serum in the presence of SCIN chimeras and the supernatants were collected after opsonization. Subsequently the C5a response of human neutrophils exposed to these supernatants was determined by measuring calcium mobilization (Rooijackers et al., 2006). The C5a dependency of the supernatant-induced calcium response of neutrophils was verified by pre-incubation with the C5a receptor antagonist CHIPS<sup>30</sup> (Haas et al., 2004). Figure 4.6 indicates that opsonization in the presence of SCIN (10 µg/ml) completely blocks the C5a responses whereas ORF-D has no effect. Strikingly, the C5a response is not blocked by incubation in presence of chimeras CH- $\alpha$ <sub>1C</sub> and CH- $\alpha$ <sub>2N</sub> indicating C5a production is not inhibited. Thus, similar to previously observed in C3b deposition and convertase stabilization, residues 26-48 are also crucial for SCIN mediated inhibition of C5a formation.

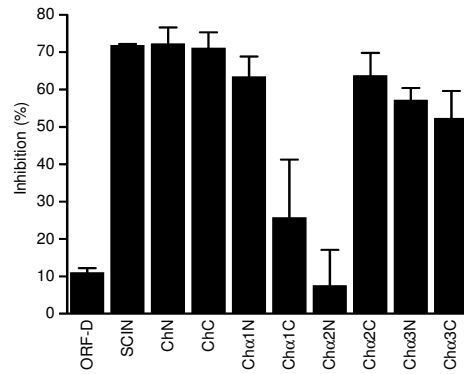


**Figure 4.6 SCIN residues 26-48 are crucial for inhibition of C5a responses.**

CH- $\alpha$ 1<sub>C</sub> and CH- $\alpha$ 2<sub>N</sub> show a reduced inhibition of C5a mediated calcium responses. SCIN effectively blocks calcium mobilization of human neutrophils when SCIN is incubated with heat-killed *S aureus* in 10% human serum to generate C5a containing supernatants. Supernatant-induced calcium mobilization was measured on fluo-3-AM loaded human neutrophils and determined by flow cytometry. Percentage of inhibition was calculated by subtraction of sample-induced calcium flux from buffer induced calcium flux, divided by buffer induced calcium flux. Data are mean  $\pm$  SEM of three independent experiments.

#### Active site of SCIN pinpointed to 18 residues (31-48)

To further pinpoint the active residues within residues 26-48 we designed four additional chimeras based on CH- $\alpha$ 1<sub>C</sub> and CH- $\alpha$ 2<sub>N</sub>; CH- $\alpha$ 1<sub>CA</sub> (26-30), CH- $\alpha$ 1<sub>CB</sub> (31-36), CH- $\alpha$ 2<sub>NA</sub> (37-42) and CH- $\alpha$ 2<sub>NB</sub> (43-48) (Figure 4.3). Structural integrity of these 4 chimeras was verified by the previously used monoclonal antibodies that recognize conformational epitopes on SCIN. Chimera CH- $\alpha$ 1<sub>CA</sub> but not CH- $\alpha$ 1<sub>CB</sub> blocks C5a responses (Figure 4.7A). Similarly, CH- $\alpha$ 1<sub>CA</sub> stabilized C4b2a and C3bBb on the bacterial surface while CH- $\alpha$ 1<sub>CB</sub> does not affect convertase stability (Figure 4.7B). The fact that CH- $\alpha$ 1<sub>CA</sub> blocks complement while CH- $\alpha$ 1<sub>CB</sub> is not active indicates that residues 26-30 are not involved in SCIN activity. For residue 37-48 we could not pinpoint the activity to a smaller region; CH- $\alpha$ 2<sub>N</sub> lacks inhibitory activity whereas the smaller chimeras, CH- $\alpha$ 2<sub>NA</sub> and CH- $\alpha$ 2<sub>NB</sub>, both inhibit the C5a response and stabilize surface bound convertases (Figure 4.7). Altogether a stretch of 18 residues (31-48) is identified that is crucial in SCIN mediated complement inhibition.

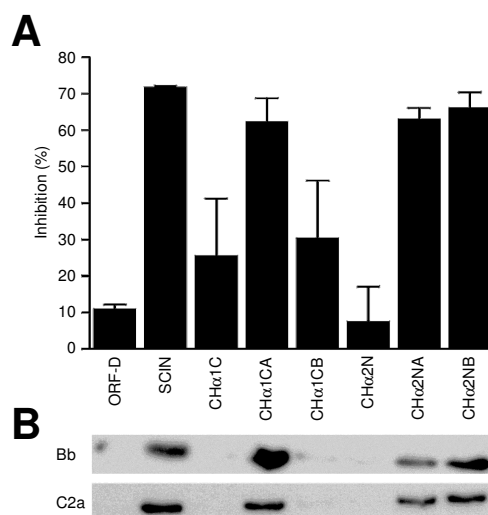


**Figure 4.7 SCIN residues 31-48 are crucial for complement inhibition and stabilization of C3 convertases.**

A) CH- $\alpha$ 1<sub>CA</sub>, CH- $\alpha$ 2<sub>NA</sub> and CH- $\alpha$ 2<sub>NB</sub> show a reduced inhibition of C5a mediated calcium responses. CH- $\alpha$ 1<sub>CB</sub> could not block C5a responses. Data are mean  $\pm$  SEM of three independent experiments. B) CH- $\alpha$ 1<sub>CA</sub>, CH- $\alpha$ 2<sub>NA</sub> and CH- $\alpha$ 2<sub>NB</sub> stabilize C3bBb and C4b2a on bacterial surfaces, whereas CH- $\alpha$ 1<sub>CB</sub> did not stabilize C3 convertases. Blot is a representative of three separate experiments.

## Discussion

Ninety percent of *S. aureus* strains express SCIN, an important factor in the staphylococcal defense against the human innate immune system. SCIN is a regulator of C3 convertases that, already at a low concentration, strongly prevents inflammatory reactions evoked by complement. Convertase regulation by SCIN differs significantly from other described convertase regulators. The human Regulators of Complement Activation (RCA) are cell-bound or fluid-phase proteins that protect cells from excessive complement activation by down regulation of the convertases. Most RCA proteins both promote dissociation of already formed convertases and inhibit formation of new convertases (Kirkitadze et al., 2001). The RCA family includes relatively large proteins that primarily consist of tandem repeats of complement control protein (CCP) domains that adopt a typical  $\beta$ -sandwich fold stabilized by pairs of disulphide bonds. Several bacteria protect themselves from complement eradication by attracting RCA proteins to their surface (Jarva et al., 2003; Ram et al., 2001; Kraiczky et al., 2003). Viruses have copied genetic material and express RCA-like molecules on virus-infected cells (Finlay et al., 2006; Mullick et al., 2005). SCIN is a small *S. aureus* convertase

inhibitor that functions in a completely different way. SCIN exclusively binds to the activated complex and does not bind individual convertase components (Rooijackers et al., 2005). SCIN binding increases convertase stability, a remarkable property that, in this paper, was shown to be crucial for SCIN activity. The crystal structure of SCIN reveals an all-helical protein with a flexible N-terminus. The SCIN fold deviates significantly from other convertase regulators, indicating SCIN belongs to a new class of convertase inhibitors.

Next to SCIN, *S. aureus* produces two SCIN homologs that function in a similar way. In the majority of clinical strains we find co-expression of either SCIN-B or SCIN-C in combination with SCIN. All SCIN molecules are human-specific, produced in vivo and expressed simultaneously during bacterial growth. Why *S. aureus* encodes three convertase inhibitors that bind the same epitope on C3bBb remains an intriguing question. Certainly it illustrates that convertase modulation strongly contributes to the organism's ability to infect humans.

The compact all helical structure of SCIN indicates a new mechanism for convertase inhibition. Recent structural determination of the C3-binding domain of Efb (Efb-C) from *S. aureus* revealed this is an all helical protein as well (Hammel et al., 2007). We have recently discovered that this C3/C3b-binding protein also regulates surface-bound convertases (Jongerius et al, Submitted, manuscript added). By binding to C3b, Efb-C blocks substrate cleavage of the convertases that harbor a C3b molecule (AP C3 convertase and all C5 convertases). In contrast to SCIN, Efb-C does not stabilize convertases and directly binds isolated C3b. Comparison of the SCIN and Efb-C structures reveals that the topological arrangement of the three helices differs significantly (Figure 4.8). Although SCIN does not directly bind isolated C3b, it is possible that SCIN does bind to C3b molecules in the context of the convertase complex. Because SCIN inhibits both the AP convertase (C3bBb) and the CP/LP convertase (C4b2a), putative binding to C3/C3b indicates a mechanism in which SCIN interacts with the substrate C3. Alternatively, direct binding to activated C2 and factor B, which provide the catalytic center to the C3 convertase (Milder et al., 2006; 2007), could explain the inhibitory activity of SCIN. In such a model SCIN would lock the convertase catalytic center in an inactive conformation and/or block substrate binding. However, residues Leu26 to Gly48, essential for the inhibiting activity of SCIN, adopt a distinct helix-loop-helix conformation that deviates significantly from the large and flexible inhibitory loops observed in trypsin inhibitors. The absence of SCIN affinity towards the isolated components of the convertases indicates specific conformations within the convertase are pivotal for SCIN binding.

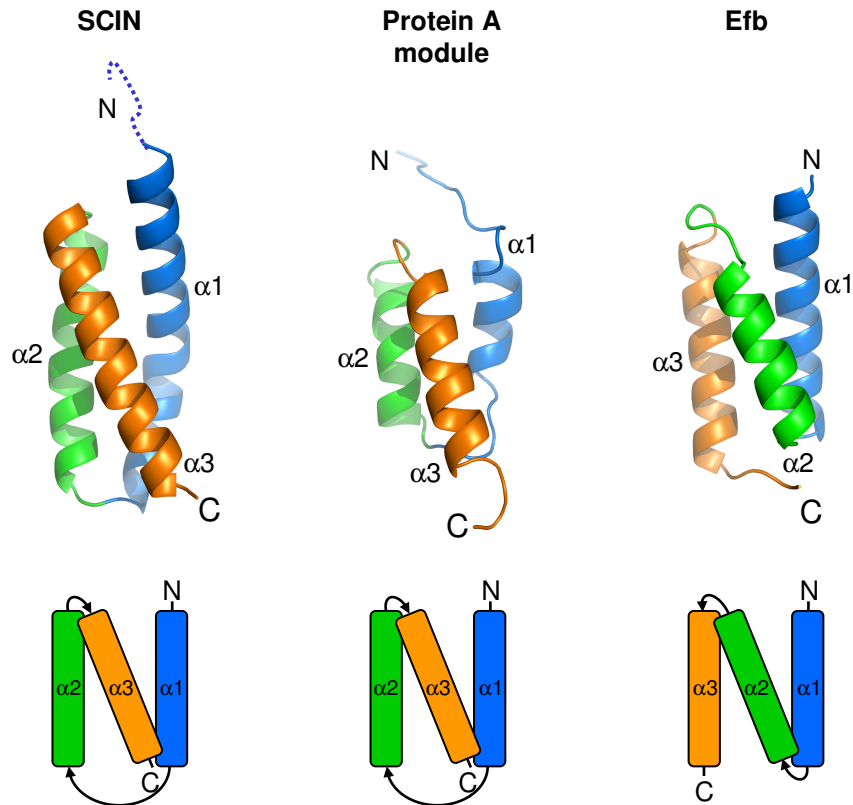


**Figure 4.8 Structural comparison of three *S. aureus* immune modulators.**

SCIN (left panel), Protein A module (middle panel, pdb 1bdd), and Efb-C (right panel, pdb 2gom) in ribbon and schematic representation. Helices are colored blue (helix 1), green (helix 2) and orange (helix 3).

Within the active helix-loop-helix segment, 6 residues (28-VxxxAxGSxNxxY-40) are conserved among the three active SCIN molecules and are absent in the structural but non-functional homolog ORF-D (Figure 4.9). In the structure of SCIN these residues are positioned on opposite sides which may indicate SCIN binds via two sides to the convertase. The 6 residues are positioned in a non-charged plane that is sandwiched by the positively and negatively charged top and bottom sides of SCIN respectively. Due to the relative small size, SCIN could easily fit into a pocket of one of the much larger convertase components. A two binding site model agrees with the observation that SCIN binding stabilizes the convertase. A comparable cross-linking is proposed for a single *S. aureus* protein A (SpA) domain that, despite its small size (~7 kDa), simultaneously can bind the Fc and the Fab region of immunoglobulins (Graille et al., 2000). Interestingly, comparison of SCIN with



the five extracellular Ig-binding modules of the *S. aureus* protein A (SpA) reveals a striking similarity in helical arrangement (Figure 4.8). In summary, the capacity to stabilize the convertase and the opposite orientation of conserved residues within the active site may indicate SCIN binds to both components of the C3 convertase.

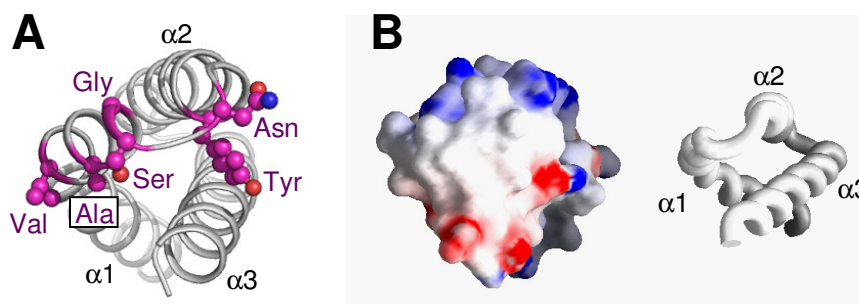


**Figure 4.9 Active site residues of SCIN for the Alternative Pathway.**

**A)** SCIN shown in ribbon representation (grey) with active site residues conserved within SCIN, SCIN-B and SCIN-C but not in ORF-D highlighted and shown in ball-and-stick representation (purple). **B)** Left panel - Electrostatic surface representation in and around the SCIN active site. Positively charged regions are represented in blue, negatively charged regions in red, and both polar and nonpolar regions are in white. Right panel - Similar view of SCIN shown in ribbon representation. Pictures were generated by GRASP (Nicholls et al., 1993).

With the current lack of proper treatment for complement mediated diseases, insights into the specific and effective complement inhibition by SCIN provide a useful tool in the development of a non-immunogenic complement inhibitor. Due to pre-existing antibodies, generation of a smaller compound with complement inhibitory capacity will be crucial for therapeutic use of SCIN. The fact that modulation of the AP is located in a distinct part (Leu-26 to Gly-48) of SCIN is promising for development of such a compound. The same stretch of residues was shown to be critical in assays in which all complement initiation routes were triggered and C5a response was analyzed. The structure and the identification of the active site of SCIN presented in this paper provide a starting point for structure-based drug design.

## Acknowledgements

We acknowledge the European Synchrotron Radiation Facility for provision of synchrotron radiation facilities and we would like to thank the beamline scientists at ID-14-EH4 for their help with data collection. We thank Jeroen Geurtsen for

providing the methionine-auxotrophic *E. coli* strain. This work was supported by grants from: NWO (Netherlands Organisation for Scientific Research)-VENI (#916-76-037), a “Pionier” programme grant (P.G.) of the Council for Chemical Sciences of NWO (NWO-CW) and NGI (Netherlands Genomics Initiative)-Horizon (#050-71-028).

## References

- Bestebroer, J.M., Poppelier, J., Ulfman, L.H., Lenting, P.J., Denis, C.V., van Kessel, K.P., van Strijp, J.A., and de Haas, C. J. (2007). Staphylococcal superantigen-like 5 binds PSGL-1 and inhibits P-selectin-mediated neutrophil rolling. *Blood*. 109, 2936-2943.
- Carroll, M.C. (2004). The complement system in regulation of adaptive immunity. *Nat. Immunol.* 5, 981-986.
- de Haas, C.J., Veldkamp, K.E., Peschel, A., Weerkamp, F., van Wamel, W.J., Heezius, E.C., Poppelier, M.J., van Kessel, K.P., and van Strijp, J.A. (2004). Chemotaxis inhibitory protein of *Staphylococcus aureus*, a bacterial antiinflammatory agent. *J. Exp. Med.* 199, 687-695
- Emsley, P., and Cowtan, K. (2004). Coot: model-building tools for molecular graphics. *Acta Crystallogr. D Biol. Crystallogr.* 60, 2126-2132.
- Graille, M., Stura, E.A., Corper, A.L., Sutton, B.J., Taussig, M.J., Charbonnier, J.B., and Silverman, G.J. (2000). Crystal structure of a *Staphylococcus aureus* protein A domain complexed with the Fab fragment of a human IgM antibody: structural basis for recognition of B-cell receptors and superantigen activity. *Proc. Natl. Acad. Sci. U. S. A.* 97, 5399-5404.
- Finlay, B. B., and McFadden, G. (2006). Anti-immunology: evasion of the host immune system by bacterial and viral pathogens. *Cell*. 124, 767-782.
- Foster, T. J. (2005). Immune evasion by staphylococci. *Nat. Rev. Microbiol.* 3, 948-958.
- Fujita, T., Matsushita, M., and Endo, Y. (2004). The lectin-complement pathway--its role in innate immunity and evolution. *Immunol. Rev.* 198, 185-202.
- Gasque, P. (2004). Complement: a unique innate immune sensor for danger signals. *Mol. Immunol.* 41, 1089-98.
- Haas, P.J., de Haas, C.J., Kleibeuker, W., Poppelier, M.J., van Kessel, K.P., Kruijtzter, J.A., Liskamp, R.M., and van Strijp, J.A. (2004). N-terminal residues of the chemotaxis inhibitory protein of *Staphylococcus aureus* are essential for blocking formylated peptide receptor but not C5a receptor. *J. Immunol.* 173, 5704-5711.
- Hammel, M., Sfyroera, G., Ricklin, D., Magotti, P., Lambris, J.D., and Geisbrecht, B.V. (2007). A structural basis for complement inhibition by *Staphylococcus aureus*. *Nat. Immunol.* 8, 430-437.
- Helmy, K.Y., Katschke, K.J., Jr., Gorgani, N.N., Kljavin, N.M., Elliott, J.M., Diehl, L., Scales, S.J., Ghilardi, N., and van Lookeren Campagne, M. (2006). CR1g: a macrophage complement receptor required for phagocytosis of circulating pathogens. *Cell* 124, 915-927.
- Ho, S.N., Hunt, H.D., Horton, R.M., Pullen, J.K., and Pease, L.R. (1989). Site-directed mutagenesis by overlap extension using the polymerase chain reaction. *Gene* 77, 51-59.
- Janssen, B.J., Christodoulidou, A., McCarthy, A., Lambris, J.D., and Gros, P. (2006). Structure of C3b reveals conformational changes that underlie complement activity. *Nature* 444, 213-216.
- Janssen, B.J., Huizinga, E.G., Raaijmakers, H.C., Roos, A., Daha, M.R., Nilsson-Ekdahl, K., Nilsson, B., and Gros, P. (2005). Structures of complement component C3 provide insights into the function and evolution of immunity. *Nature* 437, 505-511.

- Jarva, H., Jokiranta, T.S., Wurzner, R., and Meri, S. (2003). Complement resistance mechanisms of streptococci. *Mol. Immunol.* *40*, 95-107.
- Kirkitadze, M. D., and Barlow, P. N. (2001). Structure and flexibility of the multiple domain proteins that regulate complement activation. *Immunol. Rev.* *180*, 146-16.
- Kraiczky, P., Hellwage, J., Skerka, C., Kirschfink, M., Brade, V., Zipfel, P.F., and Wallich, R., (2003). Immune evasion of *Borrelia burgdorferi*: mapping of a complementinhibitor factor H-binding site of BbCRASP-3, a novel member of the Erp protein family. *Eur. J. Immunol.* *33*, 697-707.
- Lambris, J.D. (1988). The multifunctional role of C3, the third component of complement. *Immunol. Today* *9*, 387-393
- Langley, R., Wines, B., Willoughby, N., Basu, I., Proft, T., and Fraser, J.D. (2005). The staphylococcal superantigen-like protein 7 binds IgA and complement C5 and inhibits IgA-Fc alpha RI binding and serum killing of bacteria. *J. Immunol.* *174*, 2926-2933.
- Lee, L. Y., Liang, X., Hook, M., and Brown, E.L. (2004). Identification and characterization of the C3 binding domain of the *Staphylococcus aureus* extracellular fibrinogen-binding protein (Efb). *J. Biol. Chem.* *279*, 50710-50716.
- Leslie, A.G. (2006). The integration of macromolecular diffraction data. *Acta Crystallogr. D Biol. Crystallogr.* *62*, 48-57.
- Milder, F.J., Gomes, L., Schouten, A., Janssen, B.J., Huizinga, E.G., Romijn, R.A., Hemrika, W., Roos, A., Daha, M.R., and Gros, P. (2007). Factor B structure provides insights into activation of the central protease of the complement system. *Nat. Struct. Mol. Biol.* *14*, 224-228.
- Milder, F.J., Raaijmakers, H.C., Vandeputte, M.D., Schouten, A., Huizinga, E.G., Romijn, R.A., Hemrika, W., Roos, A., Daha, M.R., and Gros, P. (2006). Structure of complement component c2a: implications for convertase formation and substrate binding. *Structure* *14*, 1587-1597.
- Mullick, J., Bernet, J., Panse, Y., Hallihosur, S., Singh, A.K., and Sahu, A. (2005). Identification of complement regulatory domains in vaccinia virus complement control protein. *J. Virol.* *79*, 12382-12393.
- Nicholls, A., Bharadwaj, R., and Honig, B. (1993). GRASP: Graphical representation and analysis of surface properties *Biophys. J.* *64*, 166-170.
- Pangburn, M.K., and Rawal, N. (2002). Structure and function of complement C5 convertase enzymes. *Biochem. Soc. Trans.* *30*, 1006-1010.
- Perrakis, A., Morris, R., and Lamzin, V.S. (1999). Automated protein model building combined with iterative structure refinement. *Nat. Struct. Biol.* *6*, 458-463.
- Postma, B., Poppelier, M.J., van Galen, J.C., Prossnitz, E.R., van Strijp, J.A., de Haas, C.J., and van Kessel, K.P. (2004). Chemotaxis inhibitory protein of *Staphylococcus aureus* binds specifically to the C5a and formylated peptide receptor. *J. Immunol.* *172*, 6994-7001.
- Postma, B., Kleibeuker, W., Poppelier, M.J., Boonstra, M., van Kessel, K.P., van Strijp, J.A., and de Haas, C.J. (2005). Residues 10-18 within the C5a receptor N terminus compose a binding domain for chemotaxis inhibitory protein of *Staphylococcus aureus*. *J. Biol. Chem.* *280*, 2020-2027.
- Ram, S., Cullinane, M., Blom, A.M., Gulati, S., McQuillen, D.P., Monks, B.G., O'Connell, C., Boden, R., Elkins, C., Pangburn, M.K., Dahlback, B., and Rice, P.A., (2001). Binding of C4b-binding protein to porin: a molecular mechanism of serum resistance of *Neisseria gonorrhoeae*. *J. Exp. Med.* *193*, 281-295.
- Rooijackers, S.H.M., Ruyken, M., Roos, A., Daha, M.R., Presanis, J.S., Sim, R.B., van Wamel, W.J., van Kessel, K.P., and van Strijp, J.A. (2005). Immune evasion by a staphylococcal complement inhibitor that acts on C3 convertases. *Nat. Immunol.* *6*, 920-927.
- Rooijackers, S.H.M., van Wamel, J., Ruyken, M., van Kessel, K.P., and van Strijp, J. A. (2005). Anti-opsonic properties of staphylokinase. *Microbes. Infect.* *7*, 476-484.
- Rooijackers, S.H.M., van Kessel, K.P., and van Strijp, J. A. (2005). Staphylococcal innate immune evasion. *Trends Microbiol.* *13*, 596--601.

- Rooijackers, S.H.M., Ruyken, M., van Roon, J., van Kessel, K.P., van Strijp, J.A., and van Wamel, W.J. (2006). Early expression of SCIN and CHIPS drives instant immune evasion by *Staphylococcus aureus*. *Cell. Microbiol.* *8*, 1282-1293.
- Roos, A., Bouwman, L.H., Munoz, J., Zuiverloon, T., Faber-Krol, M.C., Fallaux-van den Houten F.C., Klar-Mohamad, N., Hack, C.E., Tilanus, M.G., and Daha, M.R. (2003). Functional characterization of the lectin pathway of complement in human serum. *Mol. Immunol.* *39*, 655-668.
- Rutten, L., Geurtsen, J., Lambert, W., Smolenaers, J.J., Bonvin, A. M., de Haan, A., van der Ley, P., Egmond, M.R., Gros, P., and Tommassen, J. (2006). Crystal structure and catalytic mechanism of the LPS 3-O-deacylase PagL from *Pseudomonas aeruginosa*. *Proc. Natl. Acad. Sci. U. S. A* *103*, 7071-7076.
- Seelen, M.A., Roos, A., and Daha, M.R. (2005) Role of complement in innate and autoimmunity. *J. Nephrol.* *18*, 642-653.
- Terwilliger, T.C. (2003). Automated main-chain model building by template matching and iterative fragment extension. *Acta Crystallogr. D Biol. Crystallogr.* *59*, 38-44.
- Trouw, L.A., Seelen, M.A., and Daha, M.R. (2003) Complement and renal disease. *Mol. Immunol.* *40*, 125-134
- Veldkamp, K.E., van Kessel, K.P., Verhoef, J., and van Strijp, J.A. (1997). Staphylococcal culture supernates stimulate human phagocytes. *Inflammation* *21*, 541-551.
- Walport, M.J. (2001a). Complement. First of two parts. *N. Engl. J. Med.* *344*, 1058-1066.
- Walport, M.J. (2001b). Complement. Second of two parts. *N. Engl. J. Med.* *344*, 1140-1144.
- Wang, Y. (2006). Complementary therapies for inflammation. *Nat. Biotechnol.* *24*, 1224-1226.
- Winn, M.D., Isupov, M.N., and Murshudov, G.N. (2001). Use of TLS parameters to model anisotropic displacements in macromolecular refinement. *Acta Crystallogr. D Biol. Crystallogr.* *57*, 122-133.
- Xu, Y., Narayana, S.V., and Volanakis, J.E. (2001). Structural biology of the alternative pathway convertase. *Immunol. Rev.* *180*, 123-135.

# 5

## **Summarizing discussion**

The immune system protects the host from invading pathogenic organisms. Essential in this process is the complement system, which recognizes and kills pathogens, presents pathogens to the adaptive immune system, and elicits inflammatory responses (Walport 2001a, 2001b; Carroll 2004). Central in the complement activation process is the formation of the C3 convertase, a bimolecular enzyme complex on the cell surface of invading pathogens or altered host cells (Fishelson et al., 1983; Pangburn and Muller-Eberhard 1986). Insight into the molecular mechanisms underlying formation and regulation of these key enzymes, is important for the understanding of pathogen immune evasion and host self-defense, and for the development of complement-immune therapies.

To gain more insight into the mechanisms that regulate C3 convertase activity, the studies described in this thesis focus on the proteins C2 and factor B that provide the catalytic center to the C3 convertases (Figure 5.1), and on the bacterial convertase-inhibitory protein SCIN. The obtained structural data provide a basis for a mechanistic model in which binding of C2 and factor B to the surface-bound cofactors C4b and C3b respectively, and their subsequent proteolytic activation are coupled to large conformational changes.

## 5.1 The catalytic component prior to convertase formation

To prevent unwanted complement activation, the catalytic component of the C3 convertase (C2 or factor B) circulates in the blood stream as pro-enzyme. To comprehend how the proteolytic activity of the 5 domain proteins, is regulated and how binding to their cofactor makes them susceptible to proteolytic activation, the crystal structure of recombinant factor B was determined (**Chapter 3**).

The overall structure of factor B consists of three lobes representing the three N-terminal complement control protein (CCP) domains, the von Willebrand factor type A (VWA) domain, and the C-terminal serine protease (SP) domain.

The CCP domains adopt a triad arrangement; CCP 2 and 3 form an anti-parallel dimer that is capped by CCP1. In the center of this compact arrangement a hydrophobic core is observed. The tight interface between CCP domains 2 and 3 likely is important for the functional activity of C2 and factor B since mutations within these domains reduces the capacity of both proteins to bind their cofactor (Hourcade et al., 1995; Xu and Volanakis 1997). The triad of CCP domains is only weakly associated with the rest of the protein, suggesting that they may dislocate upon cofactor binding.

The N-terminal part of the 45-residue linker connecting the third CCP and the VWA domain forms an  $\alpha$ -helix ( $\alpha$ L) that, surprisingly, is structurally incorporated in the VWA domain. The linker segment following helix  $\alpha$ L was not modeled in the structure of factor B due to poor electron density, indicating flexibility. The scissile bond in the C-terminal part of the linker is partially buried and the side-chain of the P1-arginine is bound to helix  $\alpha$ L and to helix  $\alpha$ 7 of the VWA domain and thereby points away from the solvent. As such the cleavage site is inaccessible for the serine proteases that activate factor B, implying that the protein must undergo conformational changes during convertase formation.

In the structure of factor B the metal ion dependent adhesion site (MIDAS) in the VWA domain adopts an ion-free distorted conformation. This conformation explains the low affinity of factor B towards divalent ions (Fishelson et al., 1983). The distortion is caused by direct and indirect interactions with the first CCP domain that partially covers the MIDAS. This suggests that the MIDAS of factor B cannot bind its ligand, i.e. cofactor C3b, unless CCP domain 1 moves aside. As shown for integrin I domains, that are homologous to VWA domains (Springer, 2006), the MIDAS conformation is directly related to the position of the activation helix  $\alpha$ 7 (Shimaoka et al., 2002; Luo and Springer 2006). In factor B helix  $\alpha$ 7 is displaced from its normal binding groove by helix  $\alpha$ L (Bhattacharya et al., 2004; Ponnuraj et al., 2004), that occupies the position of helix  $\alpha$ 7 as observed in activated, liganded I domains (Emsley et al., 2000; Shimaoka et al. 2003). The preceding loop  $\beta$ F- $\alpha$ 7 and adjacent helix  $\alpha$ 1 adopt the closed conformation similar to inactive, unliganded I domains (Emsley et al., 1997) The conformation of the VWA domain as described above shows the  $Mg^{2+}$  dependent cofactor binding site of factor B is “locked” in an inactive conformation by CCP domain 1 and helix  $\alpha$ L.

The SP domain carries the catalytic center of the C3 convertases. In the structure of factor B the loop forming the oxyanion hole displays an outward orientation similar to observed in activated trypsin. This conformation is unexpected since factor B is a pro-enzyme, and lacks a liberated N-terminus that induces the outwards orientation of the oxyanion hole-forming loop in trypsins (Khan and James 1998). Due to a  $\sim 180^\circ$  flip of a single peptide plain the oxyanion hole of factor B is ill-formed. Again this is unexpected since in trypsins the outwards orientation of the oxyanion hole-forming loop is coupled to maturation of the oxyanion hole. The arrangement of the catalytic center of factor B suggests its activity is not regulated as in trypsinogens, but rather through quaternary rearrangement of the domains during assembly of the convertase and/or following substrate binding.

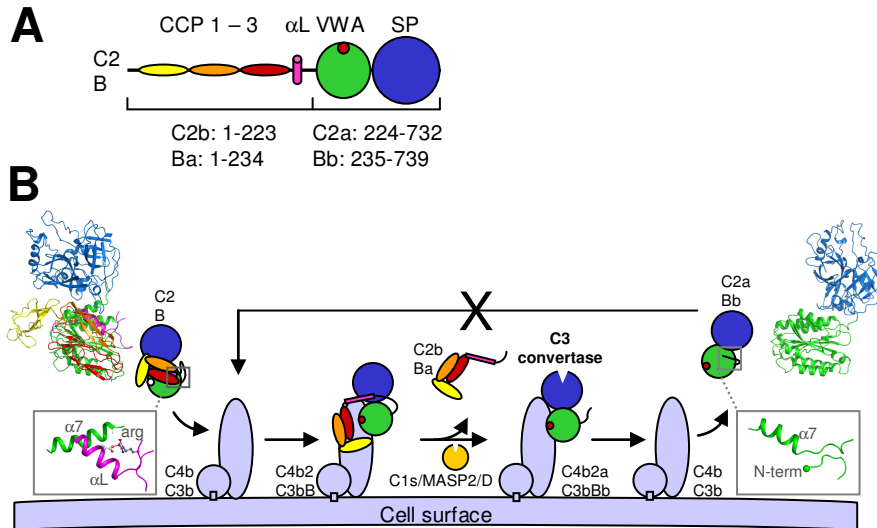


**Figure 5.1 Domain topology of C2 and factor B and convertase formation model**

**A)** Schematic representation of C2 and factor B, indicated are the domains and the linker helix ( $\alpha$ L). **B)** Cartoon representation of C3 convertase formation. Shown in ribbon representation are the crystal structures of factor B (left) and C2a (right).

## 5.2 The catalytic component after dissociation from the convertase

Once dissociated the catalytic components C2a and Bb cannot re-associate with their still functional cofactor and are no longer active (Figure 5.1). This serves as an inherent stop signal in regulation of complex formation. In order to gain insight in the mechanisms underlying irreversibility and inactivation the crystal structure of recombinant C2a was determined (**Chapter 2**).

Two structures of C2a were determined, one unliganded and one with a pseudo ligand bound to the VWA domain.

In both structures the eight residue N-terminal tail, formed upon proteolysis C2 bound to its cofactor C4b, is structurally incorporated in the VWA domain. Via hydrophobic interactions the N-terminus is immobilized in a groove near the VWA-SP domain interface and is partially covered by residues from the adjacent domain-domain linker. This arrangement suggest the N-terminal tail adopts a different conformation in the C4bC2 and C3bB complexes, otherwise the scissile bond is inaccessible for the serine proteases that activate C2 and factor B.



In both the unliganded and pseudo-liganded C2a structures the VWA domain displays a MIDAS in an open conformation. This indicates the open MIDAS occurs independent of ligand binding. The activation helix  $\alpha 7$  of the VWA domain is positioned neither in the inactive or active conformation. Putatively, this intermediate position of helix  $\alpha 7$  reduces the affinity of the VWA domain towards its ligand. The intermediate conformation is caused by the N-terminus, which also prevents helix  $\alpha 7$  to adopt the activated position. By the interaction with helix  $\alpha 7$ , the N-terminus indirectly affects the VWA-SP domain orientation.

Characteristic for the domain-domain interface in C2a, next to the presence of the N-terminus, are two N-linked glycans from the SP domain. Deletion of the first and second glycan yields almost inactive C2 and C2 with slightly enhanced activity, respectively. Deletion of both glycans yields C2 that is only a little active. This indicates the two interface glycans are important but not crucial for C2 activity.

The SP domain of C2a displays a catalytic center in which an arginine from a nearby surface loop mimics the N-terminus via which trypsinogens are activated. However, the catalytic center adopts a near-active conformation similar to observed in pro-enzyme factor B; the oxyanion hole loop points outwards whereas the oxyanion hole is ill-formed. This conformation indicates the activity of the SP domain is not regulated as in trypsins. The surface loops surrounding the catalytic center of C2a differ from trypsin due to large insertions and deletions. The largest insertion is present in the partially flexible loop 2, that harbors the arginine interacting with the catalytic center. A simple C2a-C3 enzyme-substrate model suggests the extended loops increase the contact area in between both proteins. Putatively, these interactions induce the required maturation of the oxyanion hole via stabilization of the nearby loop 2.

### 5.3 C3 convertase inhibition by Staphylococcal complement inhibitor (SCIN)

The pathogenic bacterium *Staphylococcus aureus* counteracts the host immune defense system by secretion of SCIN (Rooijackers et al., 2005). The crystal structure of this C3 convertase inhibiting protein was determined and structure based chimeric proteins and SCIN homologs were functionally characterized to increase the understanding of immune evasion by pathogens (**Chapter 4**).

SCIN adopts a coiled-coil conformation comprising three helices and a flexible N-terminus. The all-helical structure suggests a new mechanism of C3 convertase inhibition since most regulators are formed by consecutive CCP domains (Kirkitaдзе and Barlow 2001).

Functional characterization of chimeric proteins consisting of SCIN and the structurally but non-functionally homologous ORF-D, indicate an 18-residue segment that is crucial for SCIN activity. Chimeras lacking these residues show strongly reduced capacity to inhibit alternative pathway mediated opsonization (C3b deposition) and formation of the membrane attack complex (MAC). Likewise, classical/lectin pathway mediated opsonization and MAC formation is reduced, although additional sites in SCIN are involved. These chimeric proteins also lose their capacity to inhibit production of C5a.

Next to their diminished inhibitory capacity the chimeras also fail to stabilize the C3 convertases. This suggests the stabilizing effect is an important part of the mechanism by which SCIN inhibits the activity of the convertase. SCIN does not bind the isolated components of the convertases, suggesting that specific conformations within the convertase are pivotal. The conserved residues within the 18-residues segment are positioned on opposite sides of the molecule. This may indicate cross-linking of the catalytic and cofactor component underlies the observed stabilizing effect. SCIN inhibits all convertases, which may point towards an interaction with substrate C3.

#### **5.4 C3 convertase assembly and dissociation model**

The inherent instability of the C3 convertase hampers structural characterization of this central enzyme complex. However, from the structural advances presented in this thesis a model can be deduced describing the intricate conformational changes of the catalytic components during convertase formation and dissociation (Figure 5.1B). This model can form a basis for future studies to further unravel the regulatory mechanisms underlying complement activation.

The convertases are formed in two steps. First, pro-enzymes C2 and factor B bind their surface bound cofactors. Second, associated C2 and factor B are cleaved by specific complement serine proteases which yields the C3 convertases C4b2a and C3bBb. Binding of the pro-enzymes to the cofactor proceeds via two sites; a Mg<sup>2+</sup> independent one located in the small fragment (C2b/Ba) and a Mg<sup>2+</sup> dependent one located in the VWA domain of the large fragment (C2a/Bb). In the proposed mechanistic model C2 and factor B initially bind their cofactor via the site in the

small fragment, which dislocates the CCP domains and the linker helix. These displacements unlock the VWA domain. As a result the activation helix  $\alpha 7$  can take its active position, priming the  $Mg^{2+}$  dependent binding site for high affinity cofactor binding. Simultaneously, the rearrangement of the linker and activation helix expels the cleavage site from its buried position. The exposed scissile bond can now be cleaved by the proteases that activate the pro-enzyme. Following cleavage, the liberated small fragment dissociates from the complex, leaving behind the C3 convertase.

The irreversibility of C3 convertase dissociation may be explained by the arrangement of the N-terminal residues and the activation helix  $\alpha 7$  as observed in the structure of C2a. In C2a the N-terminus is structurally incorporated in the VWA domain directly adjacent to helix  $\alpha 7$ . This conformation enforces the activation helix in the intermediate position and prevents the VWA domain to adopt the active conformation that putatively is required for the catalytic component to rebind its cofactor.

## References

- Bhattacharya, A.A., Lupper, M.L., Jr., Staunton, D.E., and Liddington, R.C. (2004). Crystal structure of the A domain from complement factor B reveals an integrin-like open conformation. *Structure (Camb)* *12*, 371-378.
- Carroll, M.C. (2004). The complement system in regulation of adaptive immunity. *Nat. Immunol.* *5*, 981-986.
- Emsley, J., King, S.L., Bergelson, J.M., and Liddington, R.C. (1997). Crystal structure of the I domain from integrin  $\alpha 2\beta 1$ . *J. Biol. Chem.* *272*, 28512-28517.
- Emsley, J., Knight, C.G., Farndale, R.W., Barnes, M.J., and Liddington, R.C. (2000). Structural basis of collagen recognition by integrin  $\alpha 2\beta 1$ . *Cell* *101*, 47-56.
- Fishelson, Z., Pangburn, M.K., and Muller-Eberhard, H.J. (1983). C3 convertase of the alternative complement pathway. Demonstration of an active, stable C3b, Bb (Ni) complex. *J. Biol. Chem.* *258*, 7411-7415.
- Hourcade, D.E., Wagner, L.M., and Oglesby, T.J. (1995). Analysis of the short consensus repeats of human complement factor B by site-directed mutagenesis. *J. Biol. Chem.* *270*, 19716-19722.
- Khan, A.R. and James, M.N. (1998). Molecular mechanisms for the conversion of zymogens to active proteolytic enzymes. *Protein Sci.* *7*, 815-836.
- Kirkitadze, M. D. and Barlow, P. N. (2001). Structure and flexibility of the multiple domain proteins that regulate complement activation. *Immunol. Rev.* *180*, 146-161.
- Luo, B. H. and Springer, T. A. (2006). Integrin structures and conformational signaling. *Curr. Opin. Cell. Biol.* *18*, 579-586.
- Pangburn, M. K. and Muller-Eberhard, H. J. (1986). The C3 convertase of the alternative pathway of human complement. Enzymic properties of the bimolecular proteinase. *Biochem. J.* *235*, 723-730.

- Ponnuraj, K., Xu, Y., Macon, K., Moore, D., Volanakis, J.E., and Narayana, S.V. (2004). Structural analysis of engineered Bb fragment of complement factor B: insights into the activation mechanism of the alternative pathway C3-convertase. *Mol. Cell* *14*, 17-28.
- Rooijackers, S.H.M, Ruyken, M., Roos, A., Daha, M.R., Presanis, J.S., Sim, R.B., van Wamel, W.J., van Kessel, K.P., and van Strijp, J.A. (2005). Immune evasion by a staphylococcal complement inhibitor that acts on C3 convertases. *Nat. Immunol.* *6*, 920-927.
- Shimaoka, M., Takagi, J., and Springer, T.A. (2002). Conformational regulation of integrin structure and function. *Annu. Rev. Biophys. Biomol. Struct.* *31*, 485-516.
- Shimaoka, M., Xiao, T., Liu, J.H., Yang, Y., Dong, Y., Jun, C.D., McCormack, A., Zhang, R., Joachimiak, A., Takagi, J., Wang, J.H., and Springer, T.A. (2003). Structures of the alpha L I domain and its complex with ICAM-1 reveal a shape-shifting pathway for integrin regulation. *Cell* *112*, 99-111.
- Springer, T. A. (2006). Complement and the Multifaceted Functions of VWA and Integrin I Domains. *Structure* *14*, 1611-1616.
- Walport, M. J. (2001a). Complement. First of two parts. *N. Engl. J. Med.* *344*, 1058-1066.
- Walport, M. J. (2001b). Complement. Second of two parts. *N. Engl. J. Med.* *344*, 1140-1144.
- Xu, Y. and Volanakis, J. E. (1997). Contribution of the complement control protein modules of C2 in C4b binding assessed by analysis of C2/factor B chimeras. *J. Immunol.* *158*, 5958-5965.

## Samenvattende discussie

Het immuunsysteem beschermt de gastheer tegen binnendringende ziekteverwekkende (pathogene) organismen. Een belangrijk onderdeel van dit proces is het complementsysteem. Dit systeem herkent en doodt pathogene organismen, biedt deze aan het aangeboren immuunsysteem aan en ontstekingsreacties worden geïnitieerd. Centraal in de activering van complement staat de vorming van het C3 convertase, een uit twee eiwitten bestaand enzymcomplex op het celoppervlak van de pathogeen of een gewijzigde gastheercel. Inzicht in de vorming en regulatie van deze essentiële enzymen (en de onderliggende moleculaire mechanismen) is van belang voor het begrijpen van de wijze waarop ziekteverwekkers het immuunsysteem ontwijken en gastheercellen zichzelf beschermen tegen het immuunsysteem en voor het ontwikkelen van complement-immunotherapieën.

Om meer inzicht te krijgen in de manier waarop de activiteit van C3 convertases wordt gereguleerd, concentreerde het onderzoek beschreven in dit proefschrift zich op de eiwitten die het katalytische centrum van het C3 convertase vormen: C2 en factor B (Figuur 5.1). Daarnaast werd er onderzoek verricht aan het bacteriële eiwit SCIN, dat de activiteit van de convertases remt. De verkregen structuurdata vormen een basis voor een mechanistisch model waarin de binding van C2 en factor B aan hun cofactoren (respectievelijk C4b en C3b) en hun proteolytische activering gepaard gaat met grote conformationele veranderingen.

### 5.1 De catalytische component voorafgaande aan convertase vorming

Om ongewenste activering van het complementsysteem te voorkomen, circuleren de katalytische componenten van het C3 convertase (C2 en factor B), als pro-enzymen in het bloed. Om te begrijpen hoe de activiteit van deze uit 5 domeinen bestaande eiwitten is gereguleerd en hoe de binding aan de cofactor ze vatbaar maakt voor proteolytische activering, is de kristalstructuur van recombinant factor B bepaald (**Hoofdstuk 3**).

De globale structuur van factor B bestaat uit drie delen; de drie N-terminale “complement control protein” (CCP) domeinen, het von Willebrand factor type A (VWA) domein, en het C-terminale serine protease (SP) domein.

De CCP domeinen zijn gepositioneerd in een triade; CCP 2 en 3 staan antiparallel t.o.v. elkaar en vormen een dimeer die is afgedekt door CCP1. Een hydrofobe kern vormt het centrum van de compacte rangschikking. Waarschijnlijk is de hechte interface tussen het tweede en derde CCP domein van belang voor de functionele activiteit van C2 en factor B, omdat mutaties in deze domeinen zorgen voor een verlaging van de cofactor-bindingscapaciteit van de twee eiwitten. De triade van CCP domeinen is slechts zwak gebonden aan de rest van het eiwit, wat aangeeft dat deze domeinen mogelijk verplaatsen tengevolge van cofactor-associatie.

Het N-terminale gedeelte van de uit 45 residuen bestaande verbinding/linker tussen CCP 3 en het VWA domein, vormt een  $\alpha$  helix ( $\alpha$ L) die een structureel onderdeel is van het VWA domein. Het daarop volgende deel van de linker is niet gemodelleerd in de structuur van factor B, omdat de elektronendichtheid hiervan van slechte kwaliteit was. Deze slechte kwaliteit wordt waarschijnlijk veroorzaakt door locale flexibiliteit van het molecuul. De te splitsen peptide binding, de “scissile bond”, in het C-terminale gedeelte van de verbinding is gedeeltelijk onttrokken aan het eiwitoppervlak. De zijketen van de P1-arginine keert zich af van het oplosmiddel, omdat deze gebonden is aan zowel helix  $\alpha$ L als helix  $\alpha$ 7 van het VWA domein. Als zodanig is de “scissile bond” dus niet beschikbaar voor de serine proteases die factor B activeren, wat suggereert dat het eiwit conformationele veranderingen moet ondergaan gedurende vorming van het convertase.

De “metal ion dependent adhesion site” (MIDAS) in het VWA domein neemt een misvormde conformatie aan in de structuur van factor B. Deze conformatie verklaart de lage affiniteit van factor B ten opzichte van divalente ionen. De misvorming wordt veroorzaakt door directe en indirecte wisselwerkingen met het CCP 1, welke gedeeltelijk de MIDAS bedekt. Dit duidt erop dat de MIDAS in factor B geen ligand (cofactor) kan binden, tenzij CCP1 verplaatst. Zoals aangetoond voor Integrine I domeinen, welke homoloog zijn aan de VWA domeinen, is er een directe relatie tussen de conformatie van de MIDAS en de positie van de activeringshelix  $\alpha$ 7. In factor B is de activeringshelix verdrongen van zijn normale groeve door helix  $\alpha$ L, die de positie inneemt van helix  $\alpha$ 7, zoals in geactiveerde, ligand gebonden I domeinen. De voorafgaande lus  $\beta$ F- $\alpha$ 7 en naastgelegen helix  $\alpha$ 1 nemen de gesloten conformatie aan zoals in inactieve, niet ligand gebonden I domeinen. De hierboven beschreven conformatie van het VWA domein laat zien hoe de  $Mg^{2+}$  afhankelijke cofactor-bindingsplaats van factor B is “vastgezet” in de inactieve conformatie door CCP 1 en helix  $\alpha$ L.

Het SP domein bevat het katalytische centrum van de C3 convertases. In de structuur van factor B neemt de oxyanionholte-vormende lus de naar buiten

gerichte conformatie aan zoals in geactiveerde trypsines. Dit is een onverwachte conformatie aangezien factor B een pro-enzym is en niet beschikt over een vrije N-terminus die bij trypsines juist zorgt voor de naar buiten gerichte oriëntatie van de oxyanionholte-vormende lus. De oxyanionholte zelf is niet compleet wegens een  $\sim 180^\circ$  draai van één peptidevlak. Dit is opvallend, omdat in trypsines de naar buiten gerichte conformatie altijd samen met een volledig gevormde oxyanionholte voorkomt. De conformatie, zoals aanwezig in factor B, suggereert dat de activiteit van het katalytische centrum niet gereguleerd wordt zoals bij trypsine, maar eerder afhankelijk is van herschikkingen van domeinen gedurende de vorming van het convertase en/of door binding van het substraat.

## 5.2 De catalytische component na dissociatie van het convertase

Eénmaal gedissocieerd kunnen de katalytische componenten niet opnieuw associëren met hun nog steeds functionele cofactor en zijn ze dus niet langer actief. Dit functioneert als een stopsignaal in de regulatie van complexvorming. Om meer inzicht te krijgen in de mechanismen die zorgen voor de irreversibele en inactiverende dissociatie, werd de kristalstructuur van C2a bepaald (**Hoofdstuk 2**).

Er zijn twee structuren van C2a bepaald: één zonder ligand en één met een pseudo-ligand gebonden aan het VWA domein.

In beide structuren zijn de acht N-terminale residuen die gevormd worden na proteolyse van aan cofactor C4b gebonden C2, een structureel onderdeel van het VWA domein. Door hydrofobe interacties zit de N-terminus vast in een groeve naast de interface tussen het VWA-en het SP domein en is deze gedeeltelijk bedekt door de linker tussen beide domeinen. Deze rangschikking laat zien dat de N-terminus een andere conformatie heeft in het C4b2 en C3bB complex, anders zou de “scissile bond” niet beschikbaar zijn voor de serine proteases die C2 en factor B activeren.

In zowel de ligand-vrije als ligand-gebonden structuur van C2a neemt de MIDAS in het VWA domein een open conformatie aan. Dit suggereert dat de open MIDAS conformatie onafhankelijk is van ligandbinding. De activerings-helix  $\alpha 7$  in het VWA domein is gepositioneerd tussen de actieve en inactieve conformatie. Deze middenpositie van helix  $\alpha 7$  verlaagt de affiniteit van het VWA domein voor ligand. De middenconformatie wordt veroorzaakt door de N-terminus die er ook voor zorgt dat helix  $\alpha 7$  niet zijn geactiveerde positie kan aannemen. Door de interactie met helix  $\alpha 7$  beïnvloedt de N-terminus indirect de onderlinge oriëntatie van de VWA en SP domeinen.

Kenmerkend voor de domein-domein interface (naast de aanwezigheid van de N-terminus) zijn twee op het SP domein aanwezige asparagine gebonden suikers. Deletie van de eerste suiker resulteert in nagenoeg geheel inactief C2. Deletie van de tweede suiker, daarentegen leidt tot een iets verhoogde activiteit. Indien beide suikers afwezig zijn is C2 nog maar enigszins actief. Dit geeft aan dat de suikers belangrijk, maar niet cruciaal zijn voor de activiteit van C2.

Het SP domein van C2a laat een katalytisch centrum zien waarin een arginine uit een nabijgelegen oppervlakte lus (Lus 2) de vrije N-terminus nabootst via welke trypsines geactiveerd worden. Het katalytisch centrum verkeert echter in een bijna actieve conformatie, vergelijkbaar met de conformatie in pro-enzym factor B: de oxyanionholte-vormende lus wijst naar buiten, terwijl de oxyanionholte zelf niet compleet is. Deze conformatie laat zien dat de activiteit van het SP domein niet gereguleerd wordt zoals bij trypsines. De lussen aan de oppervlakte die het katalytische centrum van C2a omringen verschillen van trypsine door grote inserties en deleties. Lus 2 bevat de grootste insertie, is gedeeltelijk flexibel en bevat de arginine die de interactie aangaat met het katalytische centrum. Een eenvoudig C2a-C3 enzymsubstraat model geeft aan dat de verlengde lussen de raakvlakken tussen beide eiwitten misschien vergroten. Mogelijkerwijs resulteren deze interacties in een volledig gevormd oxyanionholte middels stabilisatie van de nabijgelegen lus 2.

### 5.3 C3 convertase remming door Staphylococcal complement inhibitor (SCIN)

De pathogene bacterie *Staphylococcus aureus* werkt de immuunverdediging van de gastheer tegen door middel van het uitscheiden van SCIN. Om beter te begrijpen hoe pathogene organismen het immuunsysteem omzeilen is de kristalstructuur van dit C3 convertase remmende eiwit bepaald en zijn op deze structuur gebaseerde chimera eiwitten en eiwitten homoloog aan SCIN functioneel gekarakteriseerd (**Hoofdstuk 4**).

SCIN neemt een coiled-coil conformatie aan bestaande uit drie helices en een flexibele N-terminus. De meeste regulatoren bestaan uit opeenvolgende CCP domeinen, terwijl SCIN enkel uit helices bestaat. Dit suggereert een nieuw C3 convertase remmend mechanisme.

Functionele karakterisatie van chimera eiwitten bestaande uit SCIN en het eiwit ORF-D (structureel maar niet functioneel vergelijkbaar met SCIN) geeft aan dat een segment van 18 residuen van cruciaal belang is voor de activiteit van SCIN.



Chimera eiwitten die deze residuen missen zijn een stuk minder goed in staat de door de alternatieve activatie-route geïnduceerde opsonisatie (C3b depositie) en vorming van het “membrane attack complex” (MAC) te remmen. Eveneens is de remming van opsonisatie en de vorming van het MAC middels de klassieke/lectin activatie-route gereduceerd. Hiervoor zijn waarschijnlijk nog additionele plaatsen in SCIN benodigd. Deze chimera eiwitten verliezen ook hun capaciteit om de C5a - productie te remmen.

Naast het verlies van de remmende werking zijn deze eiwitten ook niet meer in staat het C3 convertase te stabiliseren. Dit geeft aan dat het stabiliserende effect een belangrijk onderdeel is van het mechanisme waarmee SCIN de convertases remt. SCIN bindt niet aan de geïsoleerde componenten van de convertases, wat erop wijst dat specifieke conformaties in het convertase van cruciaal belang zijn. De residuen die geconserveerd zijn in het 18 residuen segment zijn gepositioneerd aan tegenoverstaande kanten van het molecuul. Dit doet vermoeden dat de stabilisatie mogelijk een gevolg is van cross-linking van de katalytische en cofactor component. SCIN remt alle convertases, wat mogelijk wijst op een interactie met substraat C3.

#### 5.4 C3 convertase associatie en dissociatie model

De instabiliteit van C3 convertase verhindert de structuurbepaling van dit centrale enzymcomplex. Evenwel kan er op basis van de verkregen structurele inzichten, zoals beschreven in dit proefschrift, een model gemaakt worden dat de ingewikkelde conformationele veranderingen van de katalytische component gedurende convertase associatie en dissociatie beschrijft (Figuur 5.1B). Dit model kan mogelijk gebruikt worden als ondersteuning voor toekomstige studies ter opheldering van de mechanismen die complement activering reguleren.

De convertases worden gevormd in twee stappen. Eerst binden de pro-enzymen C2 en factor B aan hun oppervlaktegebonden cofactoren. Vervolgens worden C2 en factor B geknipt door specifieke complement serine proteases, resulterend in de C3 convertases C4b2a en C3bBb. De pro-enzymen hebben twee cofactor bindingsplaatsen; een Mg<sup>2+</sup>-onafhankelijke bindingsplaats in het kleine fragment (C2b/Ba) en een Mg<sup>2+</sup>-afhankelijke bindingsplaats in het grote fragment (C2a/Bb). In het hier voorgestelde mechanistische model binden C2 en factor B hun cofactor initieel via de bindingsplaats in het kleine fragment. Dit zorgt voor de verplaatsing van de CCP domeinen en de linker-helix  $\alpha$ L. Deze herschikking ontsluit het VWA domein. Als gevolg hiervan kan de activerings-helix  $\alpha$ 7 zijn actieve positie

innemen en ervoor zorgen dat de  $Mg^{2+}$ -afhankelijke bindingsplaats met hoge affiniteit kan binden aan de cofactor. Gelijktijdig zorgt de herschikking van de linker en de activerings-helix ervoor dat de knipplaats tevoorschijn komt uit zijn verscholen positie. De “scissile bond” is nu beschikbaar voor proteases die de pro-enzymen activeren middels een knip. Na de knip laat het nu vrije, kleine fragment los van het complex en blijft het C3 convertase achter.

De irreversibele dissociatie van de C3 convertases kan mogelijk verklaard worden aan de hand van de rangschikking van de N-terminale residuen en de activerings-helix  $\alpha 7$ , zoals aanwezig in de structuur van C2a. In C2a is de N-terminus opgenomen in het VWA domein direct naast helix  $\alpha 7$ . Deze conformatie dwingt de activeringshelix in de middenpositie en voorkomt dat het VWA domein de actieve conformatie aan kan nemen die mogelijk nodig is om opnieuw te binden aan zijn cofactor.

## Dankwoord

Met het schrijven van het dankwoord is het boekje dan toch echt bijna af. Een beetje vreemd maar wel lekker. Bij deze wil ik de mensen bedanken die hebben geholpen bij de totstandkoming van dit proefschrift.

Allereerst wil ik de mensen van ons eigen lab bedanken. Piet, ik heb veel geleerd van jouw kritische kijk op de (tussentijdse) resultaten en het was erg prettig dat ik ten alle tijden voor raad bij je binnen kon lopen. Mitja, bedankt voor de eerste praktijklessen moleculaire biologie. Shizuko, it was very kind of you to introduce cell culturing to me, arigato. Arie, we vormden een goed team. Zonder jouw hulp was ik niet zover gekomen, erg bedankt. Wieger, Roland en Niels, met jullie was er van een cellentekort gelukkig nooit sprake. Loes, naast jouw hulp in het lab was het ook erg gezellig om met je op de tennisbaan te staan. Martin, onze discussies over de meest veelzijdige onderwerpen en jouw gastvrijheid in het Schwarzwald zal ik niet vergeten. Eric, bedankt voor het meedenken en je scherpe opmerkingen tijdens de werkbeprekingen en gangconferenties. Lucio, het door jouw gemaakte factor B kwam precies op het juiste moment, super! Marjan, het was fijn dat ik altijd gelijk bij je terecht kon voor het regelen van allerlei administratieve zaken en bedank sinterklaas voor me als je hem ziet. Toine, zonder een goed systeem staat alles stil. Gelukkig konden we er, mede dankzij jou, op vertrouwen dat alles goed liep en bleef lopen. Huub, samen hebben wij een tijdje het college Structuuranalyse verzorgd. Ik vond het erg leuk. Lucy, fijn dat je me bij stond met de laatste loodjes en bedankt voor de altijd gezellige klimavonden. Hans, hartelijk dank voor jouw hulp bij het C2a project en niet te vergeten voor het doorgeven van het 'recept' voor Bountyflapjes. Bert, het was leuk dat we samen aan de convertases werkten, daarnaast was het ook altijd erg gezellig gedurende de diverse vakanties. Michael, jouw enthousiasme werkt aanstekelijk en had zo zijn positieve invloed op de sfeer in de computerkamer. Xinyi, het was leuk jouw, als 'niet-complementoloog', als kamergenoot te hebben en bedankt voor alle zoete versnaperingen. Jin, the 'Beijing – what to do-list' was very useful. It was a perfect preparation for a perfect holiday in China. Els en Dennis, hartelijk dank voor de inzet tijdens jullie stage. Het was leuk om jullie te mogen begeleiden.

Naast mijn directe collega's in het Kruidgebouw wil ik ook de mensen van de afdeling Nephrology van het LUMC en de afdeling Experimentele Microbiologie van het UMC bedanken voor de prettige samenwerking. Moh, jouw enthousiaste

en onuitputtelijke stroom aan ideeën zal ik niet vergeten. Anja, jouw proeven waren essentieel voor ons werk. Hartelijk dank voor je hulp. Jos en Suzan, de combinatie tussen de SCIN structuur en de functionele proeven pakte goed uit. Ik vond het een hele fijne samenwerking.

Verder wil ik graag de AiO's van de andere labs van het Bijvoet centrum bedanken. De AiO-avonden met de borrels en diners waren altijd erg gezellig en het was goed om met mede ploeters te praten over geslaagde en minder geslaagde experimenten.

Graag wil ik ook de vrienden buiten het lab bedanken voor de noodzakelijke ontspanning. De NIOO'ers ben ik dankbaar voor hun altijd geslaagde sociale gelegenheden in en om Nieuwersluis. Erg leuk dat ik daar als nep-NIOO'er bij betrokken werd. Veel 'collega's van' zijn inmiddels vrienden geworden en dat is heel tof. Verder wil ik hier ook een woord van dank richten aan 'De Gendtenaren'. De jaarlijkse eet-, bowl- en bieravonden vormden altijd een welkome afwisseling op het leven van alledag. Dat er nog maar vele mogen volgen! Ook ben ik dank verschuldigd aan 'De Roosendalers'. De Brabantse hartelijkheid was en is altijd erg aangenaam.

Een goede thuisbasis is onontbeerlijk. Jody, broertje ; ) als jij er bent is het onmogelijk om aan werk te denken. Volhouden zou ik zeggen! Nata, bedankt voor de gastvrijheid in Eindhoven en succes met het afronden van jouw eigen boekje. Dave, wanneer gaan we weer motorrijden, duiken, skieën,.... ? Saskia bedankt voor de gezelligheid en de vele mooie kaartjes. Riet, dank voor jouw goede zorgen en zoete kadootjes. Dik, helaas kun je er niet bij zijn. Dankzij jouw hulp op ons steekje in De Bilt was het makkelijk me er thuis te voelen. Lieve ouders, bedankt voor jullie onvoorwaardelijke steun en eeuwig vertrouwen. Gabi, als we samen zijn is het goed, dank voor alles.

# Curriculum vitae

De schrijver van dit proefschrift werd op 30 april 1977 geboren te Arnhem. In 1994 behaalde hij zijn HAVO-diploma en in 1996 zijn VWO-diploma aan de scholengemeenschap Oost-Betuwe te Bommel. Aansluitend ging hij naar de Internationale Agrarische Hogeschool Larenstein en behaalde daar in 1997 het propedeuse diploma van de studierichting Land, Water en Milieubeheer. Daarna studeerde hij tot juni 2002 Moleculaire Wetenschappen aan het Wageningen Universiteit en Research Center (WUR). Tijdens die studie volgde hij afstudeervakken bij (1) de vakgroep Biochemie van het WUR (onder begeleiding van M.H. Hefti en J. Vervoort) en (2) het European Molecular Biology Laboratory (EMBL) te Hamburg, Duitsland (onder begeleiding van C. Enroth en J. Vervoort). In juli 2002 begon hij als assistent in opleiding bij de sectie Kristal- en Structuurchemie van de Universiteit Utrecht. In deze functie werd het in dit proefschrift beschreven onderzoek verricht onder begeleiding van Prof. Dr. P. Gros.



## List of publications

- Hefti, M.H., Milder, F.J., Boeren, S., Vervoort, J., and van Berkel, W.J. (2003). A His-tag based immobilization method for the preparation and reconstitution of apoflavoproteins. *Biochimica et Biophysica Acta*, 1619, 139-143.
- Milder, F.J., Raaijmakers, H.C.A., Vandeputte, D.A.A., Schouten, A., Huizinga, E.G., Romijn, R.A., Hemrika, W., Roos, A., Daha, M.R., and Gros, P. (2006). Structure of complement component C2a: implications for convertase formation and substrate binding. *Structure*, 14, 1587-1597.
- Milder, F.J., Gomes, L., Schouten, A., Janssen, B.J.C., Huizinga, E.G., Romijn, R.A., Hemrika, W., Roos, A., Daha, M.R., and Gros, P. (2007). Factor B structure provides insights into activation of the central protease of the complement system. *Nature Structural and Molecular Biology*, 3, 224-228.
- Milder, F.J.\*, Rooijackers, S.H.M.\*, Bardoel, B.W., Ruyken, M, Van Strijp, J.A.G, and Gros, P. (2007). Staphylococcal complement inhibitor: Structure and active sites. Accepted for publication in *The Journal of Immunology*

\*these authors contributed equally to this work





# Appendix: color figures

## Color figures chapter 1

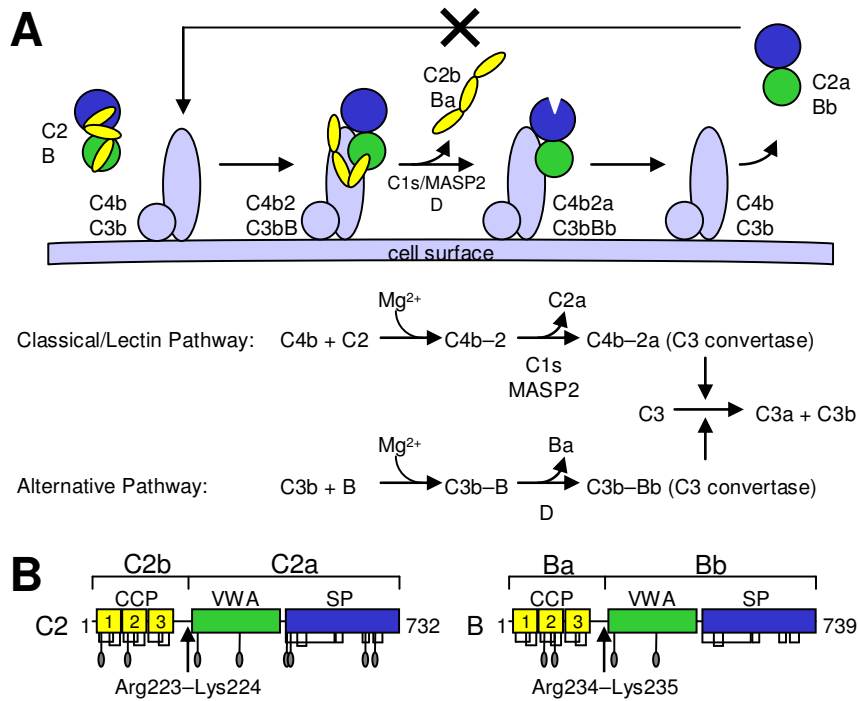


**Figure 1.2 Convertase formation and domain topology of C2 and factor B**  
**A)** Cartoon and schematic representation of C3 convertase formation. **B)** Schematic representation of C2 and factor B, indicated are the domains, N-linked glycans, and disulfide bridges.

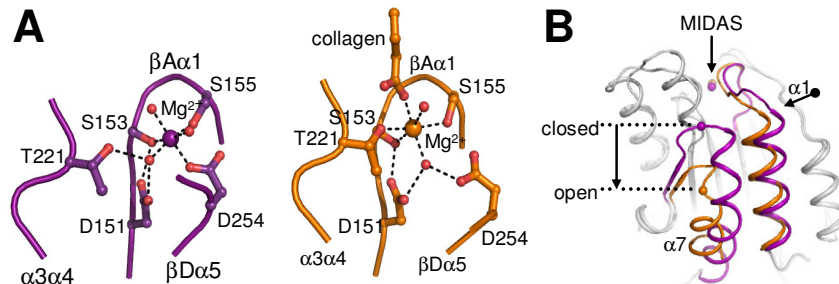


**Figure 1.3 Integrin I domain**  
**A)** Metal ion dependent adhesion site of integrin  $\alpha_2\beta_1$ . The MIDAS residues (residue number and loop names are indicated), waters (small spheres), and  $Mg^{2+}$  ion (large sphere). Left panel – unliganded closed MIDAS (PDB 1aox), right panel – liganded open MIDAS (PDB 1dzi). **B)** Conformational changes of the I domain following ligand binding. I domain shown in ribbon representation, highlighted are the MIDAS, helix  $\alpha 1$  and the C-terminal helix  $\alpha 7$ .

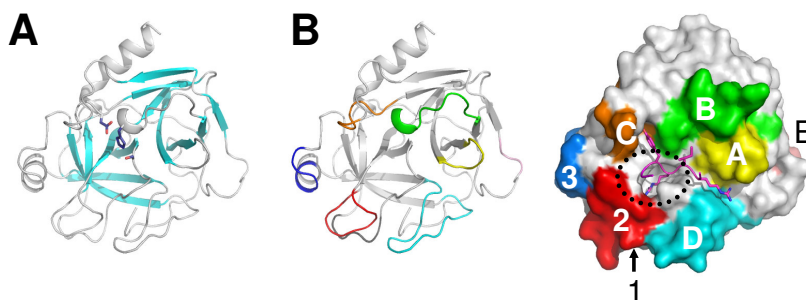


**Figure 1.4 Serine proteases; fold and substrate binding**

**A**) The chymotrypsin fold. The catalytic triad residues (dark blue) are positioned in between the two  $\beta$ -barrels (light blue). **B**) The 8 conserved substrate-binding loops surrounding the catalytic center shown in cartoon (left) and surface (right) representation (pdb 1avw). In the right panel a part of the soybean trypsin inhibitor is shown (purple), indicated are the P1-arginine (in sticks) that occupies the S1 pocket (dotted circle), and four adjacent residues interacting with the surface loops.

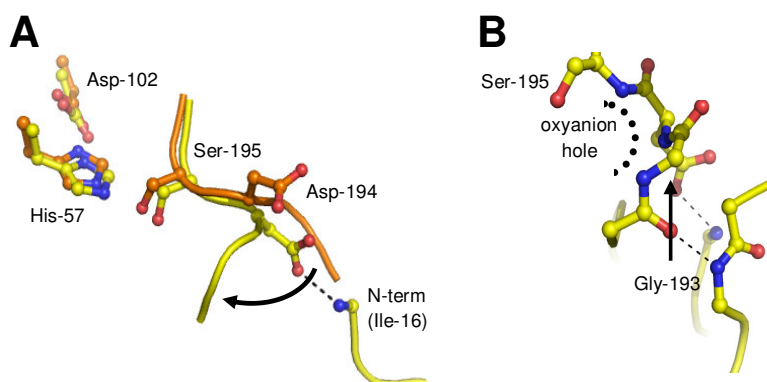


**Figure 1.5 The serine protease catalytic center**

**A**) Overlay of the catalytic center of chymotrypsinogen (orange; PDB 2cga) and chymotrypsin (yellow; 4cha). Shown in sticks are the catalytic triad (His-57, Asp-102, and Ser-195) and the Asp-194 interaction with the liberated N-terminus in the activate protease. **B**) The amides of the catalytic serine and glycine 193 pointing inwards form the oxyanionhole.

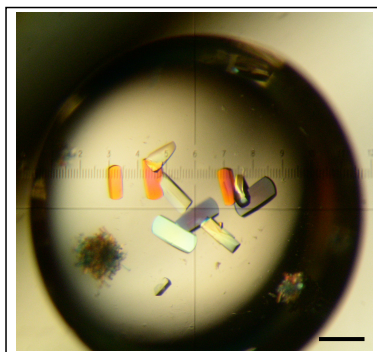


**Figure 1.6 SCIN crystals**

A drop containing SCIN crystals. Both clusters of small crystals and larger single crystals are present. Due to their birefringence, protein crystals are highlighted in different colors using polarized light. The bar indicates 100  $\mu$ m.

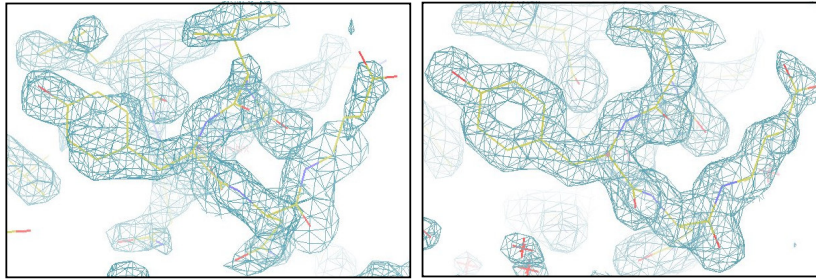


**Figure 1.7 Electron density**  
 A 1.8 Å resolution electron density map (1.4  $\sigma$ ) before (left) and after (right) refinement of the model.

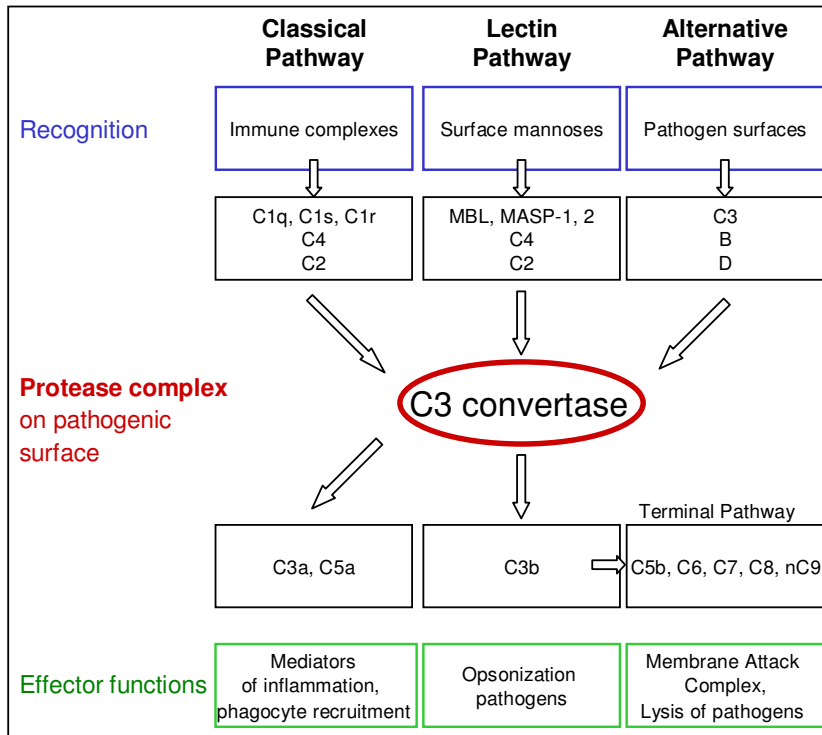


**Figure 1.1 The complement cascade**

## Color figures chapter 2

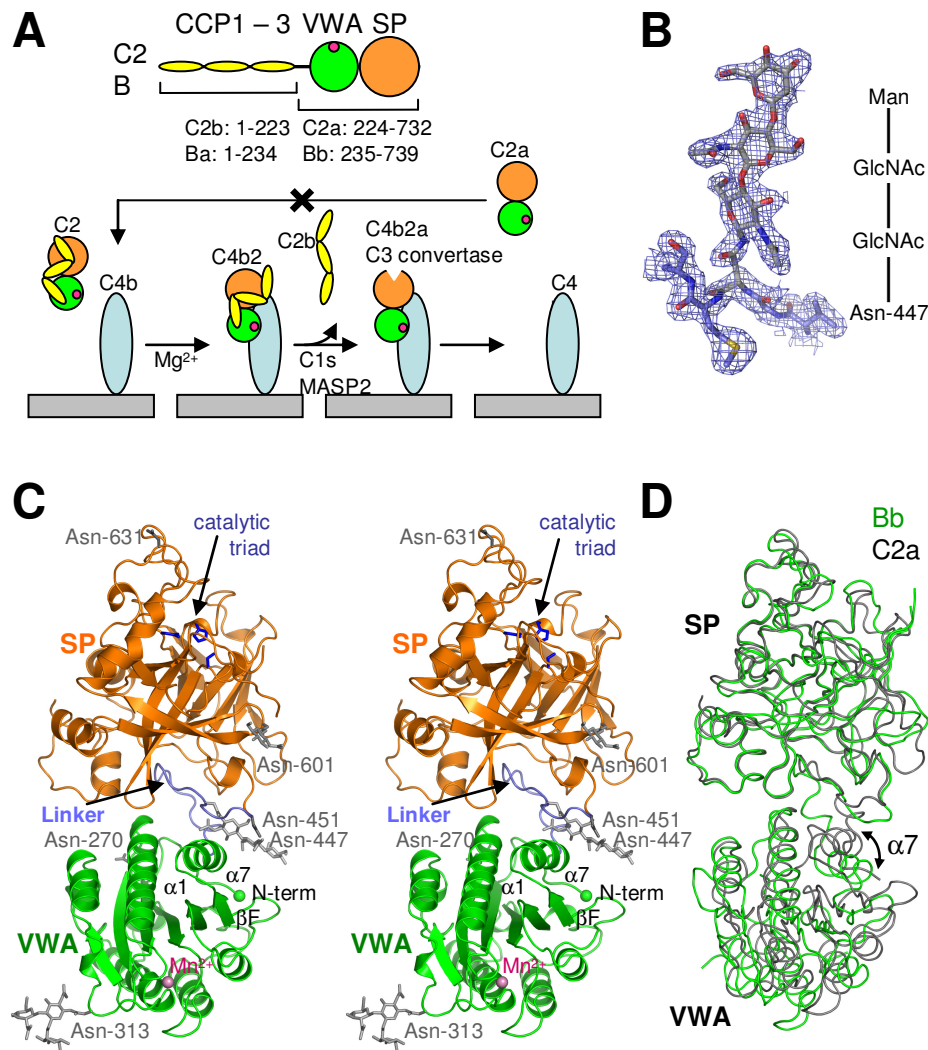


**Figure 2.1 Crystal structure of C2a.**

**A)** Schematic representation of domain topology of C2 and formation of the C3 convertase. **B)** Electron density ( $2mF_o - DF_c$ ,  $\phi_c$ ) of the glycan attached to Asn-447, shown are Asn-447-GlcNAc-GlcNAc-Man. **C)** Stereo ribbon representation of the C2a-Mn<sup>2+</sup> structure, indicated are the catalytic triad (blue) in the SP domain (orange), the linker region (light blue) between the SP and VWA domain (green with its N-terminal residue indicated by a green sphere), the manganese ion (pink) bound at the MIDAS motif; and, the six glycosylation sites (grey). **D)** Overlay of C2a (black) and Bb (1rrk, green) (Ponnuraj et al., 2004) superimposed on the SP domains, indicated is the different positions of the  $\alpha 7$  helix in the VWA domains.

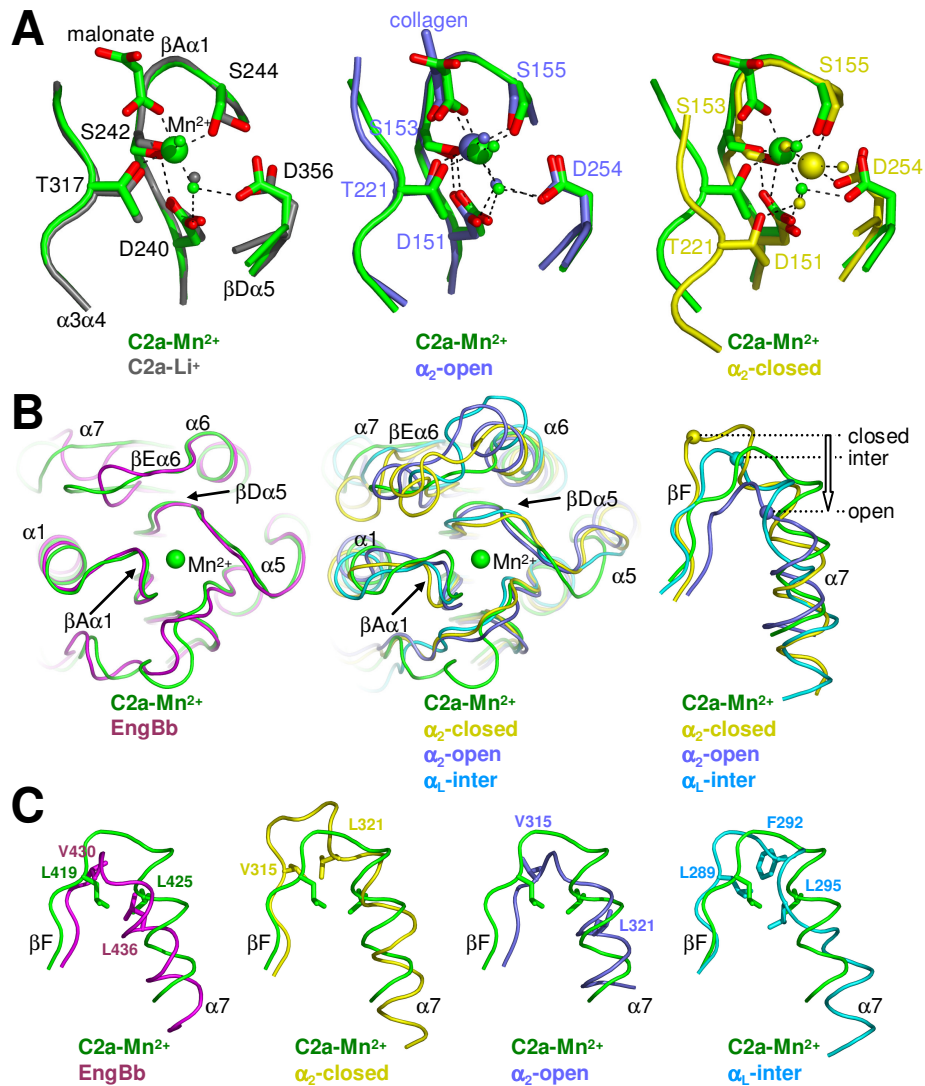


**Figure 2.2** Activation state of the VWA domain.

**A** Left panel: the MIDAS motif of C2a as observed in the structures of C2a-Li<sup>+</sup> (grey) and C2a-Mn<sup>2+</sup> (green). Shown are the MIDAS residues (residue number and loop names as indicated), pseudo-ligand malonate, waters (small spheres), and Mn<sup>2+</sup> (large sphere). Middle and right panel: the MIDAS motif of C2a-Mn<sup>2+</sup> and the  $\alpha_2$  I domain in an open (1dzi, blue) and closed (1aox, yellow) conformation (Emsley et al., 1997; 2000). **B** View of the VWA domain. Left panel: C2a-Mn<sup>2+</sup> (green) and engineered open Bb (1rrk, magenta) (Ponnuraj et al., 2004); middle panel: C2a-Mn<sup>2+</sup> (green), closed (1aox, yellow) and open (1dzi, blue)  $\alpha_2$  (Emsley et al., 1997; 2000) and intermediate (1mjn, light blue)  $\alpha_L$  (Shimaoka et al., 2003) I domains; and, right panel: coil representation of the strand  $\beta F$  and helix  $\alpha 7$ , coloured as in the middle panel. Indicated is the conformation of loops  $\beta A\alpha 1$  and  $\beta D\alpha 5$  and helix  $\alpha 1$  transmitting structural changes between the MIDAS motif and helix  $\alpha 7$ . **C** Position of hydrophobic 'ratchet' residues of loop  $\beta F\alpha 7$  and helix  $\alpha 7$ , coloured as in B. From left to right; C2a-Mn<sup>2+</sup> and engineered open Bb, C2a-Mn<sup>2+</sup> and closed  $\alpha_2$ , C2a-Mn<sup>2+</sup> and open  $\alpha_2$ ; and, C2a-Mn<sup>2+</sup> and intermediate  $\alpha_L$ .

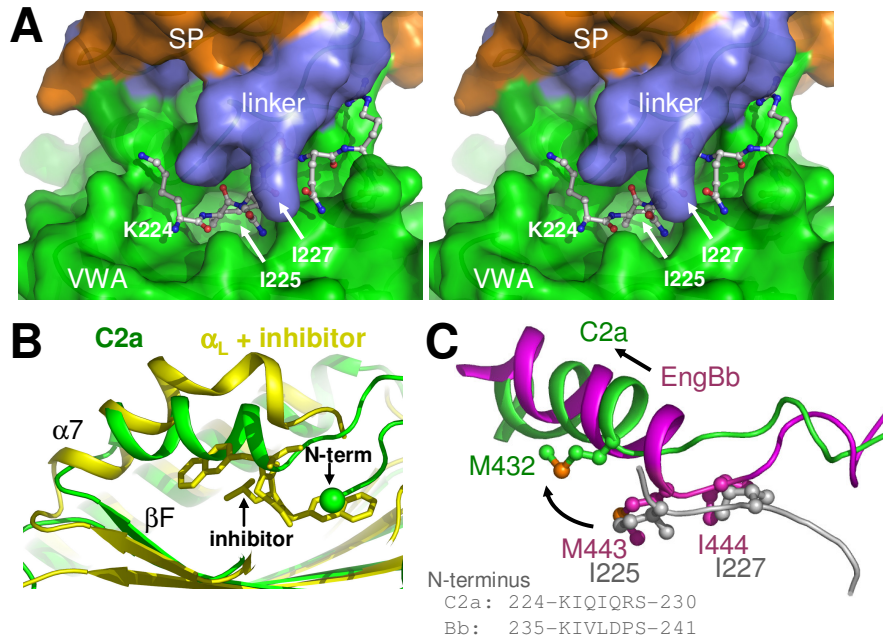


**Figure 2.3 N-terminal residues of C2a.**

**A** Stereo figure showing the N-terminal residues (ball-and-stick) of C2a positioned in a crevice near the linker (blue) connecting the VWA (green) and SP (orange) domains. The C2a N-terminus is anchored via Ile-225 and Ile-227 that are buried in underlying hydrophobic pockets. **B** Overlay of C2a-Mn<sup>2+</sup> (green) and the closed  $\alpha_L$  I domain (1xuo, yellow) in complex with a small molecule antagonist (Wattanasin et al., 2005). The binding site for the N-terminal segment in C2a and the antagonist partially overlap. **C** Overlay of the N and C-terminal regions of the VWA domain of C2a (green) and engineered Bb (1rrk, magenta) (Ponnuraj et al., 2004). In C2a the N-terminal residues interact with  $\alpha_7$  and Ile-225 and Ile-227 occupy hydrophobic pockets. In engineered Bb residues of the C-terminal end of  $\alpha_7$  (Met-443 and Ile-444) occupy these hydrophobic pockets.

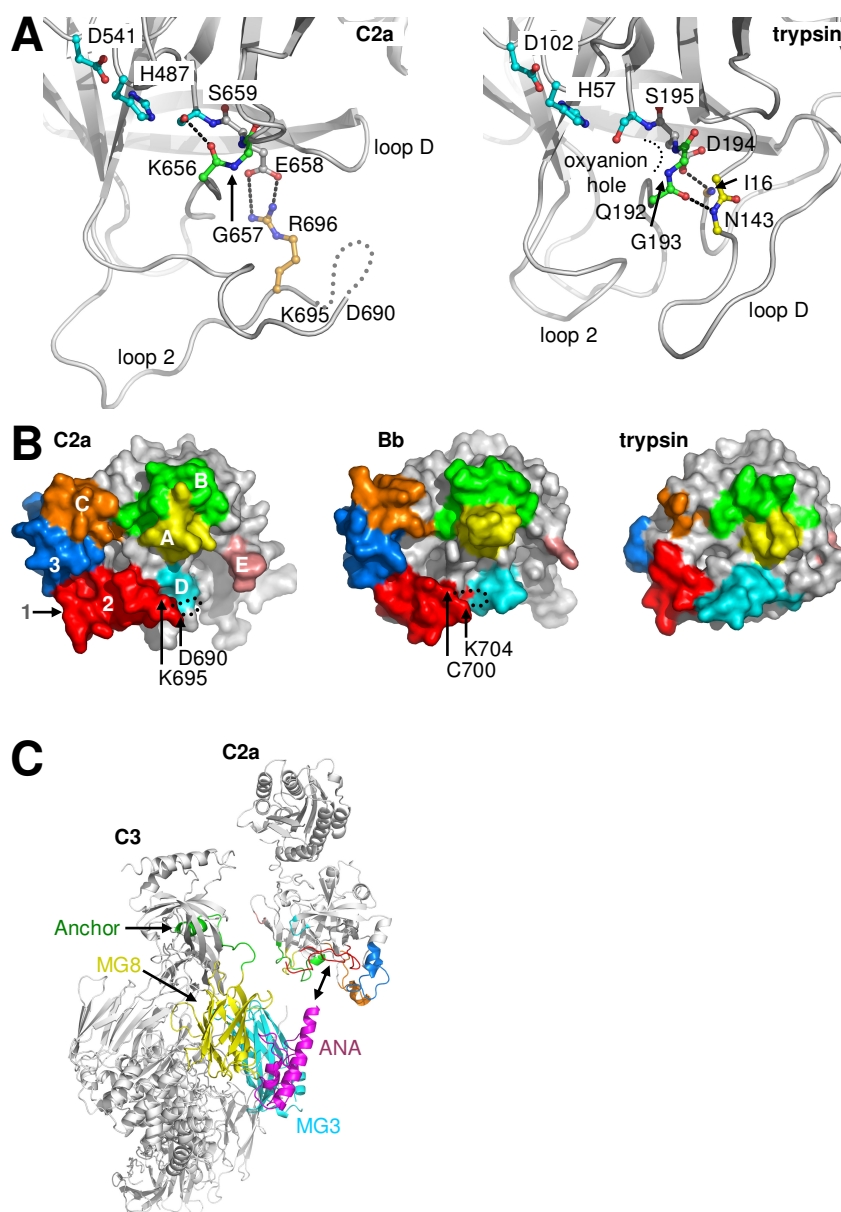


**Figure 2.4 The SP domain.**

**A)** Catalytic center and oxyanion hole in C2a-Li<sup>+</sup> (left panel) and trypsin (1aww, right panel) (Song and Suh 1998); indicated are the catalytic triad Asp-His-Ser (light blue), the oxyanion hole (green) and Arg-696 (orange) in C2a replacing the N-terminal Ile-16 in trypsin. In trypsin the main-chain of Asn-143 (yellow) forms a hydrogen bond with the main chain of 192-193. A similar interaction is absent in C2a. Instead, the peptide plane of 656-657 is flipped and makes a hydrogen bond with the catalytic serine. **B)** Surface representation of the putative substrate-binding grooves;

shown are C2a-Li<sup>+</sup> (left panel), Bb (1rrk, middle panel) (Ponnuraj et al., 2004) and trypsin (1avw, right panel) (Song and Suh 1998). Surface loops 1 (grey), 2 (red), 3 (blue), A (yellow), B (green), C (orange), D (light blue), and E (pink) are highlighted **C**) Hypothetical model of C2a placed onto C3 (2a73, (Janssen et al., 2005)); shown are the SP domain of C2a with substrate-binding loops coloured as in B; and, substrate C3 with the flexible scissile loop indicated by a dotted line; domains of C3 are labelled as defined in (Janssen et al., 2005).

### Color figures chapter 3

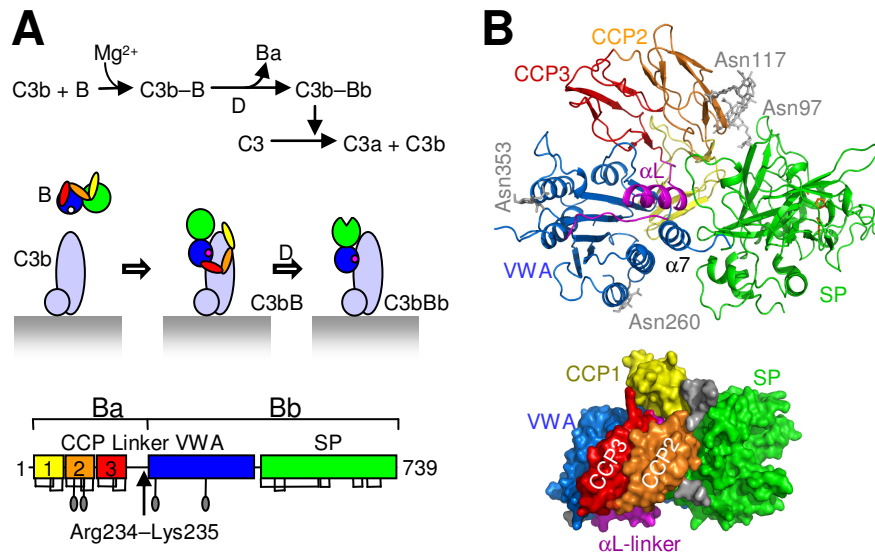


**Figure 3.1 C3-convertase formation and crystal structure of complement factor B.**

**A**) Schematic and cartoon representation of C3-convertase formation (top and middle panel; cartoon of C3b is based on crystal structure (Janssen et al., 2006; Wiesmann et al., 2006)); and, domain topology of factor B, indicated are the N-linked glycans, the disulphide bridges and the Arg234-Lys235 scissile bond (lower panel). **B**) Structure of factor B shown in ribbon representation colored by domains as in **a** (top panel). The linker connecting CCP3 and VWA is colored purple. The N-linked glycans (grey) and the catalytic triad Asp-His-Ser (brown) are presented in stick model. Labels indicate the centrally positioned helices αL and α7. Bottom panel – factor B shown in surface representation, domains colored as indicated and glycans shown in grey (rotated by 90° with respect to figure in top panel).



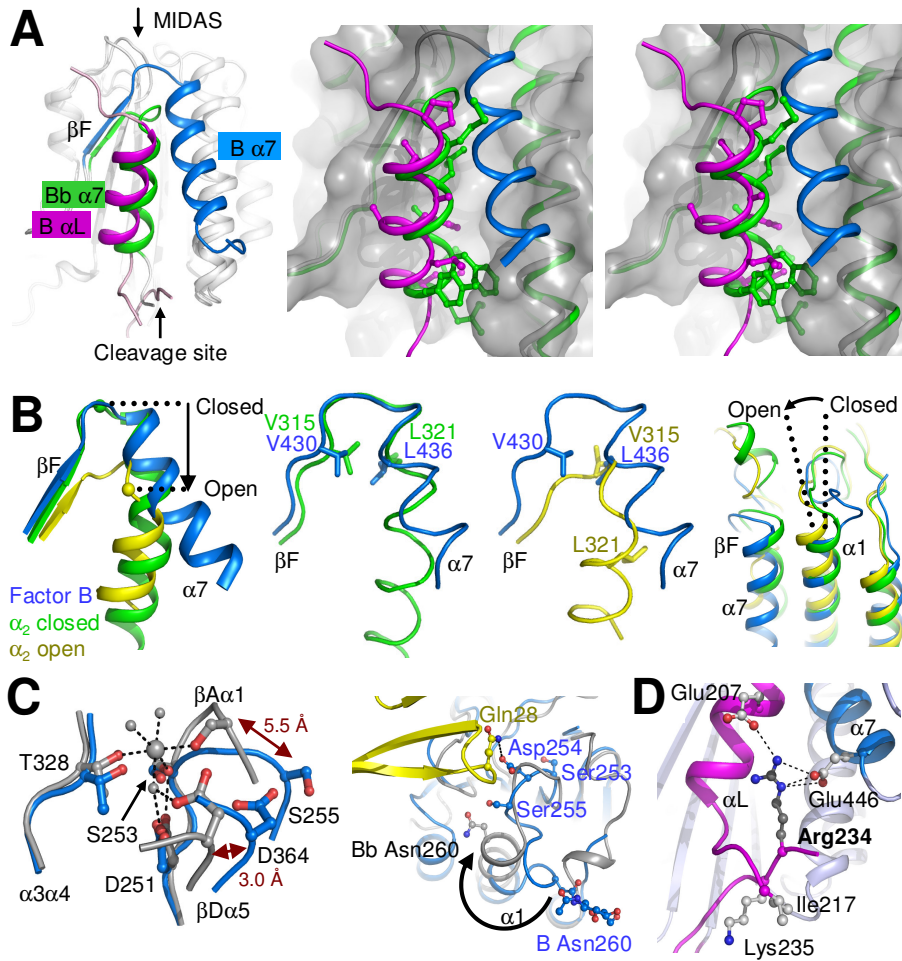


**Figure 3.2 Regulatory elements in the VWA domain.**

**A**) Dislocation of helix  $\alpha 7$  by helix  $\alpha L$ . Overlay of the VWA domains of factor B and Bb (PDB entry 1rrk) showing the displacement of helix  $\alpha 7$  (blue in factor B, green in Bb) by linker helix  $\alpha L$  (purple); and, stereo figure showing the packing of helices  $\alpha 7$  and  $\alpha L$  against the body of the VWA domain of factor B (grey, surface representation). Factor B (white) and Bb (green) are shown in ribbon representation with factor B helices  $\alpha L$  and  $\alpha 7$  colored purple and blue respectively. Hydrophobic residues of helices  $\alpha L$  (B) and  $\alpha 7$  (Bb) are shown in ball-and-stick. **B**) Conformation of loop  $\beta F \alpha 7$  and helices  $\alpha 7$  and  $\alpha 1$ . Overlay of VWA domains of factor B (blue) with closed (green) and open (yellow) conformations of the  $\alpha 2$  I-domain (PDB entries 1aox and 1dzi respectively), showing strand  $\beta F$  and helix  $\alpha 7$  (left panel), positions of hydrophobic 'ratchet' residues (sticks) of loop  $\beta F \alpha 7$  and helix  $\alpha 7$  (middle two panels) and position of helix  $\alpha 1$  (right-panel). **C**) Distortion of the  $Mg^{2+}$ -dependent MIDAS C3b binding site. Superposition of the MIDAS motif in factor B (blue) and Bb (grey) in stick model (left panel). Grey spheres represent water molecules (small spheres) and the bound ion (large sphere) as observed in Bb. Orientation of CCP1 (yellow) and VWA (blue) in factor B with the VWA domain of Bb (grey) superposed (right panel). Shown in ball-and-stick representation are the adjoining residues Gln28 and Asp254 and the glycosylation site Asn260. **D**) The P1 residue of the buried scissile bond (Arg234 – Lys235) interacts with helices  $\alpha 7$  (blue) and linker helix  $\alpha L$  (purple) via salt-bridges.

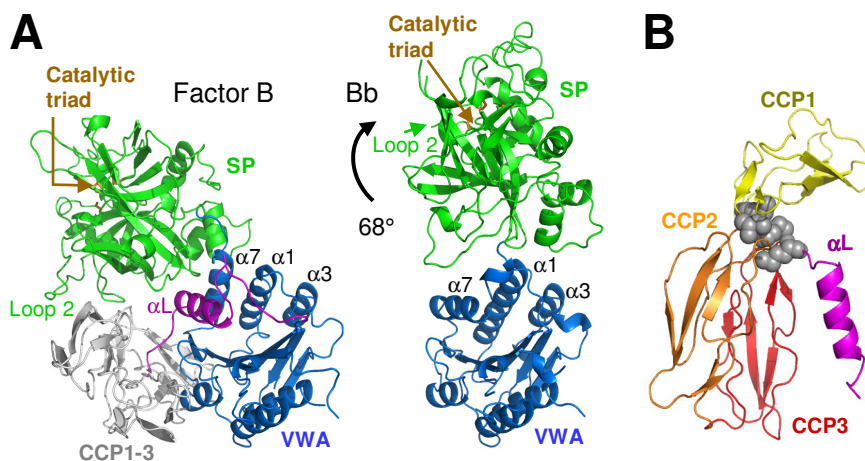


**Figure 3.3 Domain orientations in factor B and Bb.**

**A)** Orientation of VWA (blue) and SP (green) in factor B with linker and linker helix  $\alpha$ L shown in purple and CCP1-3 domains in grey (left panel); and orientation of VWA and SP in Bb (PDB entry 1rrk). Indicated are helices  $\alpha$ L,  $\alpha$ 1,  $\alpha$ 3 and  $\alpha$ 7, which are involved in the VWA-SP interfaces. **B)** The CCP triad arrangement in ribbon representation with CCP1 (yellow), CCP2 (orange) and CCP3 (red). Grey spheres indicate the four residues (Tyr42, Ile76, Phe197 and Met198) forming the hydrophobic triad center. The adjoining linker containing helix  $\alpha$ L is colored purple.

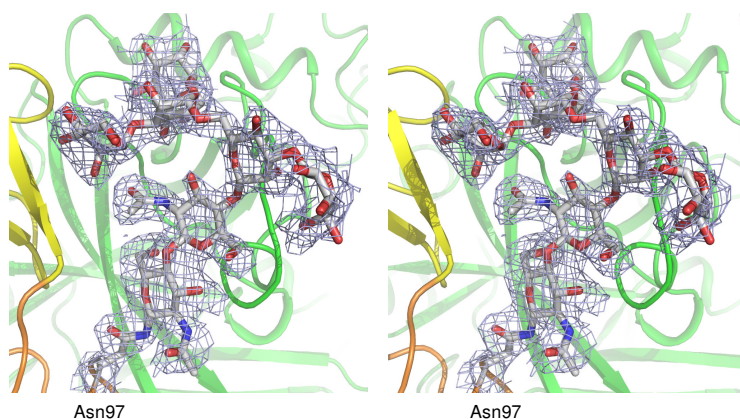


**Figure S3.1 Stereo figure showing the electron density for the N-linked glycan at Asn97.**

Electron density ( $2mF_{obs}-DF_{calc}$ ,  $\phi_{calc}$ ) contoured at  $1 \sigma$  of Man5-GlcNac2-Asn97 (shown in stick model), domains are shown in ribbon representation with CCP1 in yellow, CCP2 in orange, and the SP domain in green

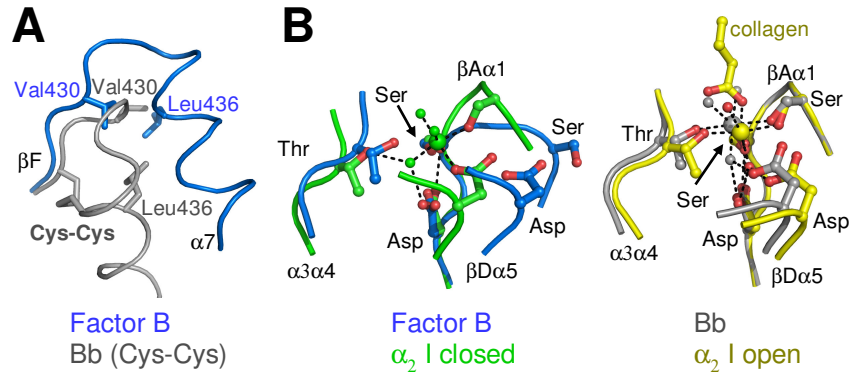


**Figure S3.2 Activation state of the VWA domain.**

**A**) Overlay of the VWA domain from factor B (blue) with Bb (1rrk, grey); position of hydrophobic 'ratchet' residues (stick) of loop  $\beta$ F $\alpha$ 7 and helix  $\alpha$ 7. **B**) Distortion of the MIDAS. Left panel – Superposition of the MIDAS motif in factor B (blue) and the closed  $\alpha$ 2 I-domain (1aox, green). Right panel – Superposition of the MIDAS motif in Bb (1rrk, grey) and the open collagen bound  $\alpha$ 2 I-domain (1dzi, yellow).

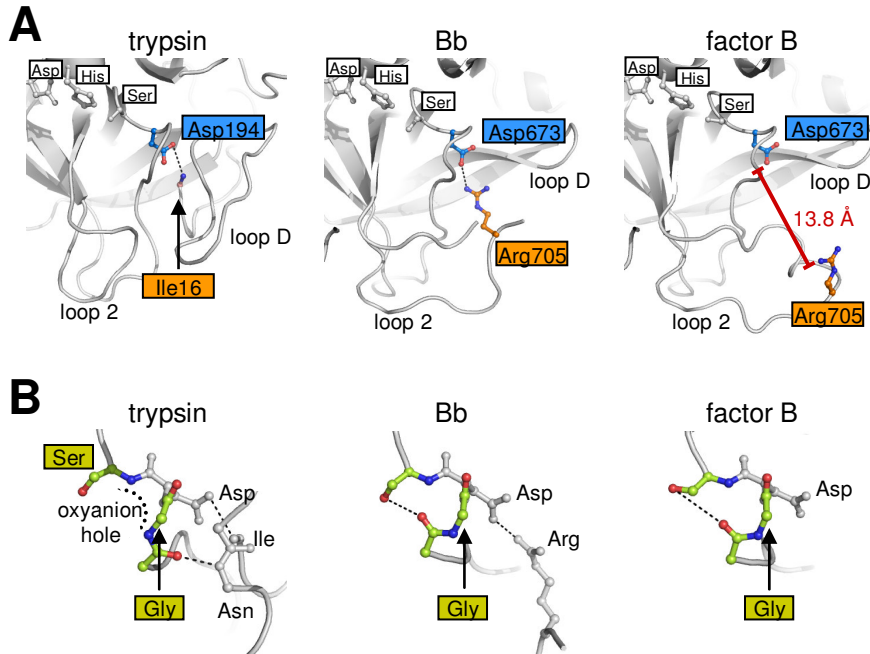


**Figure S3.3 The serine protease domain catalytic center.**

**A**) The catalytic center of trypsin (Song and Suh 1998) (1avw), Bb (Ponnuraj et al., 2004) (1rrk) and factor B. Indicated is the interaction between the N-terminal Ile16 (orange) and Asp194 (blue), which is characteristic for activated trypsins. In Bb Arg705 replaces Ile-16. In factor B this arginine is positioned away from Asp-673. **B**) The oxyanion holes of Bb (1rrk) and factor B are in an identical, near-active conformation with to an outward orientation of the glycine amide.

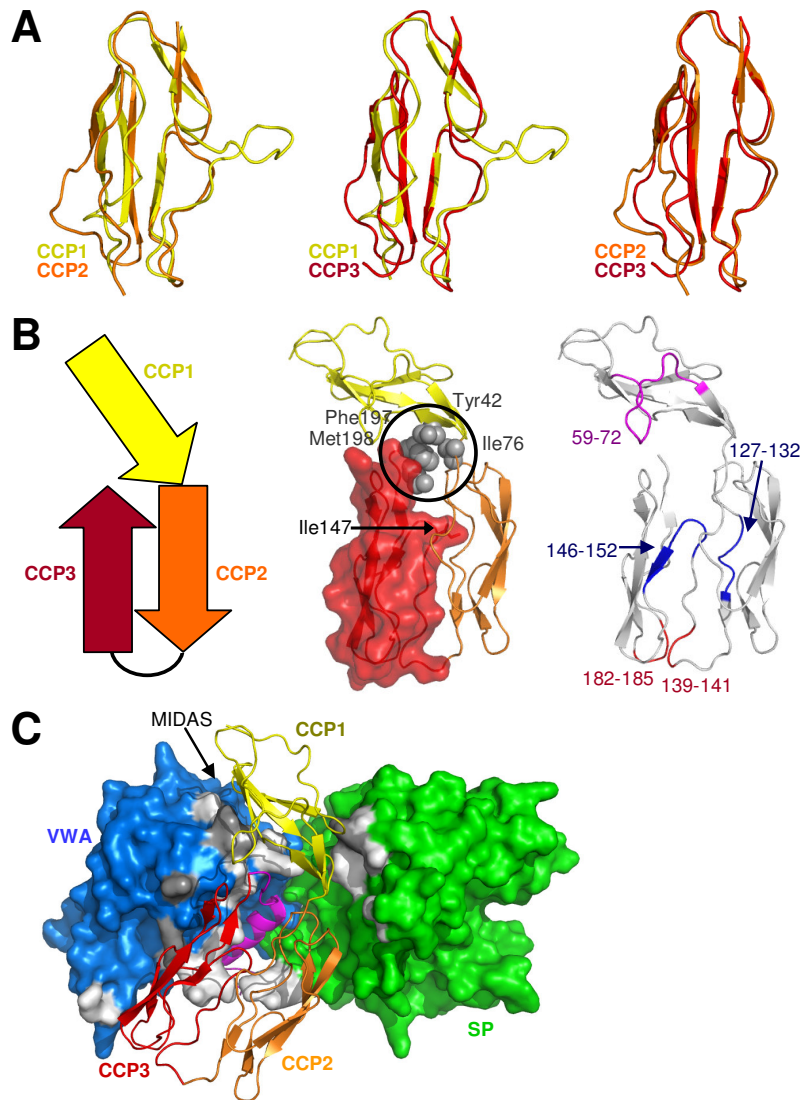


**Figure S3.4 The CCP triad arrangement.**

**A)** Overlays of the CCP domains shown in ribbon representation. **B)** Left panel - Schematic representation of the orientation of CCP domains 1 to 3. Middle panel - The CCP triad arrangement with CCP1 (yellow ribbons), CCP2 (orange ribbons) and CCP3 (red ribbon and transparent surface representation). Indicated are the four hydrophobic residues of the triad center and Ile147 of CCP3 that packs tightly into CCP2. Additional information is given in Supplemental Table S1. Right panel - Ribbon representation of CCP1-3; highlighted are segments (blue) in the CCP2-3 interface crucial for the factor B function (Hourcade et al., 1995; Xu and Volanakis 1997) and epitopes for monoclonal antibodies that reduce hemolytic activity upon binding; residues 59-728 and residues 138-141 with 182-185 (Thurman et al., 2005). **C)** Packing of CCP1-3 onto the VWA and SP domains. Shown are VWA (blue) and SP (green) in surface representation and CCP1-3 (yellow, orange and red) in ribbon representation. Grey areas represent contact area with dark grey indicating residues that yield gain in solvation energy upon formation of the interface (see Supplemental Table S2).

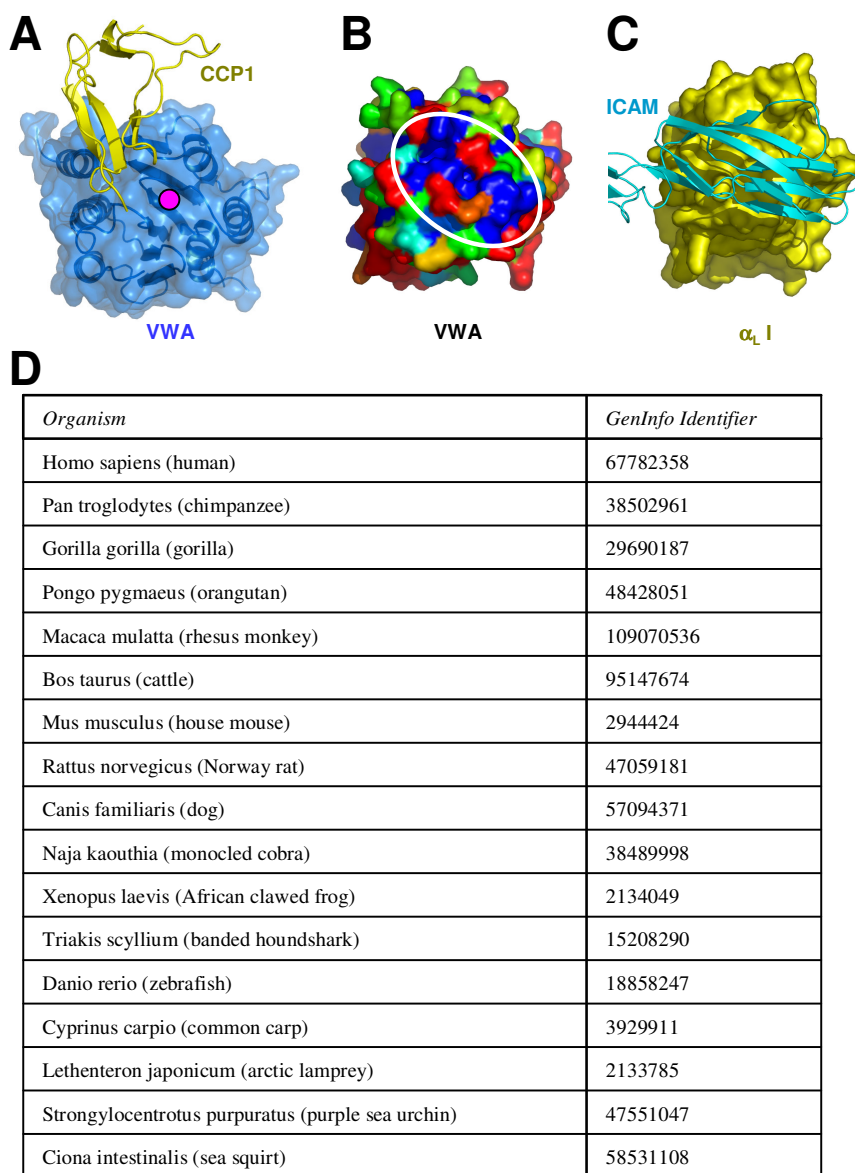


**Figure S3.5 The  $Mg^{2+}$ -dependent C3b binding site.**

**A**) VWA domain in surface (transparent blue) and ribbon representation (green) with the position of CCP1 indicated in ribbon representation (yellow). The position of  $Mg^{2+}$  binding is indicated by a pink sphere. **B**) Sequence conservation of the VWA domain based on a factor B alignment. In surface representation the VWA domain of Bb (Ponnuraj et al., 2004) (1rrk) colored from red (not conserved) to blue (conserved) (Landau et al., 2005). The white oval indicates the putative C3b contact site. **C**) Shown for comparison is ICAM binding (light blue ribbons) to the same site of the I domain of integrin  $\alpha_L$  (Shimaoka et al., 2003) (1mq8, yellow surface representation). **D**) List of sequences used for the alignment in b.

Color figures chapter 4

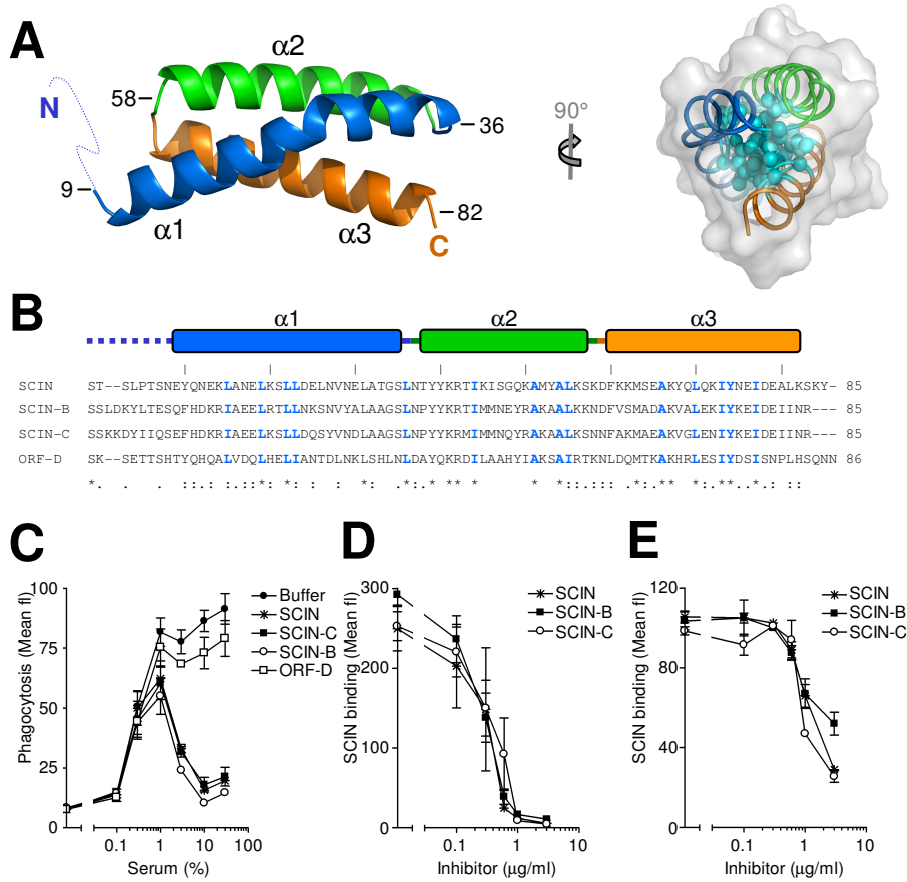


**Figure 4.2 Structure of SCIN and characterization of SCIN homologs.**

**A** left panel - Structure of SCIN shown in ribbon representation. Helices are colored blue (helix 1), green (helix 2), and orange (helix 3), the dotted line represents the flexible N-terminus. right panel - SCIN structure in ribbon and surface representation with side chains forming the conserved hydrophobic core in ball-and-stick (light blue) representation, helical coloring as in left panel. **B** Alignment of SCIN, SCIN B, SCIN C, and ORF-D. "\*" indicate identical residues, ":" indicate conserved substitutions and "." indicate semi-conserved substitutions (CLUSTAL W (1.83)). Highlighted in light blue are the conserved residues that form the hydrophobic core. **C** SCIN-B and SCIN-C (10  $\mu$ g/ml) strongly reduce phagocytosis of *S. aureus* at different serum concentrations. ORF-D does not reduce phagocytic uptake. **D,E** Binding of SCIN-FITC (1  $\mu$ g/ml) to *S. aureus* in 20% human sera in the presence of non-labeled SCIN, SCIN-B or SCIN-C. SCIN binding was analyzed by flow cytometry and is expressed as mean fluorescence of 10,000 bacteria. **D**, Non-labeled SCIN, SCIN-B and SCIN-C compete with SCIN-FITC for binding to surface-bound C3bBb. Binding to C3bBb was performed in the presence of MgEGTA. **E**, Non-labeled SCIN, SCIN-B and SCIN-C compete with SCIN-FITC for binding to surface-bound C4b2a. Binding to C4b2a was analyzed using factor D-deficient serum. All panels - data are mean  $\pm$  SEM of three independent experiments.

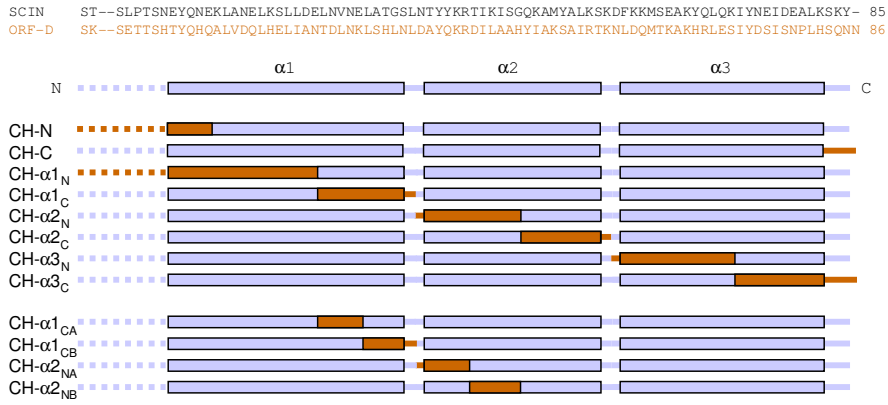


**Figure 4.3 Schematic representation of chimeric constructs used in this study.**

SCIN residues (grey) were exchanged with corresponding residues in ORF-D (orange). Exchanged residues: CH-N (res. 1-13), CH-C (res. 83-85), CH- $\alpha$ 1<sub>N</sub> (res. 1-25), CH- $\alpha$ 1<sub>C</sub> (res. 26-36), CH- $\alpha$ 2<sub>N</sub> (res. 37-48), CH- $\alpha$ 2<sub>C</sub> (res. 49-58), CH- $\alpha$ 3<sub>N</sub> (res. 59-72), and CH- $\alpha$ 3<sub>C</sub> (res. 73-86). CH- $\alpha$ 1<sub>CA</sub> (res. 26-30), CH- $\alpha$ 1<sub>CB</sub> (res. 31-36), CH- $\alpha$ 2<sub>NA</sub> (res. 37-42) and CH- $\alpha$ 2<sub>NB</sub> (res. 43-48).

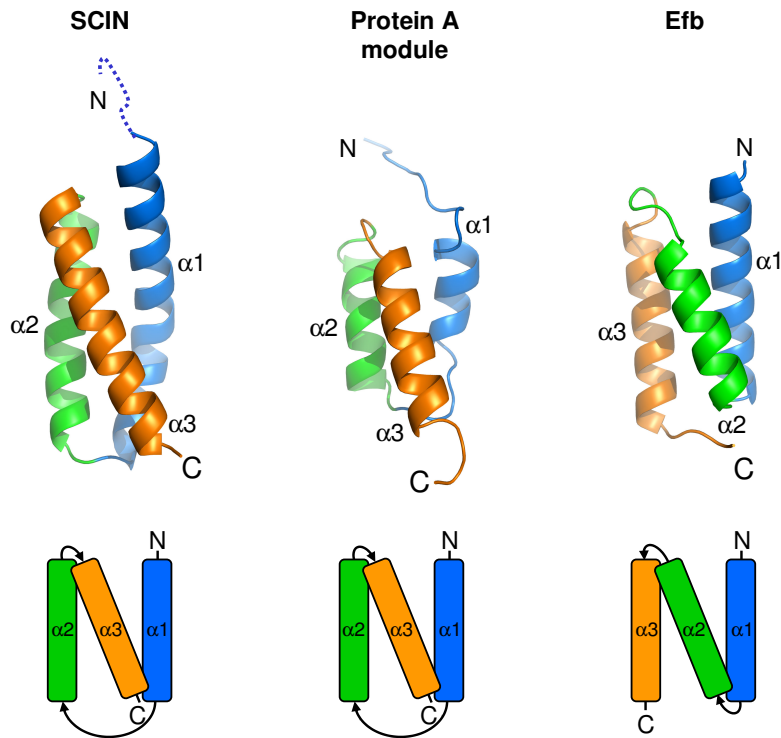


**Figure 4.8 Structural comparison of three *S. aureus* immune modulators.**

SCIN (left panel), Protein A module (middle panel, pdb 1bdd), and Efb-C (right panel, pdb 2gom) in ribbon and schematic representation. Helices are colored blue (helix 1), green (helix 2) and orange (helix 3).

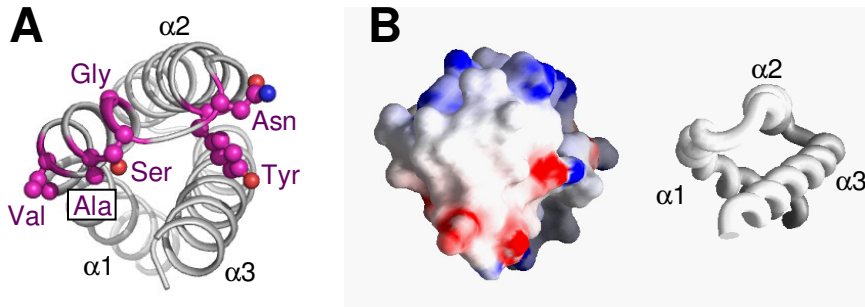


**Figure 4.9 Active site residues of SCIN for the Alternative Pathway.**

**A)** SCIN show in ribbon representation (grey) with active site residues conserved within SCIN, SCIN-B and SCIN-C but not in ORF-D highlighted and shown in ball-and stick representation (purple). **B)** Left panel - Electrostatic surface representation in and around the SCIN active site. Positively charged regions are represented in blue, negatively charged regions in red, and both polar and nonpolar regions are in white. Right panel – Similar view of SCIN shown in ribbon representation. Pictures were generated by GRASP (Nicholls et al., 1993).

## Color figures chapter 5

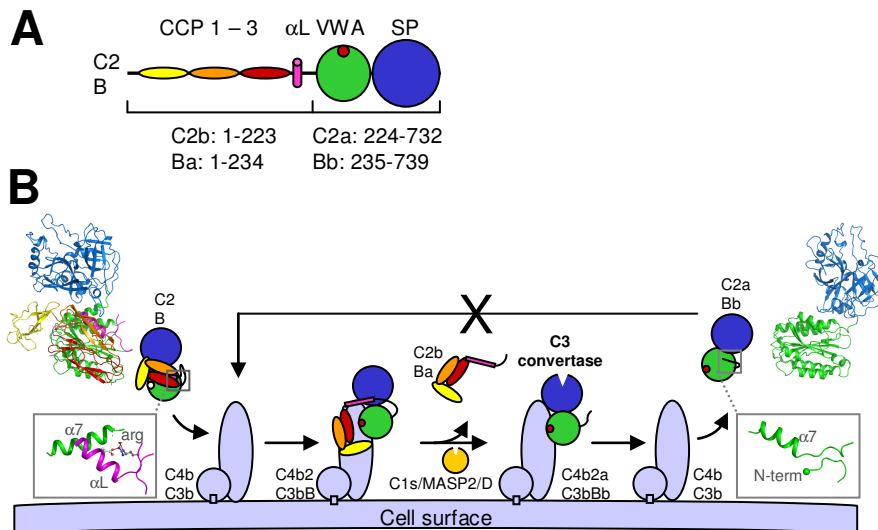


**Figure 5.1 Domain topology of C2 and factor B and convertase formation model**

**A)** Schematic representation of C2 and factor B, indicated are the domains and the linker helix ( $\alpha$ L). **B)** Cartoon representation of C3 convertase formation. Shown in ribbon representation are the crystal structures of factor B (left) and C2a (right).